INFLUENCE OF LAND USE AND LAND COVER CHANGES ON GROUNDWATER RECHARGE AND POLLUTION IN STONY ATHI SUB-CATCHMENT, KAJIADO COUNTY, KENYA

By

MORRIS WAHOME MATHENGE ***(MSc.)***

Reg. No: N85/31028/2015

A Thesis Submitted in Fulfillment of the Requirements for the Degree of Doctor of Philosophy (Environmental Science) in the School of Agriculture and Environmental Sciences of Kenyatta University

FEBRUARY, 2023

DECLARATION

This thesis is my original work and has not been presented for a degree in any other University or any other award.

Signature……. Date……..

MORRIS W. MATHENGE - N85/31028/2015
Department of Environmental Sciences and Education
Kenyatta University

We confirm that the work reported in this thesis was carried out by the student under our supervision.

Signature……. Date……..

DR. GLADYS GATHURU
Department of Environmental Sciences and Education
Kenyatta University

Signature……. Date……..

DR. ESTHER KITUR
Department of Environmental Sciences and Education
Kenyatta University

DEDICATION

To my wife Irene and my daughter Lillian, whose sacrifices and encouragement in the course of this research is something I will always cherish and remember and will continue being a source of inspiration.

ACKNOWLEDGEMENTS

First and foremost is to express my deepest appreciation to God for giving me health and strength to carry out this research. Secondly, my appreciation to my wife and daughter for their unparalleled patience. Much appreciation goes to my supervisors, Dr. Gladys Gathuru and Dr. Esther Kitur for providing professional support, intellectual stimulation and encouragement. I would also like to thank the National Research Fund for providing the funds to carry out this research. Regards also go to the Department of Research, Innovation and Outreach, Kenyatta University for the coordination of the research fund.

Gratitude also goes to the National Commission for Science, Technology and Innovation and the Administration in Kajiado County for granting me permission to collect research data during the field survey. Many thanks to my research assistant and the field crew for their assistance in field data collection. Finally, thanks to all those who gave me support and encouragement in one way or another towards the success of this research work.

TABLE OF CONTENTS

LIST OF TABLES

LIST OF FIGURES

LIST OF APPENDICES

LIST OF ABBREVIATIONS AND ACRONYMS

ASAL	Arid and Semi-Arid Land
AVI	Aquifer Vulnerability Index
CIDP	County Integrated Development Plan
DEM	Digital Elevation Map
DVI	DRASTIC Vulnerability Index
ETM	Enhanced Thematic Mapper
FAO	Food Agricultural Organization
GIS	Geographic Information System
GPS	Global Positioning System
GLEAMS	Groundwater Loading Effects of Agricultural Management Systems
GloFAS	Global Flood Awareness System
HWSD	Harmonized World Soil Data
IPCC	Inter-governmental Panel on Climate Change
KMD	Kenya Meteorological Department
KNBS	Kenya National Bureau of Statistics
LEACHM	Leaching Estimation and Chemistry Model
LULC	Land Use and Land Cover
MDVI	Modified DRASTIC Vulnerability Index
NACOSTI	National Commission for Science, Technology and Innovation
NAS	Nairobi Aquifer System
PET	Potential Evapotranspiration
PRZM	Pesticide Root Zone Model
RCMRD	Regional Centre for Mapping of Resources for Development
SRTM	Shuttle Radar Topography Mission
SSA	Sub-Saharan Africa
USDA	United States Department of Agriculture
USGS	United States Geological Survey
U.S. EPA	United States Environmental Protection Agency
WHO	World Health Organization
WRA	Water Resources Authority

DEFINITION OF TERMS

Groundwater recharge

Groundwater recharge is water that is added to the groundwater system through the vadose zone after infiltration and percolation following a rainfall event or from surface water bodies as well as from irrigation water.

Groundwater vulnerability

Groundwater vulnerability is the tendency or likelihood of contaminants to reach the groundwater system after introduction at the earth's surface**.**

Land use

Land use refers to the human utility of what is on the Earth's surface such as agriculture, urban development, grazing and mining among others.

Land cover

Land cover refers to the assemblage of the physical components on the earth's surface such as forest, water body, grassland among others.

Land use and land cover change

Land use change refers to the human modifications or alterations of the earth's terrestrial surface, that is, the way land is used or managed by humans such as agricultural activities, constructions and grazing among others. Land cover changes are the changes in land characteristics such as vegetation type and soil type among others.

Climatic characteristics

Climate describes what the weather parameters over a long period of time in a specific area. In this study, climatic characteristics refer to rainfall, temperature, evapotranspiration and wind speed.

Physical characteristics

Physical characteristics are the parameters that define the terrestrial environment. In this context the parameters are topography, slope, soil texture and groundwater depth.

ABSTRACT

The global economic growth and population increase has translated into increased anthropogenic land use and land cover changes. Changes in land use and land cover have the potential of altering the hydrological cycle. In the Stony Athi sub-catchment of Kajiado County, Kenya, demographic pressure and urbanization have transformed natural rangelands into agricultural, industrial and real estate developments. The objective of this study was to investigate the influence of land use and land cover changes on groundwater recharge and pollution vulnerability between 1984 and 2017. Specifically, the study was undertaken to; (a) quantify the spatial-temporal extent and magnitude of land use and land cover changes that have occurred in Stony Athi sub-catchment between 1984 and 2017; (b) to estimate the spatial-temporal variations of groundwater recharge due to land use and land cover changes; and (c) to evaluate the influence of land use and land cover changes on groundwater vulnerability to pollution. Quantification of spatial-temporal extent and magnitude of land use and land cover changes was achieved by classifying four satellite images through the supervised classification algorithm and finally applying post-classification change detection technique. Results showed significant ($p < 0.05$) land use and land cover changes between 1984 and 2017 with an increase in built-up areas (0.04% - 3.4%), agricultural land (0.06% - 0.7%) and grasslands (58.2% - 71.6%), but a decrease in shrub land (37.1% - 21.1%) and forested areas (2.5% - 1.4%). Estimation of the spatial-temporal variation of groundwater recharge due to land use and land cover changes was done using WetSpass-M, a Geographical Information System-based Hydrologic Model. Results indicated a decrease in groundwater recharge from 13.8% in 1984 to 13.2% in 2017. However, the observed temporal variations were not significant at $p < 0.05$. Spatial variations of groundwater recharge indicated that the highest recharge occur in forested areas at 251.1 mm per year while the lowest recharge occur in bare land at 0.4 mm per year. A modified DRASTIC model was used to evaluate the influence of land use and land cover changes on groundwater vulnerability to pollution. Potential of groundwater pollution vulnerability was categorized using a vulnerability index based on the United States Environment Protection Agency classification. Results indicated that 87% of the study area remained under low vulnerability between 1984 and 2017. Areas under moderate vulnerability decreased from 12% to 9% while areas under high vulnerability increased from 1% to 4% over the same period. The observed temporal variations in groundwater pollution vulnerability were not significant at $p < 0.05$. It was concluded that the land use and land cover changes in the study area have an influence on groundwater recharge and its vulnerability to pollution, though not statistically significant at $p < 0.05$. This study recommends continuous monitoring of groundwater quantity and quality, not only in the study area, but also in areas undergoing rapid changes in land use and land cover. Such monitoring will contribute to sustainable groundwater resource management. Future research could focus on other factors, which might affect groundwater dynamics in the study area such as climate change.

CHAPTER ONE: INTRODUCTION

1.1 Background of the Study

Water is a vital resource for human well-being and contributes to socio-economic development and sustainability of ecosystems (Goswami & Bisht, 2017; Yildiz, 2017). Water scarcity hinders development and economic growth, spurs migration and can even spark conflict (World Bank, 2016). Countries can counteract the adverse impacts of water insufficiency by taking action in management of water resources more efficiently (World Bank, 2016). Goal No. 6 of the Sustainable Development Goals was meant to ensure access to safe and affordable water by 2030 (United Nations, 2018). This goal can be achieved through more international cooperation, safeguarding wetlands and advancing water-treatment technologies (United Nations, 2018).

Population growth and economic development goes along with increasing water demand due to changing consumption (Boretti & Rosa, 2019). Globally, water demand mostly for industry, domestic and agriculture has increased by 600% within the past one hundred years and will significantly increase over the coming two decades (Boretti & Rosa, 2019). Boretti and Rosa (2019) observes that need for all water uses will increase by 20% to 30% by the year 2050 when global population is predicted to reach 9.8 billion (United Nations, 2019). Yildiz (2017) notes that water is only reliably available if it is well managed such that economic opportunities are enhanced. On the contrary, economic growth will be slow where water availability is unreliable or of inadequate quality (Yildiz, 2017).

Worldwide, changes in land use due to natural and human causes coupled with changes in climatic conditions have indicated potential of modification of the hydrological cycle (Zomlot *et al*., 2015; Graf & Przybylek). Moreover, impacts on the hydrological cycle due to global land use and land cover (LULC) changes are estimated to surpass those of climate change (Zomlot *et al*., 2015). Therefore, quantifying the extent and magnitude of the influence of LULC changes on water resources is key in setting up sound water resources management and land-use planning in every region (Zomlot *et al*., 2015).

Africa has a population of about 1.4 billion currently, which is about 18% of the world's population (United Nations, 2019). Population of Africa is projected to double by 2050 and its share of the world population predicted to grow to 26% in 2050 and to about 40% by 2100 (United Nations, 2019). The growing African economies has increased demand for water supply so as to sustain the ever-increasing population, agriculture and industrial sectors (Mehran *et al*., 2017). Like other regions of the world, water availability is a major concern due to the combined effects of climate change, environmental modifications and anthropogenic pressure (Papa *et al*., 2022).

Environmental modifications such as groundwater stress and biodiversity loss make the populations in Africa vulnerable to hydro-climatic variability (Anderson *et al*., 2021). Yet, water storage and flux, spatial distribution and variability, remain highly unknown, preventing the development of sustainable strategies to manage water resources (Hall *et al*., 2014). A better understanding of hydrological processes in African is important for addressing these challenges to reduce uncertainty in future water availability in order to develop mitigation measures (Adenuga *et al*., 2021).

Within East Africa, it is estimated that economic growth has been 5.0% and above in the last ten years (African Development Bank, 2019). East Africa's dynamic socio-economic development, together with a growing rate of urbanization, changes in land use and climate will lead to increased water demand and stress on water quality (Tramberend *et al*., 2021). A key ambition of the East African Community Vision 2050 is achieving water security (Tramberend *et al.*, 2021).

Kenya is classified as water scarce because water demand exceeds renewable water supplies (Government of the Republic of Kenya, 2018). Per capita water availability was 647 m^3 in the year 2000, then dropped to 502 m^3 in 2012, and future projections indicate that this will further drop to 235 m^3 by the year 2025 (Government of the Republic of Kenya, 2018). The per capita water availability is well below the World Health Organization (WHO) recommended minimum of 1,000 m^3 per capita (Government of the Republic of Kenya, 2018). One of the Kenya Vision 2030 goals is access to water and sanitation by 2030.

Water availability in Kenya has been decreasing because of population growth, persistent droughts and LULC changes (Government of the Republic of Kenya, 2018). Water scarcity in Kenya is also exacerbated by climate change which has continued to occur over the last few decades and will continue into the 21st century (United Nations, 2018). Climate change, in particular, gives rise to uncertainties of adequate water supply since increase in temperature results to increased evaporation of available surface water (Kumar, 2016). Consequently, this influences rainfall and has an indirect impact on the flux and storage of groundwater (Kumar, 2016). Both LULC and climate change are major factors, which alter the hydrological cycle; both have attracted an interest for researchers in recent decades (Chen *et al*., 2019).

About 80% of Kenya is designated as arid and semi-arid land (ASAL) (Amwata *et al*., 2015). Despite the water scarcity in these areas, more and more people are migrating to the ASAL areas on account of demand for land for various uses (Government of the Republic of Kenya, 2014). Subsequently, such areas have experienced changes in land tenure and policies to an extent that former pastoral communal rangelands have been transformed into group and private holdings (Morara *et al*., 2014). These changes have in turn led to an emergence of various land use systems, including agriculture, urban development and commercial industries (Syombua, 2013; Morara *et al*., 2014). Consequently, populations in the ASAL areas have limited socio-economic opportunities for development mainly due to water scarcity (Morara *et al*., 2014).

Like other parts of the world, ASAL areas in Kenya are characterized by low rainfall amounts with erratic and unreliable timing associated with recurring droughts (Bobadoye *et al*., 2014). Rivers and streams are also seasonal and therefore, groundwater becomes the main source of water for the populace and for economic development (CIDP, 2018). Kajiado County is categorized as an ASAL area (CIDP, 2018). Migration from other parts of Kenya, more so from the neighbouring Nairobi County, has rapidly increased the population in the County over the years (CIDP, 2018). As per the 2019 census, the population of Kajiado County was 1,117,840 and is projected to reach 2 million by the year 2030 (Kenya National Bureau of Statistics & Statistics, 2019). The major sources of water in the County are water pans, springs and

boreholes with the latter being the most reliable (CIDP, 2018). About 70% of water resources in Kajiado County is groundwater. Therefore, much of the County largely depends on groundwater resources as is evidenced by increased borehole drilling in recent times (CIDP, 2018; Oiro *et al*., 2020).

Groundwater is often considered a reliable and seemingly unlimited resource (Salahat *et al*., 2014). However, it is under threat due to inappropriate use resulting to groundwater overdraft as well as degradation through pollution (Salahat *et al*., 2014). Groundwater is recharged mainly by rainfall or through interaction with surface water bodies or other aquifer systems (Rukundo & Dogan, 2019). Kumar *et al*. (2014) observes that groundwater needs to be managed holistically and should not be isolated from factors that it interacts with such as LULC. Understanding changes in groundwater systems due to both climatic and non-climatic reasons is of great importance to protect and manage groundwater systems (Zomlot *et al*., 2015). Assessment of the fundamental factors that control recharge including LULC, is of great importance to ensure sustainability (Owuor *et al*., 2016a).

1.2 Statement of the Problem

Stony Athi has experienced a general demographic shift from rural communities to urban populations mainly due to changes in sedentary lifestyles of the local inhabitants (Said *et al*., 2016). Urbanization has also been occasioned by migration from other parts of Kenya due to availability of relatively cheap land for settlement and employment opportunities (Morara *et al*., 2014, Said *et al*., 2016). Demographic pressure and urbanization has transformed the predominantly rangeland landscape into agricultural land and urban settlements (Morara *et al*., 2014). The economic activities of pastoralism and livestock herding are rapidly changing to agriculture, real estate developments and industry. The changes have the potential of affecting water quantity and quality (Graf & Przybylek, 2018).

Stony Athi sub-catchment is in Kajiado County, which is an ASAL area and experiences inadequate and unreliable rainfall and communities in the area face a lot of water challenges (Mundia & Njagi, 2018). The current water sources are mainly

seasonal rivers that provide unreliable and unhygienic water supply (CIDP, 2018). The alternative is groundwater, which is the primary source of water and accounts for more than 44% during the dry season in the County (CIDP, 2018; Mundia and Njagi, 2018).

The aquifer that underlies the Stony Athi sub-catchment is part of the Nairobi Aquifer System (NAS). Previous studies have indicated a decline in groundwater levels in the system (Tuinhof *et al*., 2011, Onyancha *et al*., 2012, Oiro *et al*., 2020). Oiro *et al*. (2020) observes that groundwater abstraction is highly correlated with population growth. Oiro *et al*. (2020) also reported that surface sealing due to urban development increased from 15 to 24% between 2000 and 2017 while forest cover reduced from 20% to 16% in the same period. Therefore, it was found necessary to evaluate how LULC changes influence the spatial-temporal groundwater recharge and its vulnerability to pollution in the Stony Athi sub-catchment.

1.3 Research Questions

This research aimed at answering the following questions:

1. What is the extent and magnitude of spatial-temporal land use and land cover changes in Stony Athi sub-catchment between 1984 and 2017?
2. How have the LULC changes that occurred between 1984 and 2017 influenced the spatial-temporal groundwater recharge?
3. Do the LULC changes have an influence on groundwater vulnerability to pollution in Stony Athi sub-catchment?

1.4 Research Objectives

The main objective was to evaluate the influence of LULC changes on groundwater recharge and pollution vulnerability between 1984 and 2017 in the Stony Athi sub-catchment, Kajiado County. The specific objectives were:

1. To quantify the extent and magnitude of spatial-temporal land use and land cover changes in Stony Athi sub-catchment between 1984 and 2017.

2. To estimate the spatial-temporal variations of groundwater recharge due to LULC changes using WetSpass-M, a GIS based distributed hydrologic model between 1984 and 2017.
3. To evaluate the influence of LULC changes on groundwater vulnerability to pollution in Stony Athi sub-catchment using a modified DRASTIC model.

1.5 Research Hypotheses

This research sought to test the following hypotheses.

1. The extent and magnitude of spatial-temporal LULC changes in the Stony Athi sub-catchment between 1984 and 2017 is significant.
2. The land use and land cover changes that have occurred between 1984 and 2017 have a significant influence on groundwater recharge.
3. Land use and land cover changes have a significant influence on groundwater vulnerability to pollution in the Stony Athi sub-catchment.

1.6 Justification and Significance

Patterns of LULC changes also reflect changes in groundwater flow dynamics and its vulnerability to pollution. According to Morara *et al*. (2014) and CIDP (2018), the study area has undergone rapid LULC changes over time. This study therefore sought to evaluate the extent and magnitude of the LULC changes and how the changes influence the spatial-temporal groundwater recharge and its vulnerability to pollution. The study was important in order to properly evaluate the available water and ensure judicious allocation, utilization and management of the groundwater resource, which is key to uplifting the socio-economic status of the study area and the country as a whole.

The findings of this research will assist planners in formulating appropriate measures of land use zoning to avert negative impacts of urbanization such as increased surface runoff, decreased recharge, potential of groundwater pollution, and attenuation of the natural vegetation. Information on the amount of rainfall that goes to groundwater recharge will assist the water authorities in the National and County Governments in management of water resources including optimization of the exploitation and

utilization of the groundwater resource. Moreover, information on vulnerability of groundwater to pollution will assist decision makers to put in place strategies of monitoring the groundwater quality to avoid detrimental effects of groundwater pollution. The study will also increase scientific knowledge for scholars doing similar studies not only in Kenya, but globally, now and in the future.

1.7 Conceptual Framework

The conceptual framework presented in Figure 1.1 was informed by the potential impacts of LULC changes on groundwater. Land development and agricultural growth are two primary areas of concern that influence groundwater recharge and its vulnerability to pollution in the following ways;

i) Creation of impervious surfaces through construction of buildings, roads, and other structures which inhibit surface infiltration capacity, thereby affecting groundwater recharge.
ii) Accelerate storm water flow, causing flooding and heightened erosion potential and water quality. Moreover, increase in storm water runoff, can transport pollutants to water bodies that people may rely on for domestic and other uses.
iii) Runoff from pesticides, fertilizers, and nutrients from animal manure can degrade groundwater quality.

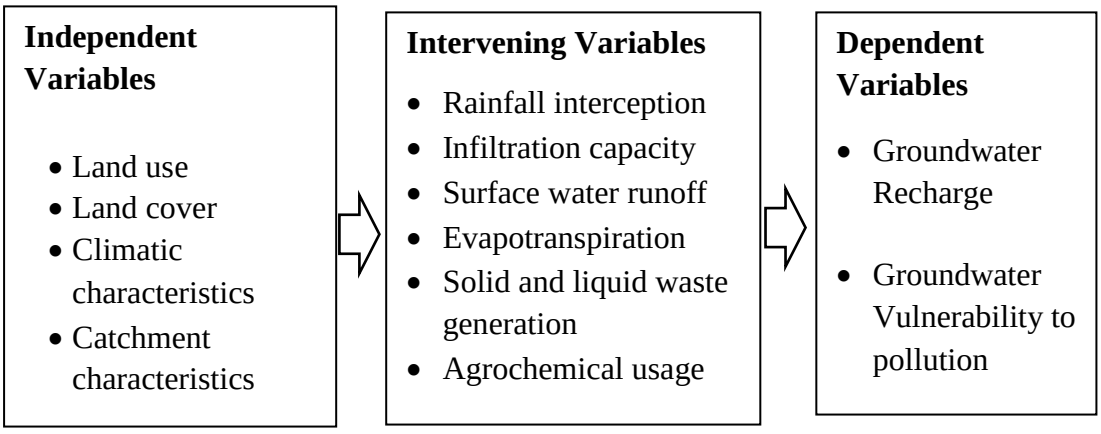

Figure 1. 1: Conceptual framework

A hydrological model, WetSpass-M, was applied for deriving the spatial-temporal relationship of the independent variables, namely, land use, land cover, climatic and physical parameters and the dependent variable comprising of groundwater recharge. On the other hand the DRASTIC model was used to evaluate the relationship between the independent variables comprisisng of land use, land cover and physical parameters and the dependent variable comprising of groundwater vulnerability to pollution. The independent variables cause changes to the intervening, which in turn causes a change in the dependent variable.

1.8 Scope and Limitations

The study focused on investigating the influence of LULC changes on groundwater recharge and pollution vulnerability between 1984 and 2017 in the Stony Athi sub-catchment, Kajiado County. The study area cover about 1,745 km^2, which is part of the headwaters of River Athi. The data used comprised of satellite images, climatic and catchment characteristics (DEM, slope. soil texture and groundwater depth. The study used descriptive modelling, where the GIS-based WetSpass-M and the Modified DRASTIC models were applied for simulation. The output data of interest was groundwater recharge and pollution vulnerability.

The major limitation was the collection of primary surface flow data for the WetSpass-M model validation since streams are highly seasonal and have no flowing water for most of the year. This was overcome by downloading stream flow discharge data from GLoFAS; a system of the European Commission for forecasting and monitoring floods across the world. The other limitation was availability of ‘clear-sky’ Landsat images captured on the same date for the years of interest. Effort was made to select images approximately ten years apart. Apart from the 1984 image, whose date of acquisition was August, the 1995 and 2005 images were captured in January while the 2017 image had an acquisition date of December.

CHAPTER TWO: LITERATURE REVIEW

2.1 Overview of Global, Regional and Local LULC Changes

Land use is the human utility of what is on the surface of the earth such as agriculture while land cover is the assemblage of the physical features on the earth's surface such as vegetation (Klemas & Pieterse, 2015). Land use changes are the human activities that modify land cover on the terrestrial surface (Klemas & Pieterse, 2015). LULC changes cannot be measured directly and so the change detection phenomenon has emerged as a tool for highlighting differences in the state of land features by observing features at different times (Parece & Campbell, 2015). The change detection phenomenon applies satellite images acquired over the years to observe LULC changes (Parece & Campbell, 2015). The technique of remote sensing in a GIS environment has been widely applied for detecting LULC changes for various purposes by several authors such as Nyamasyo and Kihima (2014), Butt *et al*. (2015), Malaki *et al*. (2017), Jiménez *et al*. (2018) Gong *et al*. *(*2018), Winkler *et al*. (2021), Potapov *et al*. (2022) among others.

From a global perspective, Klemas and Pieterse (2015) estimated that humans have modified over 50 % of the natural land cover over the years. Arneth *et al*. (2019) reported that three-quarters of the Earth's land surface has been altered by humans within the last millennium. Winkler *et al*. (2021) observes that whereas forested areas in the Global North have increased, forested areas in the developing countries of the Global South have strongly decreased. On the contrary, global cropland areas have decreased in the Global North and increased in the Global South; agricultural trade being one of the main drivers of global land use change (Winkler *et al*., 2021). Winkler *et al*. (2021) recommended that quantifying and understanding the spatial-temporal dynamics of land use change is critical in tackling global societal challenges such as food security, climate change, and biodiversity loss.

Potapov *et al*. (2022) have also documented dramatic changes in global land cover due to land use intensification through the human appropriation of natural ecosystems, and climate change during the last two decades. Potapov *et al*. (2022) reported a reduction

of global tree cover extent and expansion of cropland and settlements. (Potapov *et al*., 2022) further showed that the net forest loss was partly driven by cropland and settlement expansion. Potapov *et al*. (2022) recommended the need for sustainable development policies in regions where cropland expansion is the primary cause of natural ecosystem reduction.

Within Sub-Saharan Africa (SSA), land use changes are influenced by cultivation and population growth (Chiaka & Zhen, 2021). According to FAO (2016), there was a net loss of 7 million hectares per year in forest cover in tropical countries between 2000 and 2010 and a net gain of 6 million hectares per year in agricultural land. Large-scale commercial agriculture accounts for about 40 percent of deforestation in the tropics and sub-tropics while subsistence agriculture accounts for 33 percent (FAO, 2016). Infrastructure accounts for 10 percent while urban expansion accounts for 10 percent and for 7 percent of mining (FAO, 2016).

East Africa has also undergone rapid economic growth over the last three decades due to human development (Bullock *et al*., 2021). Bullock *et al*. (2021) reported a rapid growth in population with a 43.5% increase in the area of settlements over the last 30 years. This resulted into a 34.8%, increase in cropland area causing a large-scale reduction in woody vegetation. Bullock *et al*. (2021) noted that development of cropland continues to expand into previously intact savannah, thereby threatening ecosystems. The author recommended the need for effective land cover monitoring to address the environmental problems that may cause social impacts.

2.2 Overview of Global, Regional and Local Groundwater Resources

Groundwater is stored in and flows slowly through geological formations referred to as aquifers (Earle, 2019). Groundwater flow is one of the pathways of the global water cycle (Earle, 2019). Water from the atmosphere falls as precipitation, then infiltrates into the sub-surface, or flows on the surface as runoff, and finally gets back to the atmosphere through evapotranspiration (Edwards *et al*., 2015). Ideally, the major parameters of global water circulation are rainfall, infiltration, streamflow, groundwater flow as well as evapotranspiration (Edwards *et al*., 2015).

Groundwater is a crucial resource due to its capacity to buffer short-term climate variability, good quality and affordable abstraction (Wang *et al*., 2010). Globally, water resources amount to 1,386 million cubic kilometers, out of which 97% is salty water mainly in the oceans while only 3% is fresh water (Cassardo, 2014). About 68.9% of the fresh water is frozen while 29.9% is mainly groundwater, with only 0.3% present above ground (Cassardo, 2014). The volume of water in the upper 2 km of the lithosphere has been estimated to be 22.6 million km^3 (Gleeson *et al*., 2015). Ocean water is not directly useful for human beings, who instead rely on groundwater and the water found on the surface for use in agricultural, household, industrial, recreational and environmental activities (Cassardo, 2014; Olumuyiwa *et al*., 2017; Earle, 2019).

Groundwater forms the basis of water supplies across much of Africa and its exploitation is rising as demand for secure water increases (MacDonald *et al*., 2021). The high socio-economic and ecological importance of groundwater and its importance as a strategic resource are recognized throughout the Sub-Saharan Africa (SSA); however, data on groundwater systems are sparse and the current state of knowledge is low (Xu *et al*., 2019). Recharge rates also have not been mapped across Africa, other than from global models (MacDonald *et al*., 2021). For this reason, groundwater in SSA is so far generally under-utilized due to lack of data. Xu *et al*. (2019) recommended a very strong need for more attention to be given to SSA hydrogeology, which is mostly characterized by low-yielding, low-storage, basement aquifers.

Groundwater occurrence and distribution in Kenya is largely controlled by the geology (Kuria, 2013). The Rift Valley System is marked by the presence of intrusive rocks and volcanic flows; the coastal and northern Kenya are underlain by the sedimentary rocks while metamorphic terrains are found largely in eastern Kenya (Akech *et al*., 2013; Kuria, 2013). Groundwater systems in Kenya are closely associated with these three major rock systems. Whereas distinct aquifers are distinguished in sedimentary and volcanic areas, aquifers in areas covered by the basement rocks are largely localized (Kuria, 2013). In Kajiado County, groundwater occurs in permeable fractured zones within the basement rocks; sediments at the contact zones of the basement and volcanics as well as fractured zones within the volcanic rocks (Oiro *et al*., 2020).

2.3 Concepts of Groundwater Recharge

Recharge is infiltrated and percolated water through the soil matrix into the saturated zone (Durães & De Mello, 2013; Rukundo & Doğan, 2019). Infiltrated water flows vertically through macro-pores that are well connected and is the primary pathway of groundwater recharge (Rukundo & Doğan, 2019). Recharge plays a significant role in transporting solid and liquid contaminants to the sub-surface depending on physical and bio-chemical properties of contaminants (Talabi & Kayode, 2019).

The process of recharge is governed by the spatial and temporal patterns of various factors that include LULC, topography, climatic and soil conditions (Saghravani *et al*., 2013; Zomlot *et al*., 2015; Zarei *et al*., 2016). Among the climatic variables, the highest correlation with recharge has been found to be precipitation (Saghravani *et al*., 2013). Groundwater recharge in ASAL environments tends to occur during extreme precipitation events (Thomas *et al*., 2016). Recharge is also a function of evapotranspiration, which in turn is dependent on temperature, wind speed, solar radiation and humidity (Hughes *et al*., 2021; Dimitriadou & Nikolakopoulos, 2021). Elevation and slope gradient (topography) influence recharge and surface runoff (Mulyadi *et al*., 2020) in that steep slopes have higher surface flows, and hence the lower the recharge. Soil texture is another important factor that determines the potential of groundwater recharge as it determines the infiltration rate within the unsaturated zone before water reaches the aquifer (Guigui *et al*., 2021).

Understanding the spatial distribution of recharge and its controlling factors is a basic prerequisite for effective groundwater modeling to accurately quantify the components of the flow system (Gebremeskel & Kebede, 2017). Local and regional evaluation of groundwater recharge ought to consider the spatial and temporal variability, which improves its estimation (Salem *et al*., 2019). Recharge variability is important in ASAL regions where on a long-term analysis, evapotranspiration exceeds precipitation (Thomas *et al*., 2016). However, on a short-term analysis, high intensity of precipitation largely exceeds evapotranspiration, and therefore resulting to more water being available for recharge (Thomas *et al*., 2016).

2.4 Estimation of Groundwater Recharge

A host of methods can be used for quantification of recharge including direct measurements, Darcian approaches, water-balance methods, tracer techniques, empirical relationships and groundwater models (Abdollahi *et al*., 2018; Islam *et al*., 2016; Mohan *et al*., 2018). Selection of any one method is dependent on available data, geographical and topographical factors of an area as well as the spatial and temporal scale required (Islam *et al*., 2016; Ali & Mubarak, 2017). The detailed description of recharge estimation methods is given by several authors such as Islam *et al*. (2016), Ali and Mubarak (2017) among many others. A brief summary of each of the recharge measurement methods is described in the following sections.

2.4.1 Direct Measurement Methods

The commonly used direct recharge estimation tool is the lysimeter and is the most precise (Kohfahl *et al*., 2019). The lysimeter method determines the water quantity that flows vertically through the vadose zone to reach the water table (Kohfahl *et al*., 2019). Although lysimeter techniques are considered to be best applicable in humid conditions, they can also be employed in dry climates. The main disadvantage with the lysimeter method is that it is expensive for regional studies since it is a point measurement and cannot be upscaled to a catchment scale.

2.4.2 Darcian Approach

According to Dassargues (2018), Darcy's law describes the rate of flow of water defined by the relationship shown in Equation 2.1.

$$Q/t = KAdh / L \quad \text{.....(2.1)}$$

Where,

Q/t = flow rate

K = permeability coefficient

A = cross-sectional area;

dh = difference in elevation

L = length of flow.

The main limitation of the Darcy method is that it is valid only when flow is laminar and not turbulent (Dassargues, 2018). The Darcy method is usually applied for determining permeability of earth materials in the laboratory.

2.4.3 Water Balance Methods

Water balance methods are based on the water balance equation shown in Equation 2.2 (Saghravani *et al*., 2014; Islam *et al*., 2016) and can be stated as:

$$P + Qin = ET + Qout + \Delta S \quad \text{.....(2.2)}$$

Where,

P = precipitation

Qin and Qout = water flow into and out of the catchment

ET = evapotranspiration, and

ΔS = change in storage

The common water balance methods used include:

i) Surface water budget where upstream and downstream flows are differenced to determine transmission losses, mainly due to recharge;
ii) Soil moisture budget where rainfall is treated as the input while evapotranspiration and recharge are the outputs in a soil moisture accounting.
iii) Water table fluctuations in which difference in well water levels is equated to recharge.

2.4.4 Tracer Techniques

Tracer techniques use artificial or environmental tracers comprised of chemicals and isotopes, respectively (Scanlon *et al*., 2002). Measurable artificial tracers are applied in the soil zone such that the tracer moves with the water after which they are detected and measured in groundwater (Scanlon *et al*., 2002). The major disadvantage with artificial tracers is the long duration between tracer application and its detection because of the slow flow of groundwater (Saghravani *et al*., 2014). Environmental tracers such as chloride and tritium exist in nature and the overall mass balance of the isotope is measured to trace the groundwater flow paths (Saghravani *et al*., 2014).

2.4.5 Empirical Methods

Empirical relationships have been developed for computation of natural recharge based on studies undertaken on correlation of ground water level fluctuation and rainfall amount (Saghravani *et al*., 2013). In several instances, based on point recharge estimates, rainfall-recharge relationship is worked out to calculate recharge from rainfall events (Saghravani *et al*., 2013).

2.4.6 Groundwater Flow Models

Abdollahi *et al*. (2018) defines a model as a tool, which is an artful combination of observations and knowledge for describing the behaviour of a system. Ground water flow models are mathematical simulations of water flow through an aquifer (Abdollahi *et al*., 2018). Application of physically distributed modelling techniques has significantly increased in recent years, driven by technological advances in GIS (Batelaan & De Smedt, 2001; Abdollahi *et al*., 2018). Modelling techniques are useful tools for assessing the spatial distribution of groundwater recharge brought about by heterogeneity of the various controlling factors as well as temporal changes due to changes in LULC and climatic conditions (Abdollahi *et al*., 2018).

2.4.7 Choice of Method

Several factors must be considered in selecting an appropriate recharge quantification method (Scanlon *et al*., 2002). This Author grouped appropriate techniques on a basis of hydrological environments and climatic conditions as shown in Table 2.1. Choice of an appropriate technique depends on the study goal, but important considerations include space and time scales as well as reliability (Scanlon *et al*., 2002). Approaches for surface water as well as the saturated zone environments provide regional estimates of recharge while unsaturated zone techniques provide point or small-scale estimates (Scanlon *et al*., 2002). Numerical modelling such as the spatially distributed WetSpass-M model can be applied in all the hydrological zones and in different climatic conditions.

The main advantage of spatially distributed models is that they integrate GIS and the hydrological processes. Models also account for spatial variation of recharge due to soil

type, land-use, topography, water level as well as climate (Batelaan and De Smedt, 2001; Abdollahi *et al*., 2018). The models are especially useful in assessment of long-term impacts of LULC changes on the water flow in a catchment (Abdollahi *et al*., 2018).

Table 2. 1: Appropriate techniques for estimating recharge

Hydrological environment	**Technique**	
	Arid and Semi-arid climates	*Humid climates*
Surface water	• Channel water budget • Lysimeter • Temperature tracers • Isotopic tracers • Watershed modelling	• Channel water budget • Lysimeter • Base flow discharge • Isotopic tracers • Watershed modelling
Vadose zone	• Lysimeters • Numerical modelling • Darcy's law • Tracers (historical, environmental)	• Lysimeters • Numerical modelling • Darcy's law • Tracers (applied)
Saturated zone	• Tracers • Numerical modelling	• Water-table fluctuations • Darcy's law • Tracers • Numerical modelling

2.5 The WetSpass-M Model

The Water and Energy Transfer between Soil, Plants, and Atmosphere under quasi-Steady State (WetSpass) is a GIS based model with the ability to simulate spatially distributed groundwater recharge (Abdollahi *et al*., 2018). WetSpass-M is a downscaled model from a seasonal to a monthly scale (Abdollahi *et al*., 2018). WetSpass-M and its precursor version WetSpass, have been proven to help better characterize the water balance and is applicable in a variety of geographical areas with different environments (Batelaan and De Smedt, 2001; Armanuos *et al*., 2016; Graf & Przybyłek, 2018; Abdollahi *et al*., 2018; Salem *et al*., 2019). The model is a distributed one, which treats

a catchment as a regular pattern of grid cells, which are sub-divided into fractions of vegetated, bare soil, open water, or impervious ground (Figure 2.1).

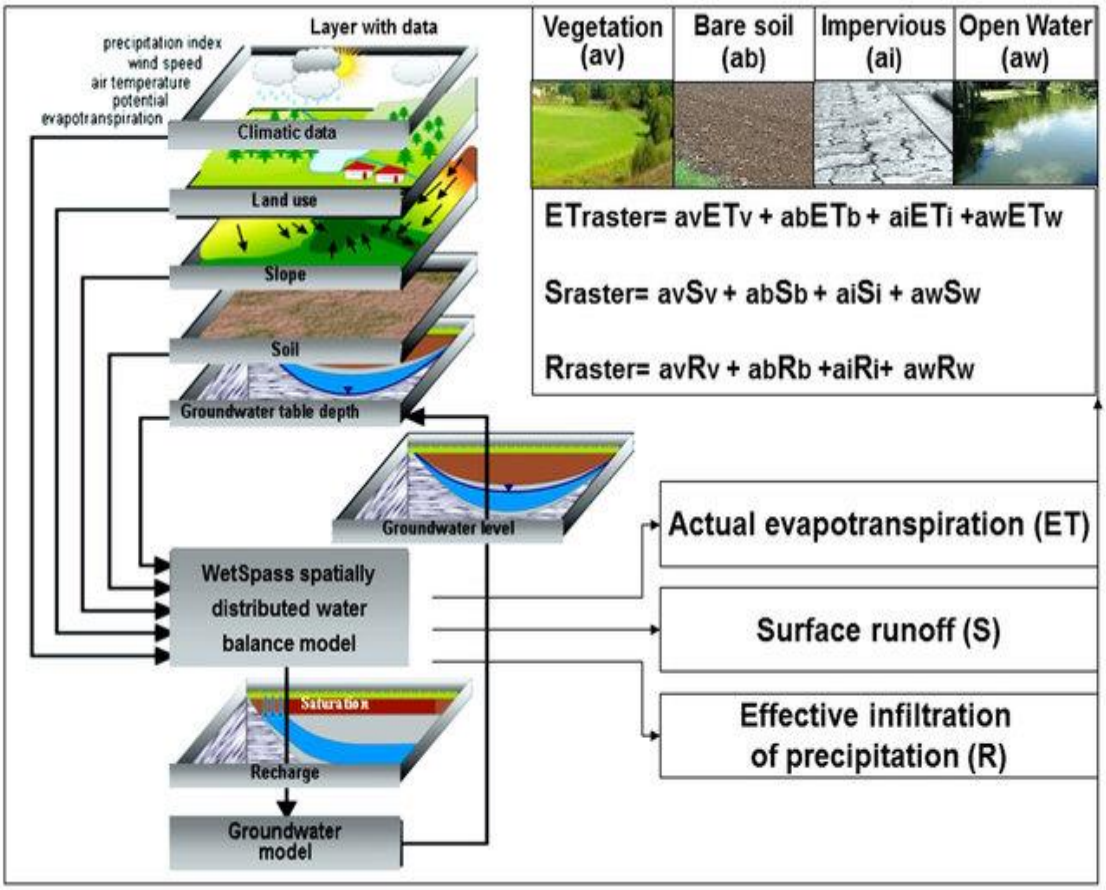

Figure 2. 1: Diagram of the WetSpass model (source: Graf & Przybyłek, 2018)

The water balance is simulated for each grid cell based on Equation 2.3.

$$P = I + SR + ET + GWR \quad \text{.....(2.3)}$$

Where;

P = precipitation

I = interception

SR = surface runoff

ET = actual evapotranspiration

GWR = groundwater recharge

Each cell has an independent water balance equation expressed by Equations 2.4 – 2.7.

$$P = Iv + SRv + ATv + GWRv \text{ for vegetated area (v)} \quad (2.4)$$

$$P = SRs + AEs + GWRs \text{ for bare soil (s)} \quad (2.5)$$

$$P = SRo + AEo + GWRo \text{ for open water (o)} \quad (2.6)$$

$$P = SRi + AEi + GWRi \text{ for impervious surface (i)} \quad (2.7)$$

The water balance components of each cell for a given time period are given in Equations 2.8 – 2.10.

$$ETraster = avETv + asETs + aoETo + aiETi \quad (2.8)$$

$$SRraster = avSRv + asSRs + aoSRo + aiSRi \quad (2.9)$$

$$GWRraster = avGWRv + asGWRs + aoGWRo + aiGWRi \quad (2.10)$$

Where; ET_{raster}, SR_{raster} and GWR_{raster} represent actual evapotranspiration, runoff, and recharge, respectively. Subscripts denote the respective cell sub-division, namely vegetation (v), bare soil (s), open water (o) and impervious ground (i) while a_v, a_s, a_o, and a_i are the fractions of each land cover in a cell. The fractions account for non-uniformity of the type of land cover in each cell.

The water balance in every grid cell is added up to give the total water balance. The initial point for simulation of the water balance in each cell is precipitation while the other processes follow in an orderly manner. Recharge is simulated as a residual component. The model calculates spatially distributed water balance as a variable that depend on LULC, catchment characteristics and climatic variables (Abdollahi *et al*., 2017). WetSpass has been widely used for various hydrological studies by different authors. Al-Kuisi and El-Naqa (2013) used the model to estimate recharge in Jordan while Albhaisi *et al*. (2013) applied it to predict impact of land use changes on recharge in upper Berg catchment, South Africa; Aish (2014) used the model to estimate the water balance components in the Gaza Strip, Palestine while Zarei *et al*. (2016) applied WetSpass-M to evaluate the water balance in the Mashhad basin, Iran; Gebreyohannes *et al*. (2013), Gebremeskel and Kebede (2017) and Meresa *et al*. (2019) used WetSpass to assess the water balance in Illala catchment, Geba basin, Werii and Birki watersheds

in Ethiopia, respectively; Graf and Przybyłek (2018) used the same method to identify factors controlling recharge in Poland. There is no study in Kenya that has documented the application of the WetSpass model.

2.6 Groundwater Pollution Vulnerability

Groundwater vulnerability is the tendency or likelihood of contaminants to reach the groundwater system after introduction at the surface (Machiwal *et al*., 2018). Groundwater is vulnerable to pollution from human activities. Assessment of vulnerability has become an important element for land use planning and groundwater resource management (Ewusi *et al*., 2016; Ghazavi & Ebrahimi, 2015; Oroji, 2018). Different techniques and methodologies have been developed to estimate groundwater vulnerability (Gupta, 2014; Maria, 2018: Rendilicha *et al*., 2018). A brief description of three methods is given in the following section.

2.6.1 Process-based Simulation Models

Process-based models are based on analytical or numerical solutions representing coupled processes that govern pollutant transport. The methods are used to predict the duration a contaminant takes to reach a given depth by mathematically modeling the processes that influence the contaminant fate from known sources in a localized area and provide site-specific information. Process-based models such as PRZM (Padilla *et al*., 2017), GLEAMS and LEACHM (Asada *et al*., 2017) predict spatial and temporal variations of water quality. Barbash and Voss (2016) constructed a process-based vulnerability assessment (P-GWAVA) system using transport-and-fate simulations to predict the concentration of any surface-derived compound at a specified depth.

2.6.2 Statistical Methods

Statistical or empirical methods are based on probability theory and are the least used vulnerability assessment methods (Zhang *et al*., 2020). Statistical methods assess specific vulnerability and require extensive site-specific monitored regional database to predict the occurrence or non-occurrence of a contaminant in the area of interest (Zhang *et al*., 2020).

2.6.3 Overlay and Index Methods

Overlay and index methods are GIS-based qualitative methods based on subjective rating of hydrogeological parameters. The methods combine maps of various physiographic attributes such as geology, water depth, soil texture and aquifer properties by assigning a weighted value to the attributes. The weights are then rated to generate a composite vulnerability rating. Overlay and index procedures constitute the most popular class of methods used in vulnerability assessment. Though they are subjective in nature, the application of these methods are useful tools for decision-making towards sustainable management of water resources. Olumuyiwa *et al*., (2017) applied AVI and GOD approaches to assess vulnerability of a water bearing formation in Southwestern Nigeria. Oroji (2019) applied various methods, namely, DRASTIC, SINTACS, SI and GOD in the Hamadan – Bahar Plain, Iran, and the results indicated that the DRASTIC model is better than other models. Ghazavi and Ebrahimi (2015) used the DRASTIC and GOD models in Iran, and the results also indicated that the DRASTIC is better than GOD. According to Maria (2018), DRASTIC has good accuracy compared to the others.

2.7 The DRASTIC Model

DRASTIC is the most commonly used modelling technique among the overlay and index methods (Al-Abadi *et al*., 2017, Abdulrafiu *et al*., 2017 and Duarte *et al*., 2019). The model (Figure 2.2) was developed by EPA-US to classify the pollution potential of aquifers at a regional scale (Aller *et al*., 1987). It is used to assess aquifer sensitivity by combining data sets based on several parameters with different weighting factors that describe the characteristics that control contaminant transport (Aller *et al*., 1987). The resulting index is a relative measure of intrinsic vulnerability to pollution; areas with a higher index are more vulnerable than those with a lower index. According to Aller *et al*. (1987), the DRASTIC method has the following assumptions:

i) The pollutant is sourced at the earth's surface;
ii) The pollutant is carried to the aquifer by rain water;
iii) The pollutant has the mobility of water;
iv) The size of the area under evaluation is larger than 0.4 sq. km.

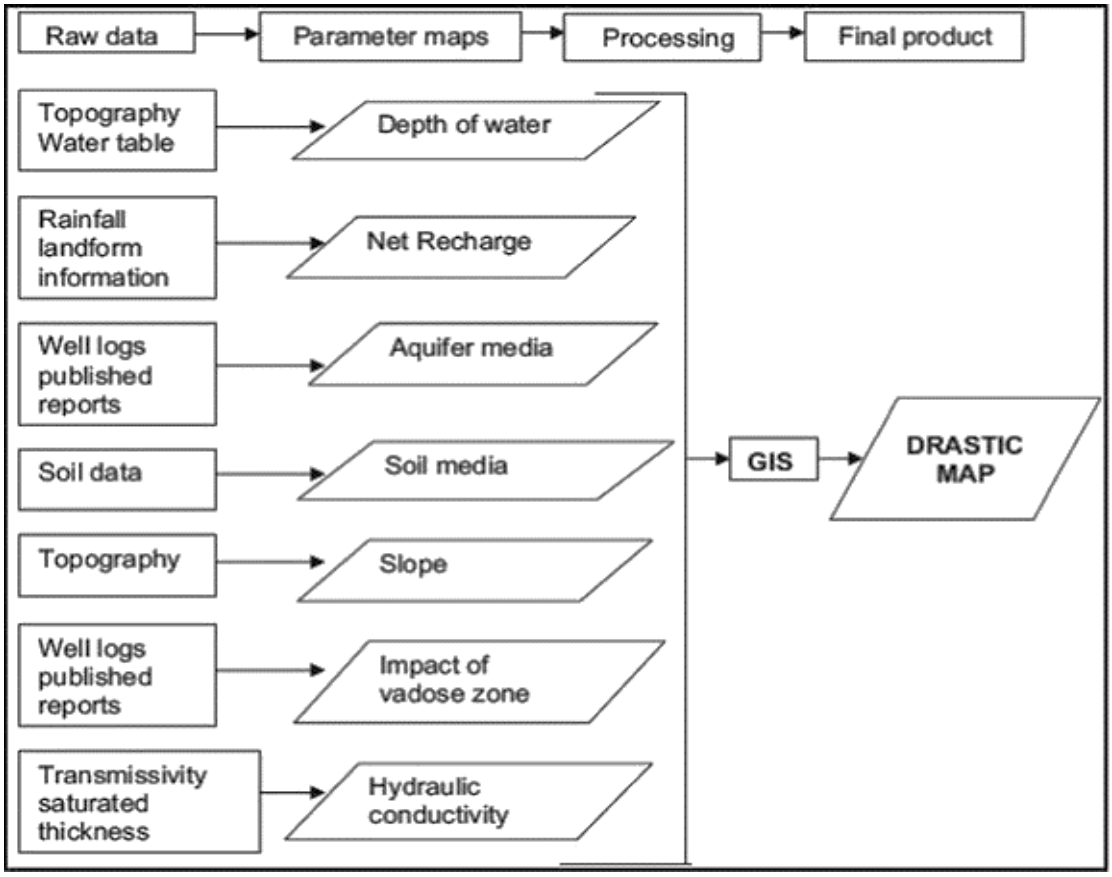

Figure 2. 2: Diagram of the DRASTIC model (source: El Mansouri *et al*., 2013)

Ratings and weights are used for each of the seven parameters to balance their importance on a scale of 1 to 10 and 1 to 5 respectively. The resulting vulnerability index (DI) is the sum of the parameters calculated using Equation 2.11:

$$DI = DrDw + RrRw + ArAw + SrSw + TrTw + IrIw + CrCw \ldots\ldots\ldots\ldots (2.11)$$

Where; subscripts r = rating and w = weight for each parameter comprising of water depth, recharge, aquifer type, soil type, topography (slope), impact of the vadose zone and hydraulic conductivity.

2.8 Linkages between LULC Changes and Groundwater

LULC changes have been indicated as one of the main human-induced factors that influence water systems (Salahat *et al*., 2014). It has been acknowledged the world over that while LULC is changing rapidly, the impact on groundwater is becoming more and

more significant (Salahat *et al*., 2014). This is especially the case in places that rely heavily on groundwater to meet their needs. Abstraction of groundwater changes the natural water distribution and affects ecosystems as well as groundwater levels (Pulido-Velazquez *et al*., 2015). Irrigation waters that return to either groundwater or surface waters may deteriorate the water quality. In areas where water availability is a problem, land use changes potentially increase water scarcity and pollution and may contribute to poor living conditions (Pulido-Velazquez *et al*., 2015).

Many researchers have observed that LULC changes due to population pressure, agricultural expansion and urbanization among others have an impact on water resources in one way or another (Salahat *et al*., 2014; Pulido-Velazquez *et al*., 2015). It is extremely important that land use is properly regulated so that groundwater resources are not adversely affected.

2.9 Summary and Knowledge Gaps

This chapter reviewed the background knowledge in understanding the global, regional and local LULC changes and groundwater conditions. The chapter also outlined developments in groundwater recharge estimation techniques and the various methods of investigating the intrinsic groundwater pollution in the context of this study's objectives. The section highlighted the importance of understanding the relationship between LULC changes and groundwater systems. The key motivations and knowledge gaps that led to the formulation of this study's objectives were as follows:

1. The extent and magnitude of spatial-temporal LULC changes in Stony Athi sub-catchment have not been quantified. This gap led to the first research question; what is the extent and magnitude of spatial-temporal LULC changes in Stony Athi sub-catchment between 1984 and 2017?

2. Much uncertainty exists on the quantitative impact of LULC changes on groundwater recharge in Stony Athi sub-catchment. This gap led to the second research question; how have the land use and land cover changes that have occurred between 1984 and 2017 influenced groundwater recharge?

3. The potential impacts of LULC changes on the groundwater quality in Stony Athi sub-catchment have not been studied. Moreover, as a result of increased urbanization and large scale agricultural activities, aquifers are vulnerable to pollution. This gap was addressed by answering the third research question; Does the land use and land cover changes have an influence on groundwater vulnerability to pollution in the study area?

CHAPTER THREE: METHODOLOGY

3.1 The Study Area

3.1.1 Location

Stony Athi sub-catchment is bounded by latitudes 1°28' S and 1°50' S and longitudes 36°40' E and 37°15' E covering an area of about 1,745 km^2 (Figure 3.1). The sub-catchment spreads across three counties, namely, Kajiado County (77%), Machakos County (21%) and Makueni County (2%).

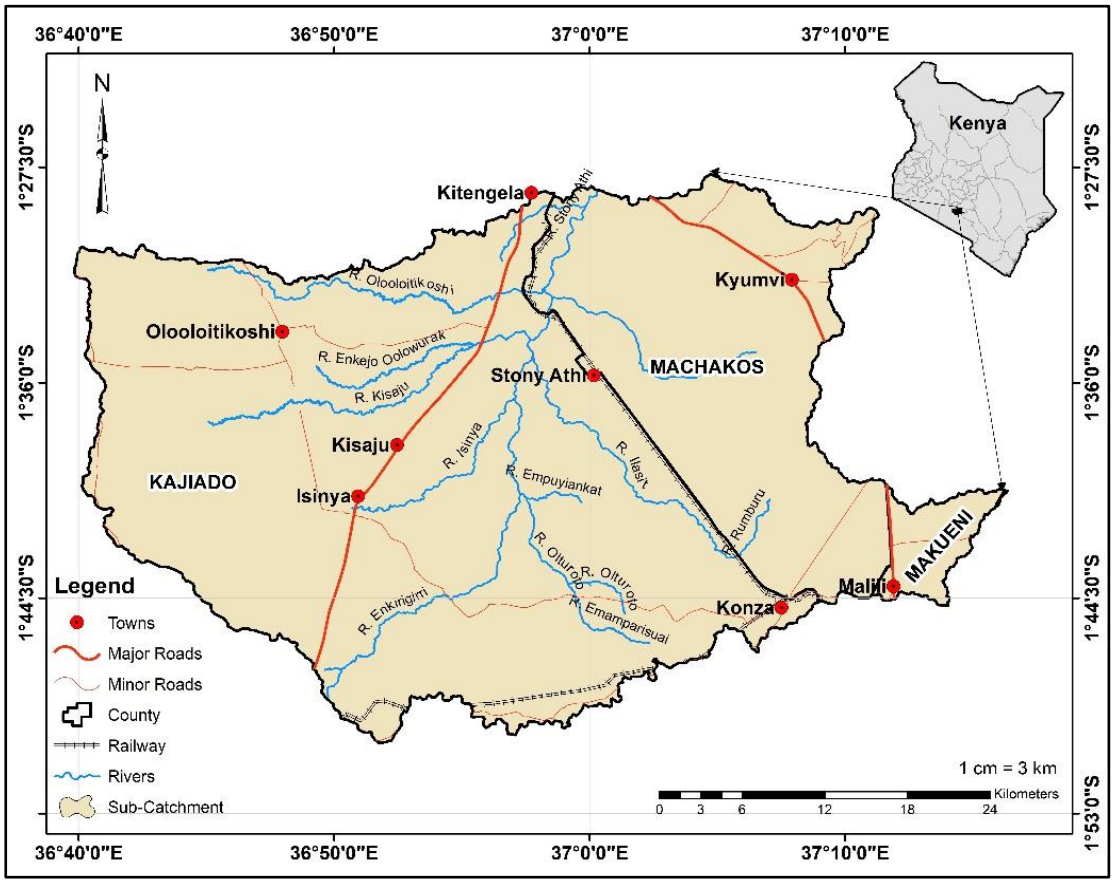

Figure 3. 1: Map of Stony Athi sub-catchment (source: present study)

3.1.2 Topography and Drainage

Stony Athi sub-catchment lies in the semi-arid Athi-Kapiti plains which gently slopes from west to east. Relief ranges from 1493 m to 2,082 m with a mean of 1787 m above sea level. The area is divided into three physiographic sub-divisions which are reflected by the dominant rock type, namely: the higher ground in the west and north-west; the

low lying eastern and south-eastern areas and the gentle undulating central and south-western area. The sub-catchment is fed by drainage from Ngong Hills and from the extensive Athi-Kapiti plains through seasonal rivers and streams which flow in a dendritic pattern to form the Stony Athi River Stony Athi River flows northwards to join the Athi River and contributes about 134 million m^3 of water annually to Athi River (Kitheka, 2019).

The sub-catchment is part of the head-waters of the Athi River drainage basin, which is the second largest drainage system in Kenya. The major drainage channels are broad and shallow while many of the smaller tributaries are ill-defined. There are significant wet season flows, but minimal or no flow occurs during the dry seasons. The main source of recharge within the sub-catchment is local precipitation and groundwater flow from the Ngong hills while the major groundwater discharge is abstraction through boreholes.

3.1.3 Climate

The study area has a semi-arid and arid climate. It lies in agro-climatic zones III to VI with IV and V being pre-dominant. Rainfall is bimodal with mean annual rainfall ranging between 300 to 800 mm (Morara *et al*., 2014, Amwata *et al*., 2015), but it is unevenly distributed. The eastern side of the area receives more rainfall during the short rainy season while in the western part, more of the rain falls during the long rains. Amwata *et al*., (2015) reported that most areas of Kajiado County receive 50% of the annual rainfall for the March to May period and 30 % for the October to December period. Bobadoye *et al*. (2014) gave 51.01 mm as the average rainfall at Isinya meteorological station, which is centrally located within Stony Athi sub-catchment. Temperatures range between 13° C and 25° C.

3.1.4 Geology and Hydro-geology

The Stony Athi sub-catchment consists of geological formations ranging from Archean to Tertiary age (Matheson, 1966; Guth & Wood, 2013). The study area can be divided into three geological groups namely; the Precambrian Mozambican system group, also referred to as the Basement System; the Tertiary volcanic rocks, mostly composed of

phonolites and tuffs and the Tertiary sediments composed of agglomerates and soft tuffs (Matheson, 1966). The oldest rocks are the quartzo-feldsphathic gneisses, which occur in the south-west and south-east as well as granitoid and augen gneisses which outcrop in sections of the north eastern parts. Tertiary volcanics are represented by phonolites and tuffs which cover the western, northern, southern and central regions (Matheson, 1966; Guth & Wood, 2013). Tertiary agglomerates are found in the north-east and parts of the western sections overlying the phonolites (Guth & Wood, 2013). The tuffs overlie the phonolites which in turn un-conformably overlie the Basement System rocks. The geological map of the sub-catchment is presented in Figure 3.2.

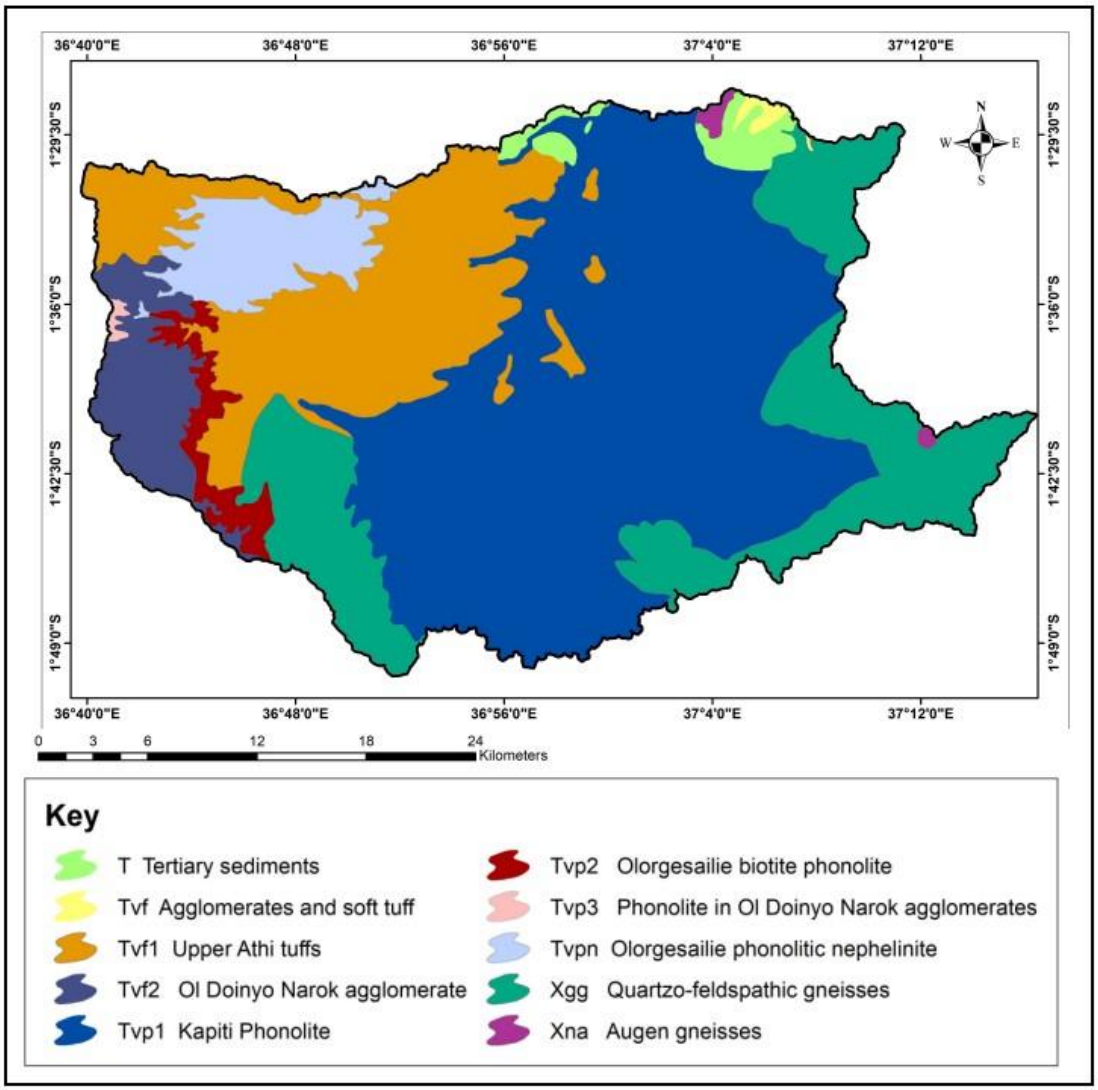

Figure 3. 2: Geological map of the study area

Hydro-geology is dependent on the nature of the underlying rocks and soils, structural features, weathering extent and the amount and frequency of precipitation. Groundwater sources in the study area are from permeable fractured zones within the basement rocks; sediments at the contact zones of the basement and volcanics as well as fractured zones within the volcanics. The hydraulic conductivities of crystalline rocks generally range between 10^{-7} and 10^{-4} m/day (Dassargues, 2018). Ozerskiy (2017) reports that the hydraulic conductivity of Archean rocks range between 0.0001 m/day and 0.001 m/day, with an average of 0.004 m/day while Owuor *et al.* (2016b) reports that the hydraulic conductivity of volcanic rocks of the Nairobi area have a range of between 0.011 and 3.84 m/day. Earle (2019) gives a range of hydraulic conductivity for fractured volcanic rocks as 10^{-2} to 10^{2} m/day and 10^{-4} to 10^{1} m/day for fractured metamorphic rocks while for unconsolidated material, the range is almost similar to fractured volcanic rocks.

3.1.5 Socio-economic Activities

Traditionally, the area is inhabited by the Maasai community, whose main economic occupation is semi-nomadic pastoralism. Over 75% of the population's livelihood is derived from livestock and livestock products (CIDP, 2018). A study done in the pastoral peri-urban area of Kajiado North indicated that land use over the years has been affected by migration by people from other areas of the country, especially the neighbouring Nairobi County (Morara *et al*., 2014).

The ensuing effect of migration has seen an increased land use changes from rangelands to urban settlements, agricultural and commercial use. Morara *et al.* (2014) classifies the major LULC into seven classes, namely rangeland, bare ground, water body, rocky area, built-up areas, crop-land, riverine vegetation and woodlots. About 76% of the sub-catchment is open grassland with acacia shrubs, mainly used as livestock ranches. The ranches within the sub-catchment are presently being sub-divided for residential and commercial use. There is also increased establishment of horticultural farms within the area which use agricultural pesticides and fertilizers, which have the potential to contaminate groundwater.

3.2 Research Design

This study applied a descriptive modelling approach. Primary and secondary data was acquired, processed, modelled and analysed to detect the long term LULC changes and their impact on recharge and pollution vulnerability of groundwater. Primary data was acquired through field observations and measurements while secondary data was obtained from literature and existing archive records in Government Departments. Fig. 3.3 shows the schematic representation of the approach used in this study.

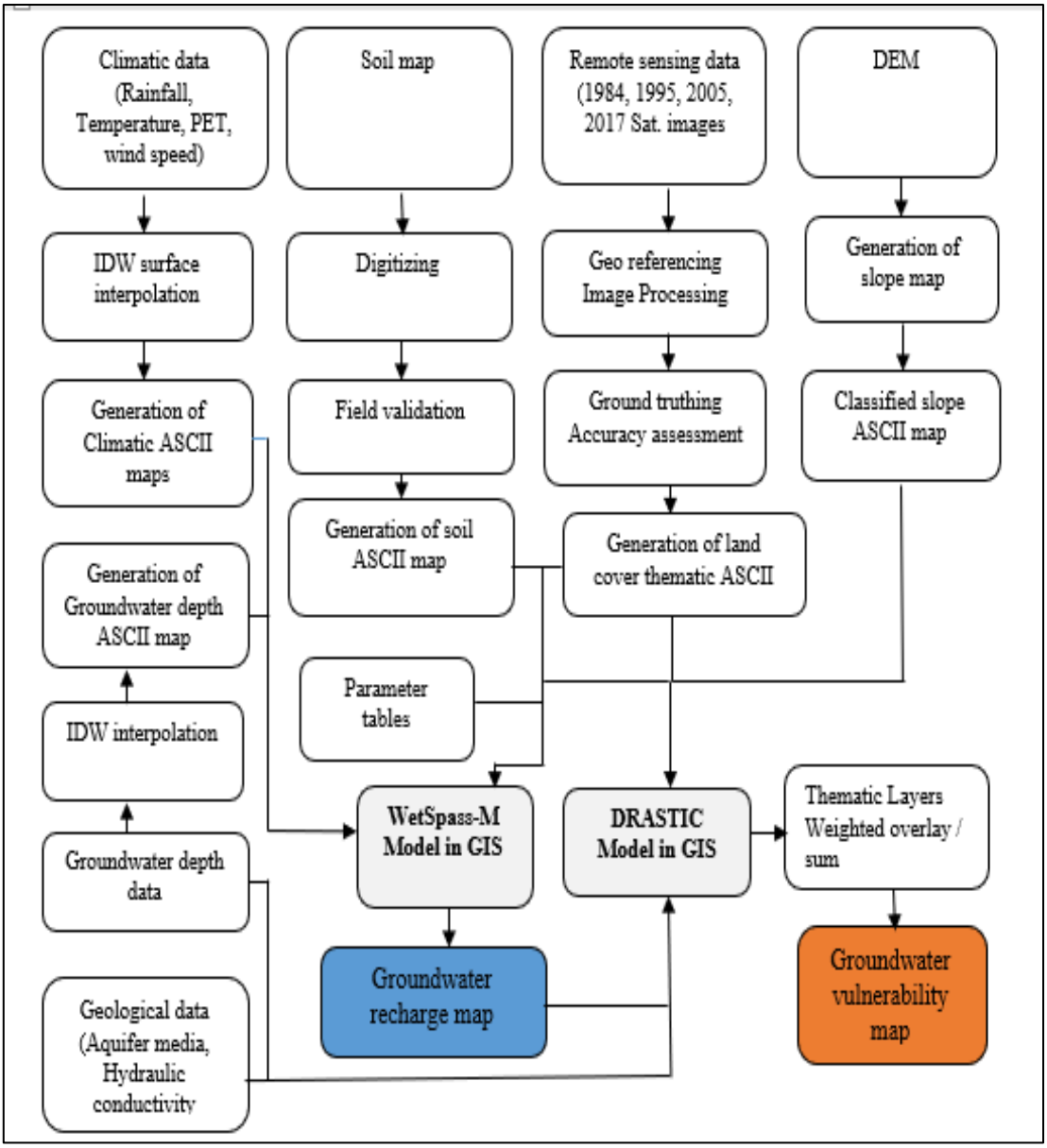

Figure 3. 3: Modeling framework used in this study

The data was manipulated using Microsoft Excel and imported into ArcMap 10.8 and used to prepare grid maps, which were used as input parameters for modelling in form of ASCII files. The modelling tool selected was the WetSpass-M model for spatial-temporal groundwater recharge (Batelaan & De Smedt, 2001; Rwanga & Ndambuki, 2017). Groundwater vulnerability to pollution due to LULC changes was analyzed using the Modified DRASTIC model (Aller *et al*., 1987; Maqsoom *et al*., 2020). The methodological steps undertaken were as follows:

1. Preparation of LULC grid maps for four temporal periods;
2. Preparation of climatic grid maps consisting of rainfall, temperature, potential evapotranspiration and wind speed;
3. Preparation of grid maps of catchment physical characteristics consisting of soil texture, elevation, slope and groundwater depth;
4. Preparation of DRASTIC grid maps.
5. Running the WetSpass and DRASTIC models and validation

3.3 Quantification of Spatial-temporal LULC Changes

The first specific objective was to quantify the extent and magnitude of the spatial-temporal LULC changes in Stony Athi sub-catchment between 1984 and 2017. This objective was achieved by classifying four satellite images (1984, 1995, 2005 and 2017) through supervised classification, followed by post-classification change detection in a GIS platform.

3.3.1 Landsat Image Acquisition

Remote sensing data was derived from temporally varied Landsat images downloaded from the USGS website (https://earthexplorer.usgs.gov/). Images selected included Landsat-5 Thematic Mapper for 1984 and 1985, Landsat-7 Enhanced Thematic Mapper for 2005 and Landsat-8 Operational Land Imager (OLI) and Thermal Infrared Sensor (TIRS) for 2017. Landsat-5 is a false color composite consisting of seven spectral bands, namely blue, green, red, near infrared, short-wave infrared, thermal infrared and mid-infrared bands (bands 1,2,3,4,5,6,7). Bands 1 to 5 and 7 have a spatial resolution of 30 meters while the spatial resolution for Band 6 (thermal infrared) is 120

meters. Landsat-7 has an additional panchromatic band (band 8) with a resolution of 15 meters. Landsat-8 images consist of nine spectral bands with a spatial resolution of 30 meters for Bands 1 to 7 and 9. Band 1 (ultra-blue) is useful for coastal and aerosol studies while band 9 is useful for cirrus cloud detection.

The present study used bands 1,2,3,4,5 and 7, all having a 30-meter pixel resolution, considered appropriate for catchment analysis. The study area is contained within the Landsat path 168, row 61 (Table 3.1). The images were selected based on availability and approximately ten years apart. Ancillary data in form of ground reference points was collected in a field survey using a hand held Global Positioning System (GPS).

Table 3. 1: Landsat multi-spectral images

Date of acquisition	Satellite Sensor	Path /Row	Bands	Spatial Resolution
27/08/1984	Landsat 5 Thematic Mapper ™	168/61	Blue, Green, Red, Near IR, Mid IR	30 m
30/01/1995	Landsat 5 Thematic Mapper ™	168/61	Blue, Green, Red, Near IR, Mid IR	30 m
01/01/2005	Landsat 7 Enhanced Thematic Mapper (ETM+)	168/61	Blue, Green, Red, Near IR, Mid IR	30 m
28/12/2017	Landsat 8 OLI/TIRS	168/61	Blue, Green, Red, Near IR, SW IR 2	30 m

OLS-TIRS - operational land imager and thematic infrared sensor, TM - thematic mapper; ETM+ - enhanced thematic mapper plus

3.3.2 Image Pre-processing and Classification

The acquired images were imported into ArchMap 10.8 for processing. The standard image pre-processing techniques of extraction, layer stacking, geo-referencing, enhancement and sub-setting were performed as described by Young *et al*. (2017). Each image was geo-referenced to the WGS-84 datum coordinate system. A supervised maximum likelihood approach in ArchMap 10.8 was employed for image spectral classification (Young *et al*., 2017).

The data was analysed by assigning signatures to the pixels and differentiating the sub-catchment into classes of the different landscape elements. For each of the pre-determined LULC class, training sites were selected by demarcating a polygon of representative sites using the signature editor in ArchMap 10.8. The maximum likelihood algorithm described by Young *et al*., (2017) was used for classification. The flow chart for LULC change detection is shown in Figure 3.4.

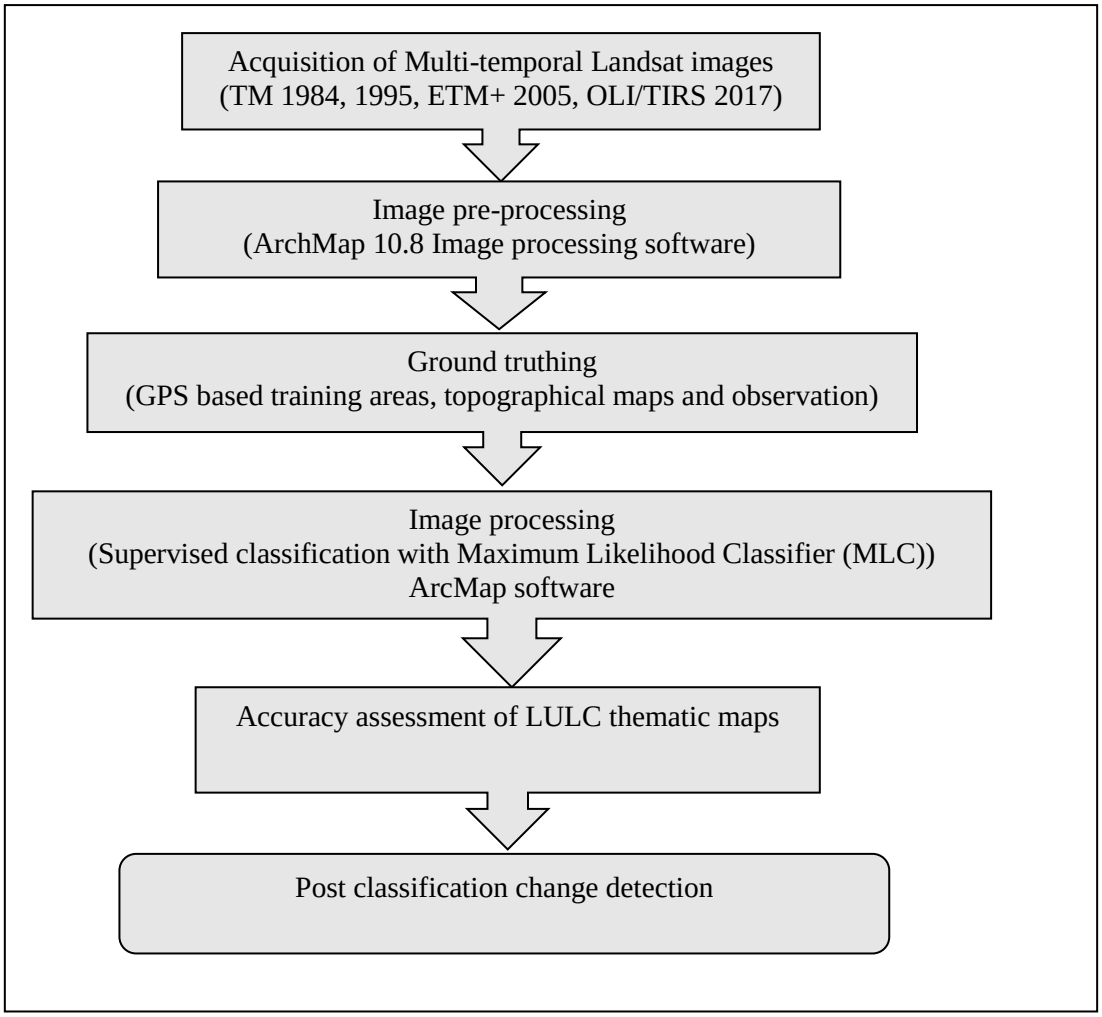

Figure 3. 4: Flow chart of post classification LULC change detection

3.3.3 Accuracy Assessment

The main goal for accuracy assessment was to obtain classified maps with minimum error of accuracy. Classification accuracy for each image was assessed using an error matrix from which the user's and producer's accuracies for each LULC class, overall accuracy and kappa index of agreement were computed according to the procedures

described by Congalton and Green (2019). The kappa index determines the agreement between maximum likelihood classification and the ground truth. The index was determined by the formula shown in Equation 3.1.

$$k = N \sum_{n=1}^{n} mi,i - \sum_{n=1}^{n}(GiCi) / N^2 - \sum_{n=1}^{n}(GiCi) \quad \text{.....(3.1)}$$

Where,

i = class number,

N = total number of classified values compared to the ground truth values,

mi,i = number of values, which belong to ground truth class *i*, that have also been assigned to class *i* (that is, values found along the diagonal of the confusion matrix)

Ci = total number of predicted values, which belong to class *i*,

Gi = total number of ground truth values, which belong to class *i*.

A kappa value of one (1) indicates perfect agreement, whereas a value of zero (0) signifies no agreement. Ancillary data in form of ground reference points collected during the field survey was incorporated and used for the overall accuracy assessment. The overall accuracy was calculated by summing the number of correctly classified values and dividing by the total number of land feature classes. The correctly classified values form the diagonal of the confusion matrix. According to Congalton and Green (2019), accuracy assessment requires that the overall accuracy to be above 90% and kappa statistics above 0.9. These conditions were successfully achieved in this study. According to USGS, a kappa coefficient of 85% is the minimum requirement for land use classification from Landsat data (Varamesh *et al*., 2017).

3.3.4 Change Detection

Change detection was done by a comparison of the classified images with field observed reference data that closely reflects the true land cover accurately. The 2017 image was used as the reference image for which the ground truth data likely equates. The post-classification change detection approach was used. This approach allowed the determination of the difference between independently classified images from each of the four temporal dates.

3.4 Estimation of Groundwater Recharge

The second specific objective was to estimate recharge using a GIS-based distributed hydrologic model (WetSpass-M). Several steps were undertaken for preparation of input data for the model to run, which included:

(i) Climatic data acquisistion (including precipitation, temperature, evapotranspiration and wind speed)
(ii) Climatic grid maps preparation
(iii) Acquisition of sub-catchment physical characteristics data (topography, slope, soil and groundwater depth)
(iv) Preparation of grid maps of the sub-catchment physical characteristics

3.4.1 Climatic Data Acquisition

Climatic data comprised of precipitation, temperature, pan evaporation and wind speed. The data was acquired from KMD for four different stations located within and surrounding the sub-catchment. The four stations were JKIA (Nairobi County) located at 1°19' S, 36°55' E, Maasai rural training centre (Kajiado County) located at 1°40' S, 36°50' E, Machakos station located at 1°35' S, 37°14' E and Kajiado DC's Office station located at 1°50' S, 36°50' E. JKIA and Machakos stations had complete data while Kajiado Maasai Rural Training Centre rainfall station and Kajiado DC's Office station had only monthly rainfall data for some years as shown on Table 3.2.

Rainfall Data

Annual and monthly rainfall records spanning from 1984 to 2017 for four stations were obtained from KMD records while additional monthly data for five other stations was downloaded from the Climate Data for Cities Worldwide website (https://en.climate-data.org).

Temperature Data

Temperature records spanning from 1984 to 2017 for two stations were obtained from KMD records while data for the other stations were downloaded from the Climate Data for Cities Worldwide website (https://en.climate-data.org). Values of monthly mean temperature were used to derive the mean annual temperature.

Table 3. 2: Sources of climatic data

Station	Parameter	Period	Sources
JKIA	Precipitation	1980 – 2017	KMD & en.climate-data.org
	Temperature	1980 – 2016	KMD & en.climate-data.org
	Wind speed	2009 – 2013	KMD
Isinya	Precipitation	1980 – 2013	KMD & en.climate-data.org
	Temperature	1982 – 2012	en.climate-data.org
Katumani	Precipitation	1980 – 2017	KMD & en.climate-data.org
	Temperature	1980 – 2026	KMD & en.climate-data.org
	Wind speed	2009 – 2013	KMD
Machakos	Precipitation	1982 – 2012	en.climate-data.org
	Temperature	1982 – 2012	en.climate-data.org
Kajiado	Precipitation	1980 – 1997	KMD
	Precipitation	1982 – 2012	en.climate-data.org
	Temperature	1982 – 2012	en.climate-data.org
Konza	Precipitation	1982 – 2012	en.climate-data.org
	Temperature	1982 – 2012	en.climate-data.org
Kitengela	Precipitation	1982 – 2012	en.climate-data.org
	Temperature	1982 – 2012	en.climate-data.org
Athi River	Precipitation	1982 – 2012	en.climate-data.org
	Temperature	1982 – 2012	en.climate-data.org
Kiserian	Precipitation	1982 – 2012	en.climate-data.org
	Temperature	1982 – 2012	en.climate-data.org

Potential Evapotranspiration Data

Pan evaporation data was obtained from KMD records for JKIA from 1984 to 2012 and Machakos Agro-meteorological station for 1984 to 2009. The WetSpass model requires potential evapotranspiration data as one of the inputs. Though a variety of models exist for derivation of potential evapotranspiration as described by Lang *et al*. (2017), pan evaporation data was used to generate the potential evapotranspiration in this study.

The evaporation pan method makes a comparison between evaporation from the water surface in the pan and evapotranspiration of standard grass (Lang *et al*., 2017). Since the water in the pan and the grass do not behave in the same way to the prevailing

environment, a pan coefficient (K pan) is used to relate one to the other. Class-A evaporation pan environment has a range of K pan values of 0.35 to 0.85. Where the pan coefficient is not known an average value of 0.70 is used (Lang *et al*., 2017). The wind speed in the study area varies between 3 and 4 m/s while relative humidity varies between 40 and 70%. A value of 0.70 was adopted to obtain the potential evapotranspiration using Equation 3.2.

$$ETo = K\ pan \times E\ pan \quad \text{.....(3.2)}$$

Where,

ETo = reference crop evapotranspiration

K pan = pan coefficient

E pan = pan evaporation

Wind Speed Data

Data for wind speed was obtained from daily summaries of KMD records for two weather stations, namely JKIA and Machakos Agro-meteorological weather stations located close to the sub-catchment. The data generated the monthly and annual averages, which were used to develop the wind raster maps.

3.4.2 Preparation of Climatic Grid Maps

Monthly climatic data was manipulated using Microsoft excel to get average annual data. Data for the stations was imported in ArcMap 10.8 and merged to create monthly and annual maps. Interpolation was done using the inverse distance weighting (IDW) technique in order to have the value of data at each point. IDW is a deterministic spatial interpolation method, which estimates an unknown value at a location using known values with corresponding weighted values (Khouni *et al*., 2021). The assumption is that values of sampled points closer to the unsampled point are more similar to it than those further away. Monthly and annual grid maps were prepared and then converted to ASCII files using ArcMap 10.8 for use in the WetSpass model.

3.4.3 Acquisition of Sub-catchment Physical Parameters

Sub-catchment physical characteristics data comprised of topography, slope, soil texture and groundwater depth. The physical parameter data was obtained from various sources shown in Table 3.3.

Table 3. 3: Sources of sub-catchment physical parameter data

Parameter	Data type	Source
Topography and slope	Secondary	Shuttle Radar Topography Mission (SRTM)
Soil texture	Secondary and primary	Soil and Agro-climatic Map of Kenya (Sombroek *et al.* 1980); Harmonized World Soil Data (HWSD) (Karim & Saeid, 2019); Field soil sampling and laboratory tests
Groundwater depth	Secondary and primary	Water Resources Authority (WRA) records; Field borehole levelling

Secondary data for elevation was obtained from STRM in form of a Digital Elevation Model (DEM) and used to generate a slope map. Apart from secondary sources, sixty-seven (67) soil samples were collected in the field through random sampling in zones which reflected different landform, drainage patterns, and slope characteristics. Each sampling site was geo-referenced using a hand-held GPS. The textural classification was determined in the laboratory by conducting the grain size analysis through sieving and hydrometer test as presented in Appendix V.

Groundwater depth was sourced from Water Resources Authority (WRA) database. However, the database suffers from gross incompleteness, that is, some boreholes lack location coordinates, elevations and water level data, while newly drilled boreholes had not yet been entered into the database. Therefore, additional groundwater depth data was obtained by direct water level measurements in 20 boreholes during the field survey using a water dipper level meter. Groundwater depth data is presented in Appendix VI.

3.4.4 Preparation of Grid Maps of Physical Characteristics

Topography and Slope

The Digital Elevation Model (DEM) was extracted from the Kenya DEM dataset using clip function in raster processing tool of ArcMap 10.8. The resulting image was then processed to prepare a topographic map at a resolution of 30 m. The slope grid map was generated from the topography map using the spatial analyst tool in ArcMap 10.8. Both maps were converted to ASCII files for use in the WetSpass-M model.

Soil Texture Data

Soil classification used for the WetSpass-M model is based on the US Department of Agriculture (USDA) (Batelaan & De Smedt, 2001). The three sources of soil texture data outlined in Table 3.3 herein were harmonized to generate the soil map, which was then converted to ASCII files for use in WetSpass-M model.

Groundwater Depth Data

Groundwater depth data was compiled using Microsoft Excel and the was imported into ArcMap 10.8. The demarcation of boreholes falling within the study area was done using clipping in Geoprocessing tool of ArcMap. Point data was interpolated to generate the groundwater level grid map, which was then converted to ASCII format required for use in the WetSpass-M model.

3.4.5 Lookup Parameter Tables for WetSpass-M Model

WetSpass-M requires parameter tables that are linked through their attributes. These parameters differ from region to region due to differences in climate. It was therefore necessary to modify the parameter tables to suit the semi-arid conditions of the area. The modified parameters were adopted from Rwanga (2018). The parameter tables used in this study are presented in the Appendix III and IV.

3.5 WetSpass-M Input and Output Parameters

Grid maps in form of ASCII files and attribute tables required by the WetSpass-M are shown in Table 3.4 while the flow chart is presented in Figure 3.5. The model was run for four temporal periods each with a different LULC grid map to generate the monthly and annual water balance components.

Table 3. 4: WetSpass-M input and output parameters

Inputs (ASCII)	Unit	Tables (dbf)	Outputs (ASCII)	Unit
Precipitation	mm	LULC	Actual	mm
Potential	mm	Soil	evapotranspiration	mm
Evaporation			Surface runoff	
Wind speed	m/s		Groundwater	mm
Temperature	^{o}C		recharge	
LULC	Type			
Soil	Texture			
Topography (slope)	%			
Water depth	m			

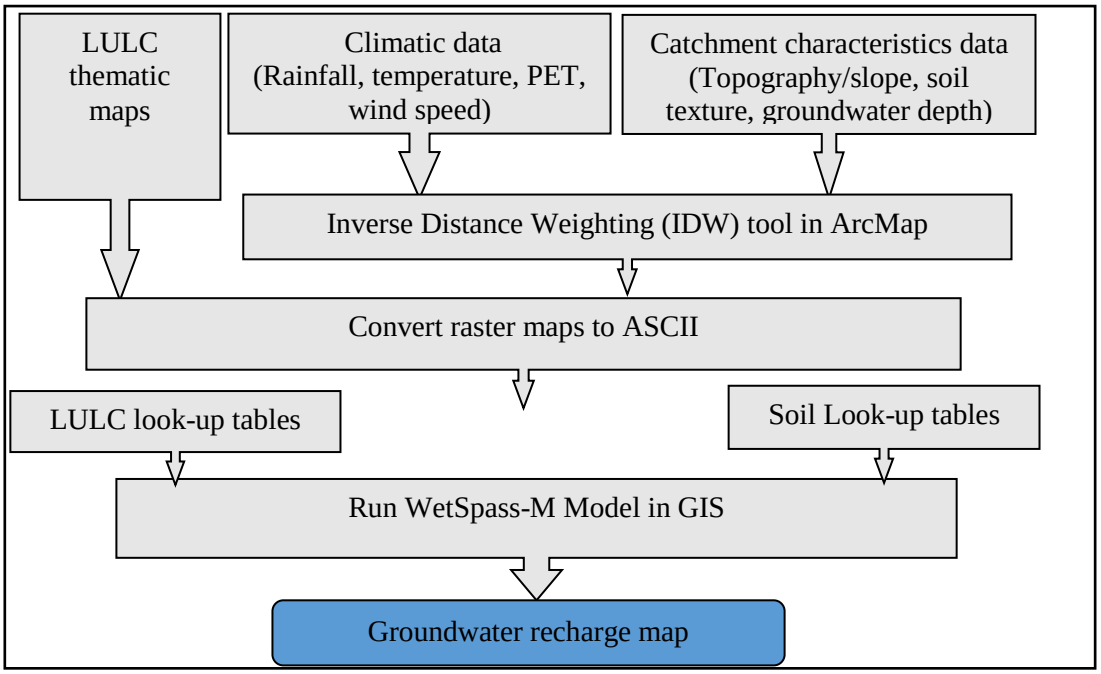

Figure 3. 5: WetSpass-M model flow chart for groundwater recharge

3.6 WetSpass-M Model Validation

Stream channels in the Stony Athi sub-catchment are usually dry for most of the year and short duration flows occur only after a rainfall event. Therefore, validation was done using surface runoff data downloaded from the Global Flood Awareness System (GloFAS), which contains global modelled daily data of river discharge**.** This dataset is simulated by forcing the hydrological river routing model with modelled gridded runoff data from global re-analysis (Harrigan *et al*., 2020; Thielen *et al*., 2012).

3.7 Evaluation of Groundwater Pollution Vulnerability

The third specific objective was to evaluate the influence of LULC changes on groundwater vulnerability to pollution in Stony Athi sub-catchment. To achieve this objective, the conventional DRASTIC model by Aller *et al*. (1987) was applied. However, the model was modified to include the LULC parameter.

3.7.1 DRASTIC Model Inputs

DRASTIC is an acronym for seven parameters which include:

1. **Depth to water –** depth to water refers to the depth of water rest level. Depth to water indicates the distance that a contaminant travels from the surface to the aquifer. A contaminant will take a longer time if the water level is deep. Shallow water table levels imply more vulnerability to contamination.

2. **Net recharge** – net recharge is the quantity of water that is added to the aquifer from the surface. Recharge is the means of transport for the pollutant. Higher recharge leads to greater chances for pollutants to reach the aquifer.

3. **Aquifer media** – aquifer media represents the properties of the saturated zone. Coarse-textured unconsolidated aquifers and fractured consolidated aquifers have higher permeabilities and are more vulnerable. Generally, aquifers are closely linked with the three major rock systems, namely, volcanic rocks, the basement metamorphic rocks, and sedimentary rocks.

4. **Soil media** – soil controls the rate at which a contaminant can infiltrate to reach the aquifer. Coarse-textured soils have higher infiltration rates, and thus the more the vulnerability of the aquifer.

5. **Topography** – topography reflects the slope of the surface. Slope determines the likelihood of a contaminant remaining long enough on the surface for infiltration to occur. Gentle slopes have little surface runoff and the potential for groundwater contamination is higher. Conversely, steep slopes have high runoff and the vulnerability for groundwater contamination is lower.

6. **Impact of the vadose zone** – this is the zone immediately above the water table that is not saturated. The time of travel of a contaminant to the saturated zone is determined by the vadose zone.

7. **Hydraulic conductivity** – hydraulic conductivity is the flow rate through an aquifer. The more the hydraulic conductivity, the higher the rate at which contaminants are spread, thereby increasing pollution vulnerability.

3.7.2 DRASTIC Data Sources

Depth to water, soil media, topography and slope was obtained and prepared as per the description given in section 3.4 herein. Net recharge was generated from the output of the WetSpass-M model while the aquifer media, vadose zone material and hydraulic conductivity were obtained from the geological map. Table 3.5 presents the sources of Drastic model parameters. The DRASTIC parameters were imported into ArcMap 10.8 software on a GIS platform as vector map layers. Ratings and weights were assigned to the parameters according to various ranges described by Aller *et al*. (1987) as shown in Table 3.6. The weights for all DRASTIC parameters were subsequently added to obtain a vulnerability index.

Table 3. 5: Sources of DRASTIC model data

Parameter	Source
Depth to water	Water Resources Authority (WRA) records; Field borehole levelling
Net recharge	WetSpass output
Aquifer media	Geological map of study area
Soil media	Soil and agro-climatic map of Kenya Harmonized world soil data (HWSD) Field soil sampling and laboratory tests
Topography	Shuttle Radar Topography Mission (SRTM)
Impact of vadose zone	Geological map of study area
Hydraulic conductivity	Geological map of study area; Physical Geology (Earle, 2019)

Table 3. 6: DRASTIC ranges, weights and ratings used in this study (After Aller *et al*. (1987)

Parameter	Range	Rating	Weight
Depth to water (m)	0.5-1.5	10	**5**
	1.5-4.6	9	
	4.6-9.1	7	
	9.1-15.2	5	
	15.2-22.8	3	
	22.8-30.4	2	
	>30.4	1	
Recharge (net) (mm)	0-50.8	1	**4**
	50.8-101.6	3	
	101.6-177.8	6	
	177.8-254	8	
	>254	9	
Aquifer media	Weathered volcanics	4	**3**
	Weathered Metamorphic	4	
	Sediments	8	
Soil media	Sandy Loam	6	**2**
	Loam	5	
	Clay Loam	3	
	Clay	1	
Topography (% slope)	0-2	10	**1**
	2-6	9	
	6-12	5	
	12-18	3	
	>18	1	
Impact of vadose zone	Confining Layer	1	**5**
	Silt/Clay	3	
	Sand and Gravel with Silt	6	
Hydraulic Conductivity (m/day)	0.04-4.1	1	**3**
	4.1-12.3	2	
	12.3-28.7	4	

3.7.3 Modified DRASTIC Model

The DRASTIC model was modified to include the LULC parameter so as to factor in the influence of LULC on groundwater vulnerability to pollution, hence the Modified DRASTIC model. The LULC parameter was assigned a weight of 5 while ratings were assigned 1 to 10. Built up areas were assigned the highest rate of 7 and forested areas the lowest rate of 2 as described by Maqsoom *et al*. (2020). Agricultural areas, bare land, grassland and shrub land were assigned rates of between 2 and 5 as shown in Table 3.7. The flow chart for the Modified DRASTIC model is shown in Figure 3.6.

Table 3. 7: Ranges, weights and ratings for LULC (After Maqsoom *et al*., 2020)

Parameter	Range	Rating	Weight
LULC	Built up area	7	**5**
	Agricultural land	5	
	Bare land	3	
	Grass land	2	
	Shrub land	2	
	Forested area	2	

3.7.4 Modified DRASTIC Vulnerability Index

Groundwater vulnerability classes were categorized according to the U.S. EPA (1993) DRASTIC Index and vulnerability classes (Table 3.8). U.S. EPA classifies DRASTIC vulnerability index into four categories namely, low, moderate, high and very high vulnerability (Jaseela *et al*., 2016).

Table 3. 8: Groundwater vulnerability index and vulnerability class

DRASTIC Index	Vulnerability category
1 – 100	Low
101 – 140	Moderate
141 – 200	High
>200	Very high

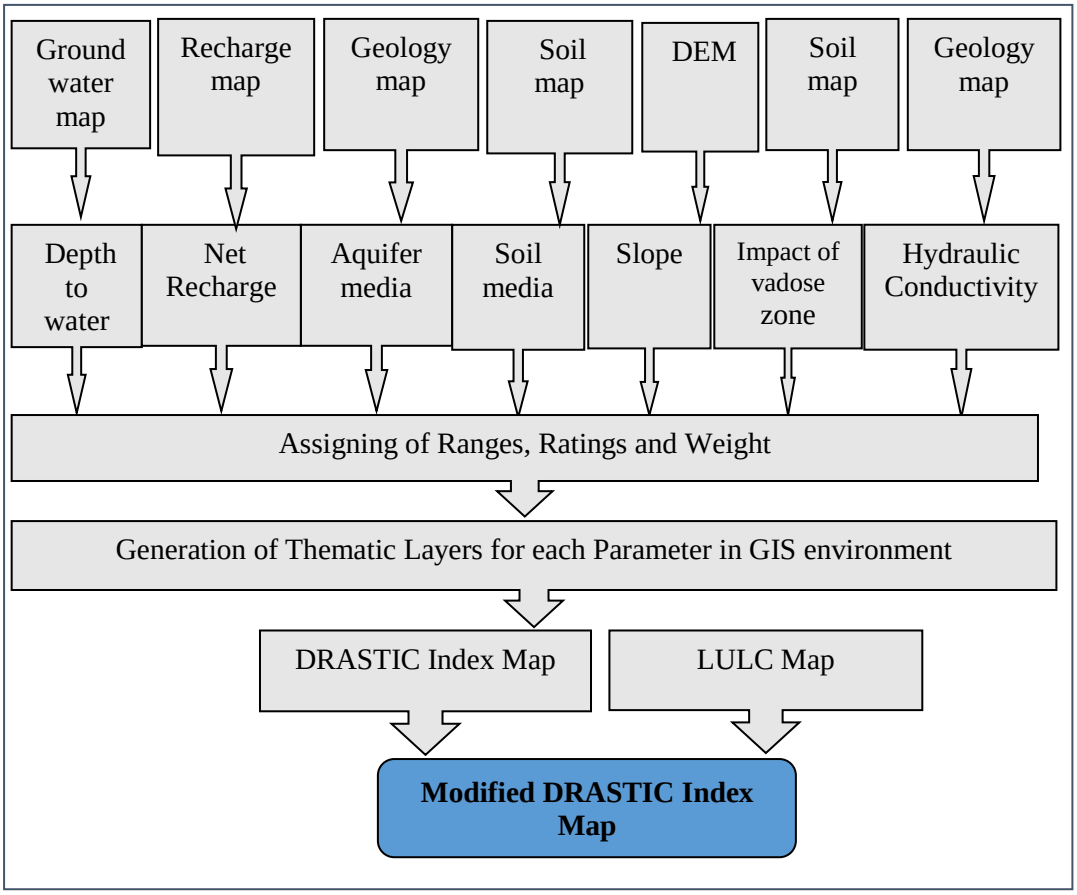

Figure 3. 6: Flow chart of the Modified DRASTIC model

3.8 Modified DRASTIC Model Validation

Nitrate is a typical groundwater contaminant associated with intensive agricultural activity and urbanization. Nitrate is highly soluble and has high mobility and as a result can pollute groundwater when carried by rain water (Khosravi *et al*., 2018). Naturally, nitrate is low in groundwater and is commonly used as a vulnerability validation parameter (Moges & Dinka, 2021). Presence of nitrate in groundwater most likely indicates pollution sources from anthropological activities. In this study, water sampling was carried out from selected boreholes, after which nitrate concentration was determined in the laboratory. The results were correlated with DRASTIC index values extracted from the DRASTIC Index map for validation. A nitrate concentration map was generated and overlaid on the modified vulnerability index map after which concentrations values were extracted and plotted on a scatter for correlation.

3.9 Data Analyses

3.9.1 LULC Changes

The classified LULC thematic maps were used to generate areas under different LULC feature using the spatial analyst and field calculator tools in ArchMap 10.8. The generated areas of each land use feature were then used to derive the LULC changes from one year to the next by subtracting the baseline value from the value after the change, then multiplying by 100 to obtain the percentages using Microsoft Excel software, that is, ((after change value – baseline value) / baseline value) x 100), for example, (Year 2017 – Year 1984) / Year 1984) x 100). Chi square goodness of fit (Equation 3.6) was applied for testing the significance of LULC changes between 1984 and 2017 accepted at $p<0.05$ as described by Zeng *et al*. (2015).

$$X^2 = \sum \frac{(\text{observed - expected})^2}{\text{expected}} \quad \text{………………………………………(3.3)}$$

3.9.2 Groundwater Recharge

The WetSpass-M model generated the monthly recharge numerical values and spatial digital maps. Monthly values were tabulated and summed up to obtain the annual groundwater recharge and percentages of the total annual rainfall were computed using Microsoft Excel. Other components of the WetSpass-M output included surface runoff and actual evapotranspiration. Chi square goodness of fit was applied for testing the significance of groundwater recharge changes between 1984 and 2017 and accepted at $p<0.05$ as decsribed by Zeng *et al*. 2015.

Spatial variations of groundwater recharge largely depend on soil texture and land cover (Batelaan & Woldeamlak, 2007). Therefore, spatial relationship between LULC and soil texture and groundwater recharge were analysed by extracting LULC classes, soil texture and groundwater recharge values from the respective digital maps using the ‘extract multi-values to points’ option in the spatial analyst option in ArchMap 10.8. The values were plotted and used to evaluate the relationships using Microsoft Excel.

3.9.3 Groundwater Pollution Vulnerability

Data sets for the seven DRASTIC layers were compiled into spread sheets using Microsoft Excel, where the ratings and weights were assigned to the parameters and then converted into shapefiles in Arc GIS as point attributes. Using the inverse distance weighting interpolation tool, the vector point attributes were then converted to raster layers and classified. The layers were then reclassified and used for overlay analysis in which each parameter was classified on a scale of one to ten, where one denotes the least vulnerable and ten the most vulnerable. The ratings were further scaled into weights according to their relative potential to contamination on a scale of 1 to 5; 1 being the least significant and 5 the most significant. The DRASTIC vulnerability index (DVI) was obtained as the sum of the product of each rating and its weight as shown in Equation 3.4.

$$\text{DVI} = \sum_{i=1}^{i=7}(\text{Wi x Ri}) \quad \text{.....(3.4)}$$

Where, DVI = DRASTIC Vulnerability Index

Wi = weighted coefficient and

Ri = rating coefficient.

The LULC index maps for the years 1984, 1995, 2005 and 2017 were added to the DRASTIC Index map to evaluate the effects of LULC changes on vulnerability to pollution. Thus, the convectional DRASTIC formula was modified to the formula shown in Equation 3.5.

$$\text{MDVI} = \sum_{i=1}^{i=7}(\text{Wi x Ri}) + LrLw \quad \text{.....(3.5)}$$

Where, MDVI = Modified DRASTIC Vulnerability Index

Lr = rating of the LULC parameter

Lw = weight of the LULC parameter

CHAPTER FOUR: RESULTS AND DISCUSSION

4.1 Quantification of Spatial-temporal LULC Changes

The first specific objective was to quantify the extent and magnitude of the spatial-temporal LULC changes in Stony Athi sub-catchment between 1984 and 2017. The objective was achieved by processing and analyzing four temporal Landsat images for 1984, 1995, 2005 and 2017 on a GIS platform using ArchMap 10.8.

4.1.1 LULC Classes

Six LULC classes were established namely; built-up area, agricultural land, grassland, shrub land, forested area and bare land (Table 4.1).

Table 4. 1: LULC classes in Stony Athi sub-catchment

LULC class	Description
Built-up areas	Urban and rural buildings including commercial, industrial and residential areas as well as roads
Agricultural land	Land areas under cultivation
Grassland	Land areas dominated by savannah grass and scattered shrubs
Shrub land	Land areas dominated by natural shrubs and bush with grass undergrowth
Forested area	Land area with tree canopy density of 10-40% and undergrowth bush including trees along drainage channels
Bare land	Land areas of exposed soil or rock with occasional scattered trees

The quantified areas and percentages covered by each LULC category is given in Table 4.2. The built-up category of land use comprised of 0.04% of the total area, which increased to 3.4% in 2017. Rangelands, comprising of grassland and shrub land dominate the land cover at 95.3%, but reduced to 92.7% in 2017. Forested area was 2.5% which reduced to 1.4% in 2017. Agricultural land comprised of 0.06%, which increased to 0.7% in 2017. Bare land category comprised of 2.1% in 1984 and 2.0% in 2017, reflecting a very small change of 0.1%.

Table 4. 2: Area coverage and percentages of LULC

	1984		1995		2005		2017	
LULC	**Area (km^2)**	**%**	**Area (km^2)**	**%**	**Area (km^2)**	**%**	**Area (km^2)**	**%**
Built-up area	0.64	0.04	4.1	0.2	33.4	2.0	59.5	3.4
Agricultural land	1.04	0.06	6.2	0.4	3.7	0.2	11.6	0.7
Grassland	1016.4	58.2	910.0	52.1	1175.5	67.4	1250.0	71.6
Shrub land	647.7	37.1	765.7	44.0	486.2	28.0	368.0	21.1
Forested area	44.0	2.5	57.5	3.3	34.0	2.0	23.7	1.4
Bare ground	35.8	2.1	2.08	0.1	12.6	0.7	32.6	2.0
Total	**1,745**	**100**	**1,745**	**100**	**1,745**	**100**	**1745**	**100**

4.1.2 Classification Accuracy

Classification accuracy was assessed using a confusion matrix to obtain classified LULC maps with minimum error of accuracy. Confusion matrices for the four temporal LULC thematic maps are presented in Appendix I while Table 4.3 presents the overall accuracy and kappa coefficient for the image classifications. Overall accuracies in all the satellite images were more than 90%, while the overall kappa index of agreement was greater than 0.90, indicating satisfactory classification accuracy and an acceptable level of agreement.

Table 4. 3: Overall accuracy assessment for the Landsat image classifications

Date of acquisition	Satellite sensor	Overall accuracy	Kappa coefficient
27/08/1984	Landsat 5 Thematic Mapper ™	94.6	0.93
30/01/1995	Landsat 5 Thematic Mapper ™	94.5	0.93
01/01/2005	Landsat 7 Enhanced Thematic Mapper $^{ETM+}$	95.8	0.95
28/12/2017	Landsat 8 OLI/TIRS	95.9	0.95

Figure 4.1 presents the overall LULC changes between 1984 and 2017. Grasslands showed the highest overall increase of 233.6 km^2 while shrub land showed the highest decrease of 279.7 km^2 representing 23% and 46.1% respectively. Bare land showed a marginal overall decrease from 35.8 km^2 in 1984 to 32.6 km^2 in 2017; a decrease of 3.2 km^2 representing 8.9%. Built up areas had an overall increase of 59 km^2 while agricultural land increased by 10.6 km^2. Forested areas decreased by 20.3 km^2 during the period under study.

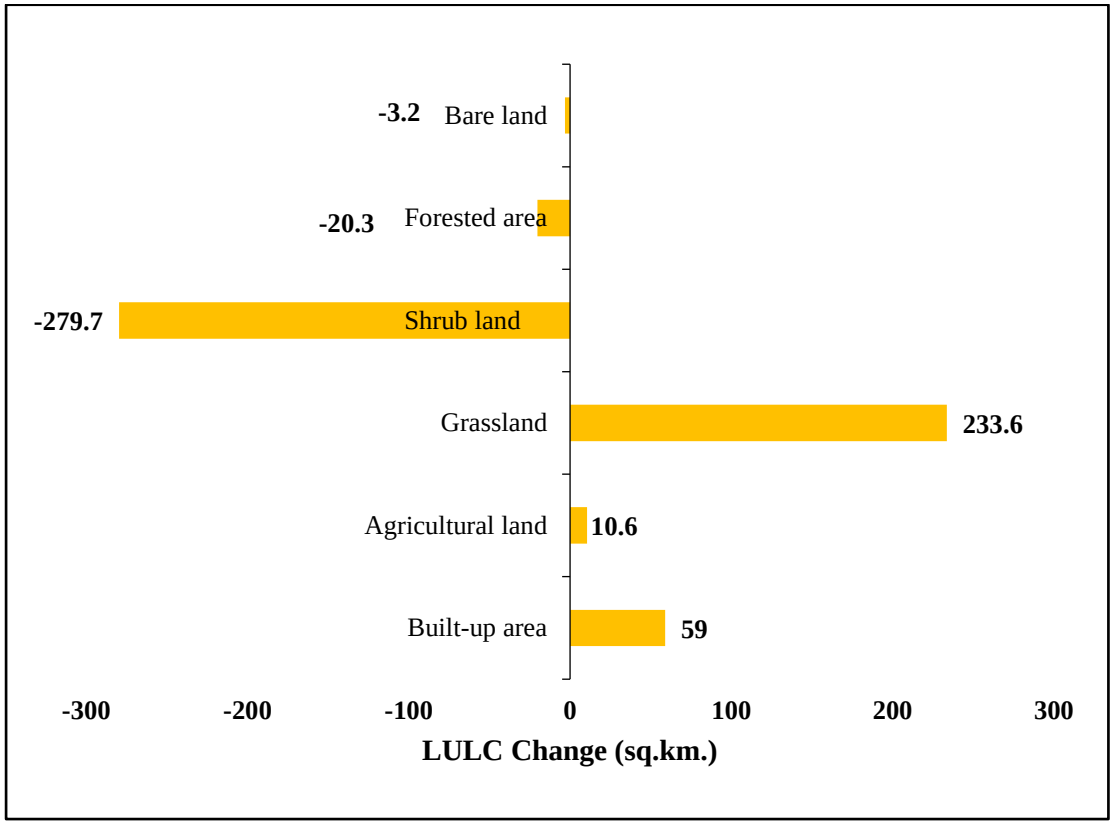

Figure 4. 1: Overall LULC changes between 1984 and 2017

4.1.3 Significance of Temporal LULC Changes

The first hypothesis stated that the extent and magnitude of land use and land cover changes that have occurred in the Stony Athi sub-catchment between 1984 and 2017 is significant. Results from the study indicated significant changes for all LULC classes as presented in Table 4.4.

Table 4. 4: Chi-Square goodness of fit for LULC changes

	1984	1995	2005	2017			
LULC	**Area (km^2)**	**Area (km^2)**	**Area (km^2)**	**Area (km^2)**	**X^2**	**df**	**p**
Built-up area	0.64	4.1	33.4	59.5	93.69	3	<0.00001
Agricultural land	1.04	6.2	3.7	11.6	10.56	3	0.0143
Grassland	1016.4	910.0	1175.5	1250.0	65	3	<0.00001
Shrub land	647.7	765.7	486.2	368.0	162.5	3	<0.00001
Forested area	44.0	57.5	34.0	23.7	15.66	3	0.0013
Bare land	35.8	2.08	12.6	32.6	37.63	3	<0.00001

4.1.4 Spatial Distribution of LULC

The spatial distribution of LULC maps for the years 1984 and 2017 are shown in Figures 4.2 and 4.3. It is evident from the maps that growth of built-up area tremendously increased between 1984 and 2017. Similarly, agricultural land was almost non-existent in 1984 but was noticeable in the thematic map for 2017.

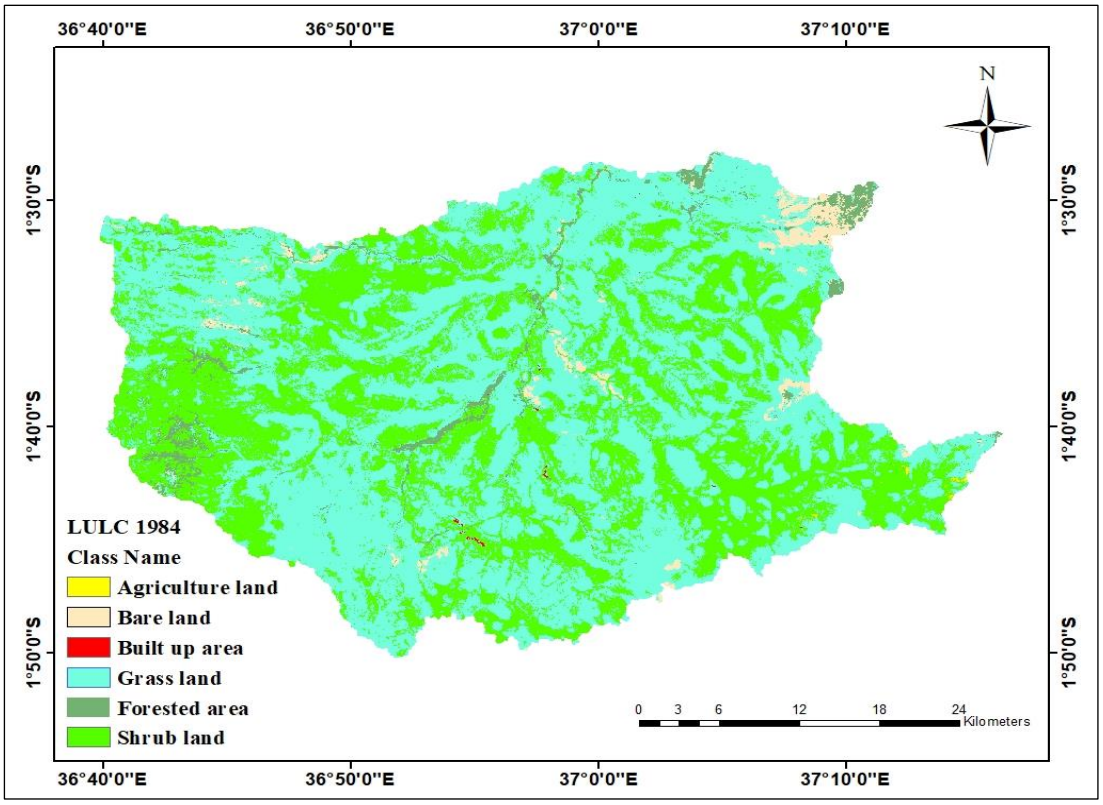

Figure 4. 2: Thematic LULC map of Stony Athi Sub-catchment for 1984

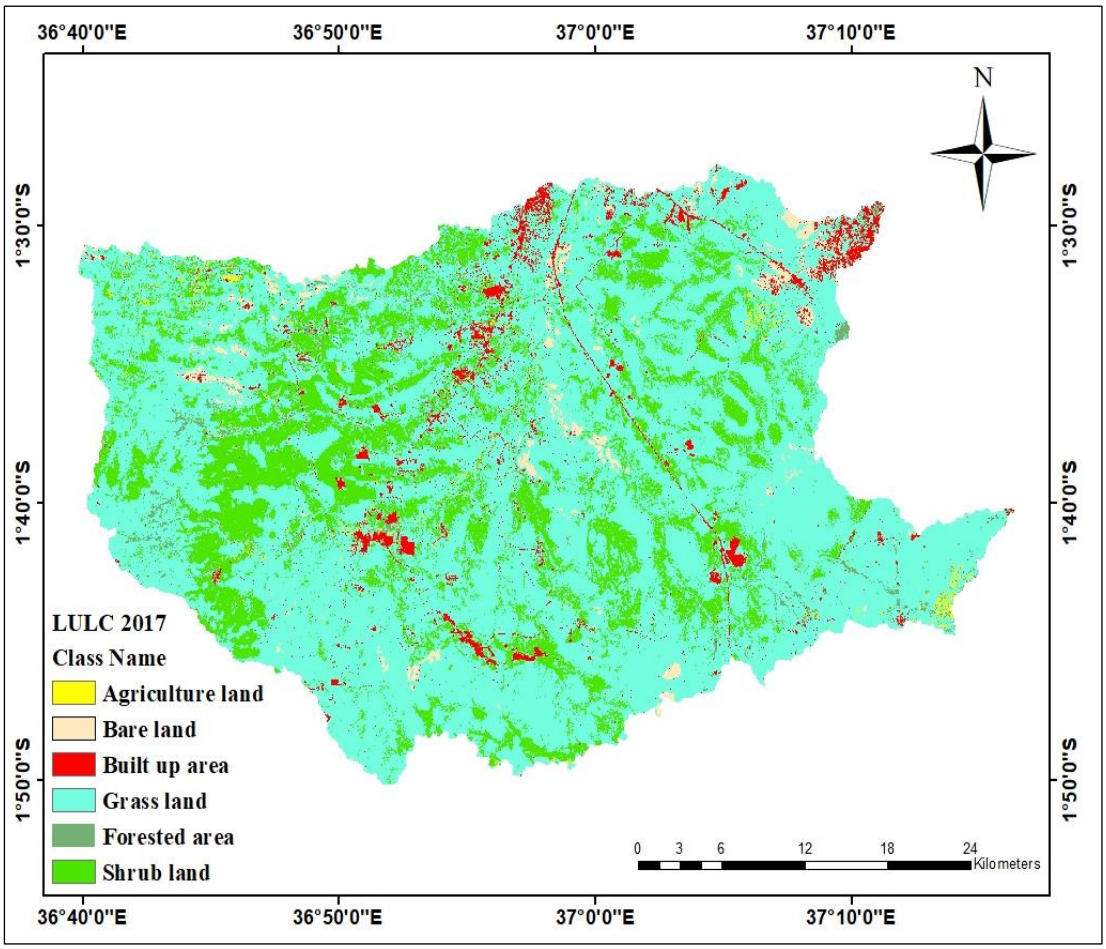

Figure 4. 3: Thematic LULC map of Stony Athi Sub-catchment for 2017

Most of the built-up area was found to be sprawled within the major towns along the main road network which include the Nairobi-Mombasa road, Athi River-Namanga road as well as Isinya-Kiserian road. However, grasslands, shrubs and forested areas still dominated the land cover; mainly used for wildlife and livestock grazing. This study also noted that rangelands still had highest percentage of land cover. Agricultural land was mostly concentrated in the north-eastern parts around Mua Hills, south eastern parts around Malili and parts of the north-western sections around Olooloitikoshi. Large scale flower and horticultural farming was mainly concentrated around Isinya and Kitengela towns.

Said *et al*. (2016) observed that LULC changes in the study area have been marked by turbulence mainly due to man-made activities. In the 1960s and 1970s, Maasai communal land was divided into group ranches collectively owned by ranch members.

According to Morara *et al*. (2014), some of these ranches have since been divided into un-economical small units owned by individual members as a result of increased sales to migrants by un-informed pastoralists. Suitable location and influx of immigrants have made pastoral peri-urban Kajiado County a centre of two conflicting interests; urban sprawl and agricultural intensification (Morara *et al*., 2014). Morara *et al*. (2014) further reported that between 1984 and 2010, significant LULC changes occurred due to increased demand of land and employment opportunities by migrants. In the present study, development was observed across much of the area, which included massive housing, industrial developments and large-scale flower and horticultural farms.

Stony Athi sub-catchment represents a case where changes in land tenure, land use policies, proximity to a major city, urbanization and immigration caused rapid land use changes, which adversely impact the natural resources (Ogutu *et al*., 2014; Morara *et al*., 2014). The location of the sub-catchment close to a rapidly expanding major city where undeveloped land has become increasingly scarce and expensive, made the area a strong magnet for those seeking relatively cheap land for settlement, industrial and other developments (Ogutu *et al*., 2014; Morara *et al*., 2014).

4.1.5 LULC Conversions

Losses and gains for the different LULC cover categories were evaluated for three episodes, namely, from 1984 to 1995, 1995 to 2015 and 2015 to 2017.

Year 2005 to 2017

From 1984 to 1995, 46.2%, 10.8%, 74.2%, 77.7%, 49.7% and 4.6% of built up, agricultural, grass, shrub, forested area and bare lands, respectively remained under the same LULC categories. However, there were conversions from agricultural land to shrub land (73.8%) and to forested area (13.9%). 17.2%, 34.2%, 28.7% and 15.1% of what was bare land in 1984 was converted to agricultural land, grassland, shrub land and forested area by the year 1995, respectively, while 29.8%, 12.8% and 10.4% of what was built up area was converted to grasslands, shrub land, and forested area, respectively. Grass land (23.3%) and forested area (39.0%) were converted to shrub land while 20.1% of shrub lands was converted to grassland.

Year 2005 to 2017

The second comparison made from 1995 to 2005 indicated that 57.8%, 2.9%, 89.5%, 51.2%, 31.5% and 57.3% of built up, agricultural, grass, shrub, forested area and bare lands, respectively, remained under the same categories. However, 34.9%, 9.42% and 26.4% of agricultural land, forested area and bare land was converted to built-up area while 33.0% and 7.2 % of built up area was converted to grassland and shrub land. Agricultural area was converted to grassland (14.8%), shrub land (29.3%) and forested area (15.5%), respectively. Conversion to grassland also emanated from shrub land (45.8%), forested area (26.8%) and bare land (11.6%). The table also shows that 7.9% and 30.3% of shrub land in 2005 resulted from to grass land and forested area.

Year 2005 to 2017

Finally, comparison made from 2005 to 2017 showed that 40.7%, 7.3%, 82.5%, 44.2%, 21.6% and 79.3% of built up area, agricultural land, grassland, shrub land, forested area and bare lands, respectively, remained under the same categories. Agricultural land (5.8%) and forested area (11.5%) were converted to built-up area while 38.5 % and 17.2% of built up area was converted to grassland and bare land, respectively. Agricultural land (62.8%), shrub land (50.1%), forested area (56.6%) and bare land (16.0%) were converted to grassland. The LULC change conversion matrices from 1984 to 2027 are presented in Table 4.5.

Table 4. 5: Change detection matrices of LULC for 1984 to 1995, 1995 to 2005, and 2015 to 2017

LULC Class	Built-up area		Agricultural land		Grass land		Shrub land		Forested area		Bare ground	
1984 - 1995	**Area (km^2)**	**% Area**	**Area (km^2)**	**% Area**	**Area (km^2)**	**% Area**	**Area (km^2)**	**% Area**	**Area (km^2)**	**% Area**	**Area (km^2)**	**% Area**
Built-up area	0.30	46.16	0.00	0.75	0.19	29.76	0.08	12.80	0.07	10.38	0.00	0.14
Agricultural land	0.00	0.13	0.11	10.84	0.01	1.27	0.77	73.84	0.14	13.92	0.00	0.00
Grass land	1.95	0.19	6.28	0.62	754.43	74.23	236.79	23.30	16.75	1.65	0.20	0.02
Shrub land	1.34	0.21	1.01	0.16	130.08	20.08	503.28	77.70	12.00	1.85	0.00	0.00
Forested area	0.00	0.27	2.68	6.10	2.16	4.91	17.12	38.92	21.87	49.71	0.04	0.09
Bare ground	0.08	0.23	6.15	17.19	12.25	34.20	10.28	28.70	5.39	15.05	1.66	4.63
TOTAL	**3.67**	**47.19**	**16.24**	**35.66**	**899.12**	**164.44**	**768.31**	**255.27**	**56.22**	**92.55**	**1.90**	**4.88**

1995 - 2005	**Area (km^2)**	**% Area**	**Area (km^2)**	**% Area**	**Area (km^2)**	**% Area**	**Area (km^2)**	**% Area**	**Area (km^2)**	**% Area**	**Area (km^2)**	**% Area**
Built-up area	0.55	57.84	0.00	0.12	0.24	33.04	0.05	7.24	0.04	1.47	1.19	0.29
Agricultural land	2.17	34.92	0.18	2.85	0.92	14.79	1.82	29.28	0.96	15.50	0.16	2.66
Grass land	11.87	1.30	0.75	0.08	814.19	89.47	71.89	7.90	3.00	0.33	8.30	0.91
Shrub land	8.05	1.05	1.68	0.22	350.88	45.82	391.80	51.17	10.78	1.41	2.50	0.33
Forested area	5.42	9.42	0.83	1.44	15.38	26.75	17.43	30.31	18.12	31.51	0.33	0.57
Bare ground	1.08	26.39	0.01	0.21	0.48	11.64	0.10	2.37	0.09	2.10	2.35	57.29
TOTAL	**29.14**	**130.9**	**3.45**	**4.92**	**1182.1**	**221.51**	**483.08**	**128.27**	**33.00**	**52.32**	**14.83**	**62.05**

2005 - 2017	**Area (km^2)**	**% Area**	**Area (km^2)**	**% Area**	**Area (km^2)**	**% Area**	**Area (km^2)**	**% Area**	**Area (km^2)**	**% Area**	**Area (km^2)**	**% Area**
Built-up area	13.58	40.65	0.19	0.58	12.86	38.51	0.40	1.20	0.62	1.85	5.75	17.23
Agricultural land	0.21	5.78	0.27	7.33	2.32	62.76	0.53	14.36	0.33	8.93	0.03	0.84
Grass land	32.32	2.75	4.59	0.39	969.85	82.51	150.47	12.80	6.30	0.54	11.96	1.02
Shrub land	8.77	1.80	5.35	1.10	243.74	50.13	215.09	44.24	9.10	1.87	4.15	0.85
Forested area	3.92	11.54	1.23	3.63	19.24	56.60	1.56	4.58	7.35	21.61	0.70	2.05
Bare ground	0.57	4.50	0.01	0.05	2.01	15.98	0.00	0.02	0.01	0.11	10.00	79.33
TOTAL	**59.37**	**67.01**	**11.65**	**13.08**	**1250.0**	**306.49**	**368.05**	**77.20**	**23.70**	**34.91**	**32.58**	**101.3**

4.2 Estimation of Spatial-temporal Groundwater Recharge

The second specific objective was to estimate the temporal variations of recharge due to LULC changes using WetSpass-M model between 1984 and 2017. The model requires grid maps comprised of LULC, climatic (rainfall, temperature, potential evapotranspiration and wind speed) and catchment characteristics (DEM, slope, soil texture and groundwater depth) as input data.

4.2.1 Climatic Characteristics

Climatic data comprising of rainfall, temperature, PET and wind speed was used for inputs in the WetSpass-M simulation. Climatic data used in this study is presented in Appendix II.

Rainfall

Table 4.6 and Figure 4.4 shows the long-term rainfall trend in the period 1984 – 2017, recorded in four weather stations within and surrounding the sub-catchment. Records showed that rainfall was highest in 1990 at 1,052 mm and lowest in 2000 at 306.2 mm. The annual average was found to be 633.5 mm.

Table 4. 6: Annual rainfall from 1984 to 2017

Year	**1984**	**1985**	**1986**	**1987**	**1988**	**1989**	**1990**	**1991**	**1992**
Amount	498	635	610	446	730	851	1052	847	605
Year	**1993**	**1994**	**1995**	**1996**	**1997**	**1998**	**1999**	**2000**	**2001**
Amount	598.5	682.3	599.7	530.7	913.1	940.6	538.4	306.2	802.6
Year	**2002**	**2003**	**2004**	**2006**	**2007**	**2008**	**2009**	**2010**	**2011**
Amount	834.9	572.5	592.6	880.4	540.3	505.0	553.7	719.9	545.9
Year	**2012**	**2013**	**2014**	**2015**	**2016**	**2017**			
Amount	595.4	646.5	479.8	785.3	517.0	484.6			

Examination of rainfall data for the period 1984–2017 showed significant inter-annual variability with a declining rainfall trend occurring at a period of increasing temperature trend. The observation could emphasize the fact that the sub-catchment is already experiencing the impact of global climate change.

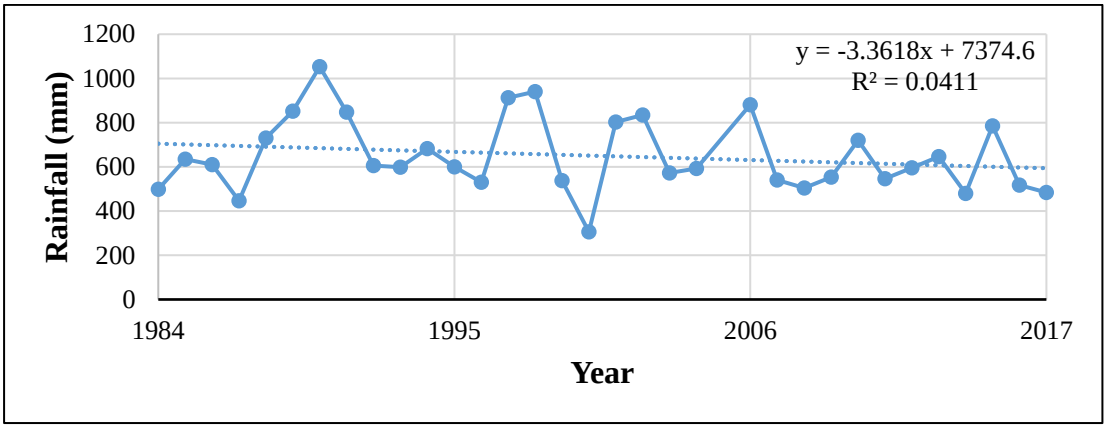

Figure 4. 4: Long term rainfall trend for the period 1984 – 2017

Figure 4.5 presents the spatial rainfall distribution in Stony Athi sub-catchment. Higher rainfall ranging between 650 and 768 mm occurs in the high-altitude areas in the north-east and north-west while most of the central and southern areas receive below average rainfall amounts ranging between 530 and 620 mm.

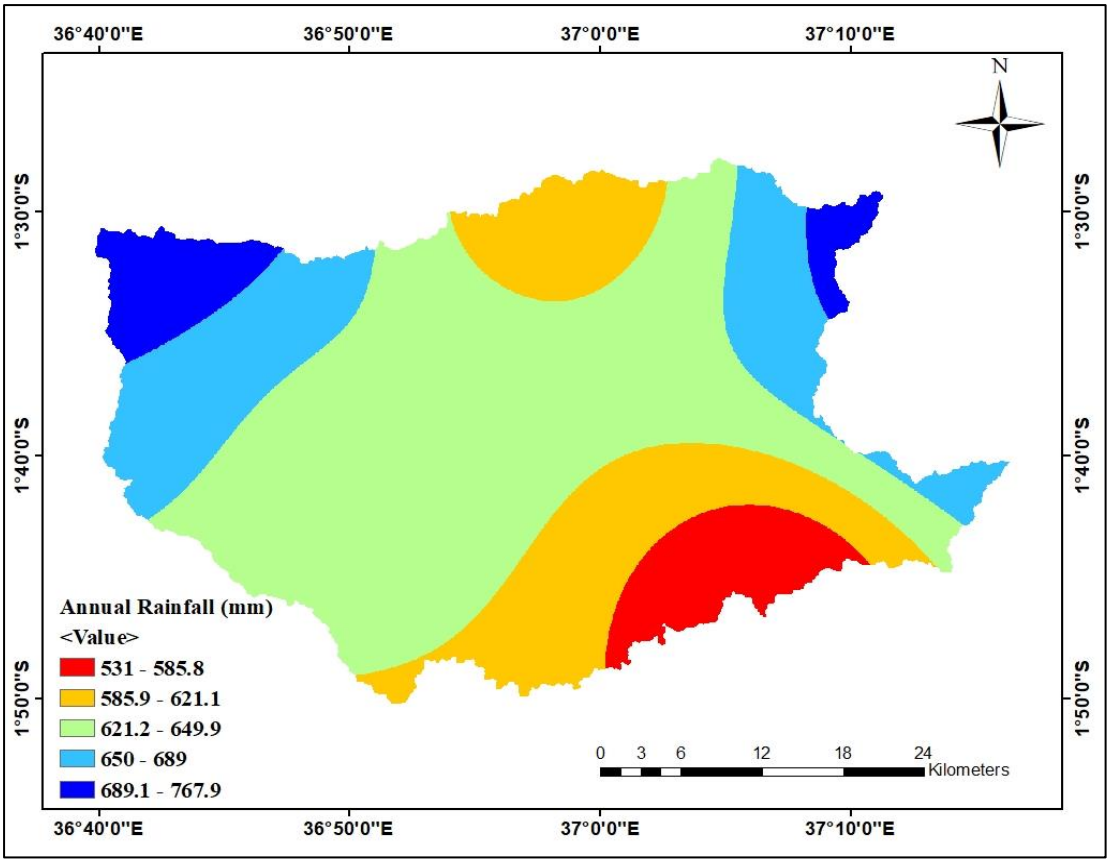

Figure 4. 5: Spatial distribution of annual rainfall in the study area

The average monthly rainfall is presented in Table 4.7 and Figure 4.6 from records of nine stations within and surrounding the sub-catchment. Stony Athi sub-catchment has two rainy periods; the March-May long rains and the October-December short rains. The short rainy season receives less amounts of rainfall than the long rainy season. Average monthly amounts are 38.7 mm, 113.1 mm and 72.3 mm for October, November and December, respectively. The study area receives 77.6 mm, 137.9 mm and 77.3 mm in March, April and May, respectively. This calculates to 46% of the annual rainfall in the long rainy season and 35% in the short rainy season. Amwata *et al*. (2015) reported that most areas of Kajiado County receive 50 % of the annual rainfall during the March to May period and 30 % during the October to December period.

The two rainy periods are separated by a dry spell between June and September which record the lowest rainfall amounts of 15.1 mm, 4.7 mm, 6.7 mm and 8.7 mm in June, July, August and September, respectively. January and February receive moderate rainfall averaging about 40 mm. The variation in precipitation between the driest and wettest months is 133.2 mm. The average monthly rainfall is about 53 mm, which agrees with Bobadoye *et al*. (2014) who gave 51.01 mm as the average rainfall at Isinya meteorological station, which is centrally located in the study area.

Table 4. 7: Monthly rainfall in Stony Athi sub-catchment

Month	**Jan.**	**Feb.**	**Mar.**	**Apr.**	**May**	**June**
Amount	41.6	39.8	77.6	137.9	77.3	15.1
Month	**July**	**Aug.**	**Sept.**	**Oct.**	**Nov.**	**Dec.**
Amount	4.7	6.7	8.7	38.7	113.1	72.3

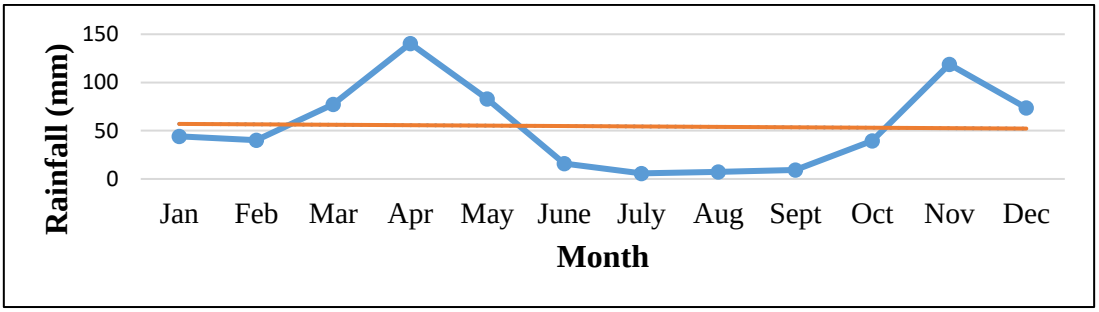

Figure 4. 6: Trend of monthly rainfall for Stony Athi sub-catchment

Temperature

The trend of annual maximum and minimum temperatures for the period 1984 – 2017 are shown in Table 4.8 and Figure 4.7. The average annual temperature is 19.0 °C with a maximum of 25.5 °C and a minimum of 13.4 °C. There was a noticeable increase in temperature over the years, which could be attributed to climate change. According to IPCC research, human-induced warming reached between 0.8°C and 1.2°C above pre-industrial levels in 2017, increase at between 0.2°C and 0.3°C per decade (Framing and Context, 2022).

Table 4. 8: Average annual temperature between 1984 and 2017

Year	**1984**	**1985**	**1986**	**1987**	**1988**	**1989**	**1990**	**1991**	**1992**
Min. Temp. (°C)	12.55	13	12.6	12.9	13.1	12.1	13.2	12.95	13.15
Max. Temp. (°C)	25.45	24.6	25.3	26.3	25.25	24.45	24.65	25.5	25.2
Year	**1993**	**1994**	**1995**	**1996**	**1997**	**1998**	**1999**	**2000**	**2001**
Min. Temp. (°C)	13.3	13.2	12.9	13.05	13.35	13.3	13.6	13.3	13.45
Max. Temp. (°C)	25.05	25.4	25.4	25.6	25.7	24.9	25.65	25.85	25.35
Year	**2002**	**2003**	**2004**	**2005**	**2006**	**2007**	**2008**	**2009**	**2010**
Min. Temp. (°C)	13.85	12.8	13.2	13.3	13.75	13.45	13.35	13.9	13.8
Max. Temp. (°C)	25.3	25.5	25.5	25.8	25.35	25.35	25.4	26.15	25.35
Year	**2011**	**2013**	**2014**	**2015**	**2016**	**2017**			
Min. Temp. (°C)	14.35	13.95	13.95	13.75	14.3	13.95			
Max. Temp. (°C)	26.2	25.85	25.9	26.4	25.65	25.9			

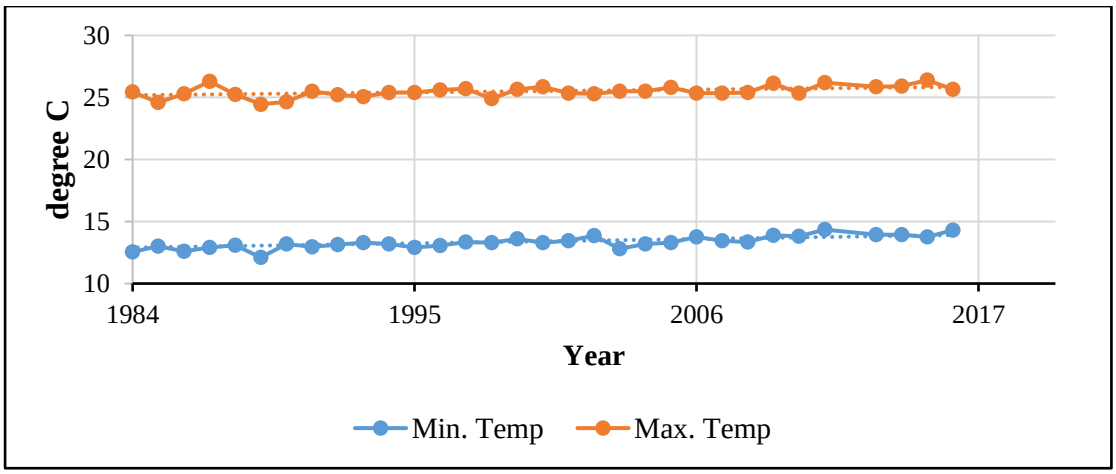

Figure 4. 7: Trend of annual minimum and maximum temperature

The spatial distribution of annual temperature is shown in Figure 4.8. Areas to the north-western parts has lower temperatures which increase towards the eastern areas of the sub-catchment. Spatial distribution of temperature was found to be controlled by elevation, with lower elevations having comparatively higher temperatures.

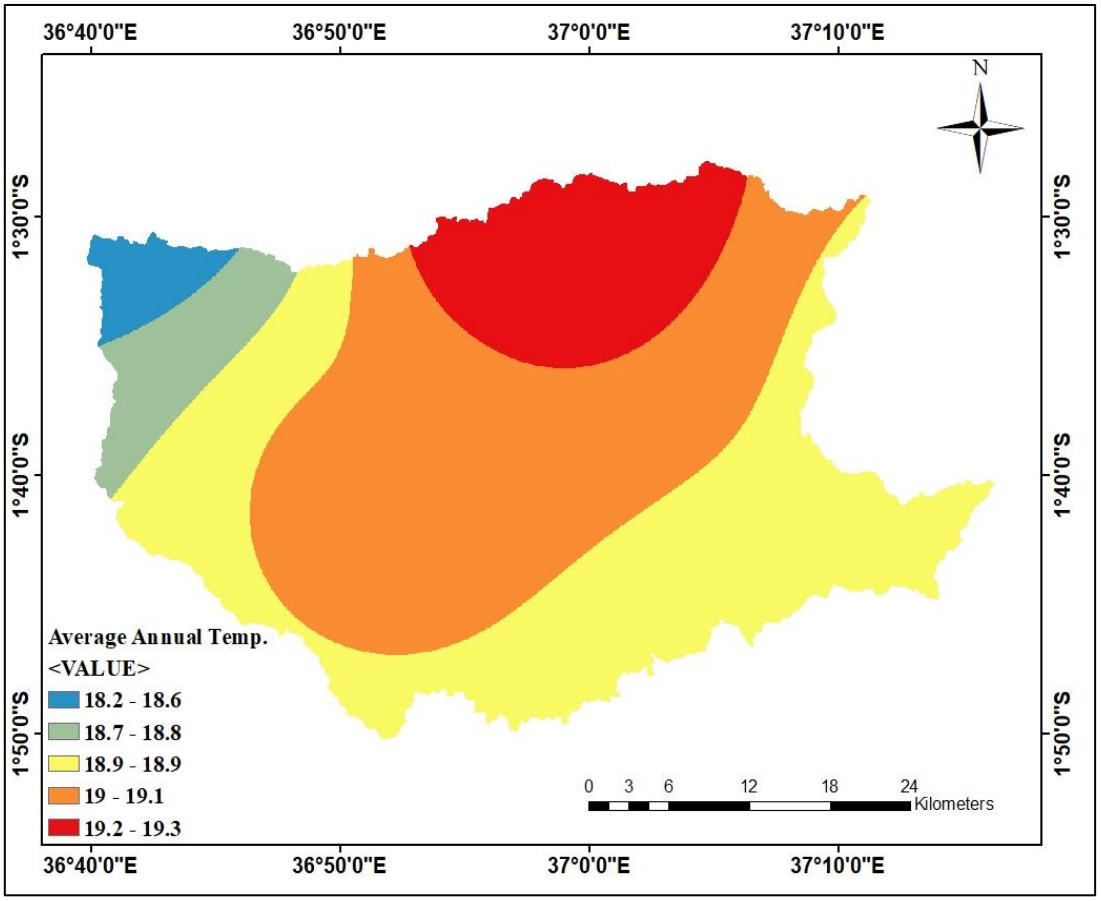

Figure 4. 8: Map of mean annual temperature

Trend of monthly temperature is presented in Table 4.9 and Figure 4.9. Average monthly temperatures showed that the month of March had the highest mean temperature of 20.5 °C followed by February and April with 20.2 °C and 20.0 °C, respectively. July, August and June had the lowest mean temperatures of 16.5 °C, 16.9 °C and 17.4 °C respectively. The highest value was recorded in February while July had the lowest temperature of the year with values of 27.4 °C and 10.8 °C, respectively. During the year, the average temperatures varied by 3.6 °C.

Table 4. 9: Monthly temperature in Stony Athi sub-catchment

Month	Jan.	Feb.	Mar.	Apr.	May	June
Temp $_{Min}$ (°C)	12.7	12.9	14.2	14.5	13.7	11.6
Temp $_{Ave}$ (°C)	19.4	20.2	20.0	20.0	19.0	17.4
Temp $_{Max}$ (°C)	26.3	27.4	27.0	25.4	24.3	23.4
Month	**July**	**Aug.**	**Sept.**	**Oct.**	**Nov.**	**Dec.**
Temp $_{Min}$ (°C)	10.8	11.0	11.5	13.0	13.8	13.8
Temp $_{Ave}$ (°C)	16.5	16.9	18.4	19.7	19.3	18.9
Temp $_{Max}$ (°C)	22.3	22.9	25.2	26.3	24.7	24.8

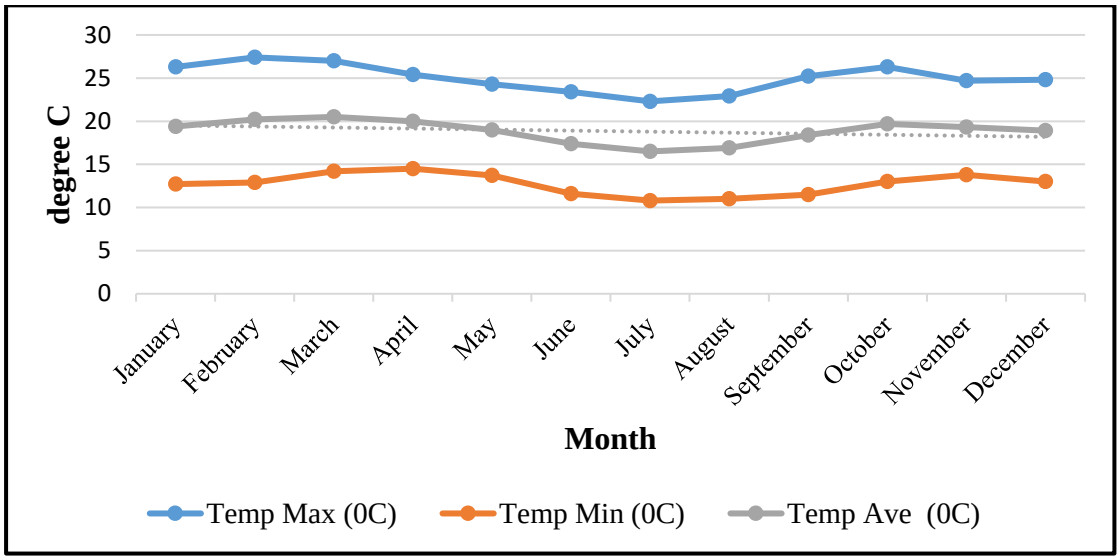

Figure 4. 9: Monthly trend of maximum, average and minimum temperature

Potential Evapotranspiration

The calculated monthly trend of potential evapotranspiration (PET) is presented in Table 4.10 and Figure 4.10. The highest PET value was for the month of March followed by February with 153.5 mm and 146.8 mm respectively while the lowest values were 86.9 mm and 93.8 mm for July and August, respectively. Annual potential evaporation calculated values ranged between 1264 mm and 1715 mm. Figure 4.11 shows the spatial distribution of annual potential evapotranspiration. Areas towards the north-west and south east were found to have lower values compared to the central sections of the study area.

Table 4. 10: Monthly PET in Stony Athi sub-catchment

Month	**Jan.**	**Feb.**	**Mar.**	**Apr.**	**May**	**June**
Amount (mm)	134	146	151	139	122	99
Month	**July**	**Aug.**	**Sept.**	**Oct.**	**Nov.**	**Dec.**
Amount (mm)	88	94	119	140	129	128

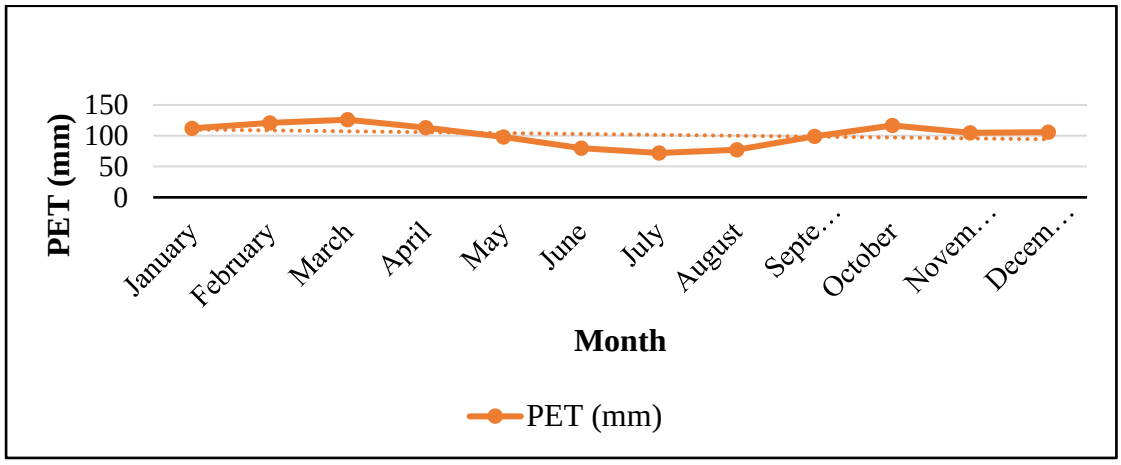

Figure 4. 10: Trend of average monthly PET

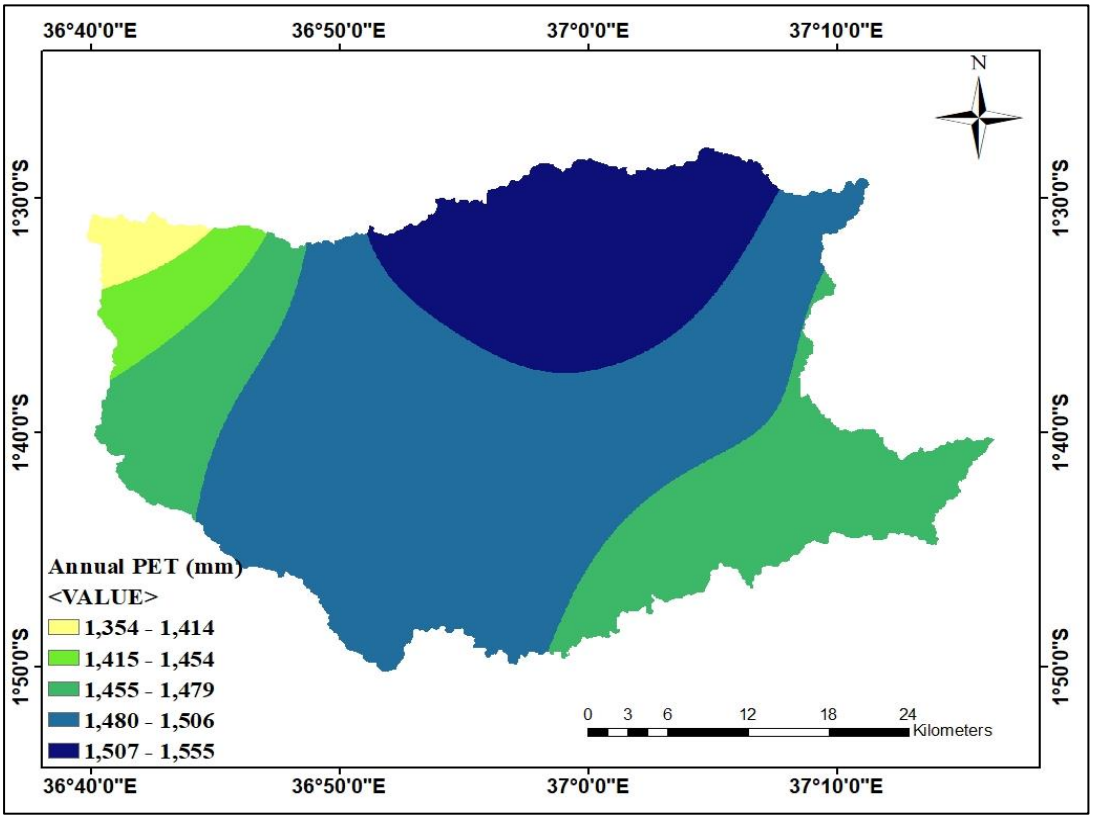

Figure 4. 11: Map of annual Potential Evapotranspiration (PET)

Wind Speed

Wind speed varied from a minimum of 2.8 m/s in June and July to a maximum of 4.5 m/s from December to February with a monthly average of 3.7 m/s. Monthly trend of wind speed is presented in Table 4.11 and Figure 4.12.

Table 4. 11: Monthly wind speed in Stony Athi sub-catchment

Month	**Jan.**	**Feb.**	**Mar.**	**Apr.**	**May**	**June**
Wind speed (m/s)	4.4	4.5	4.3	3.6	2.9	2.8
Month	**July**	**Aug.**	**Sept.**	**Oct.**	**Nov.**	**Dec.**
Wind speed (m/s)	2.8	3.0	3.4	4.1	4.2	4.5

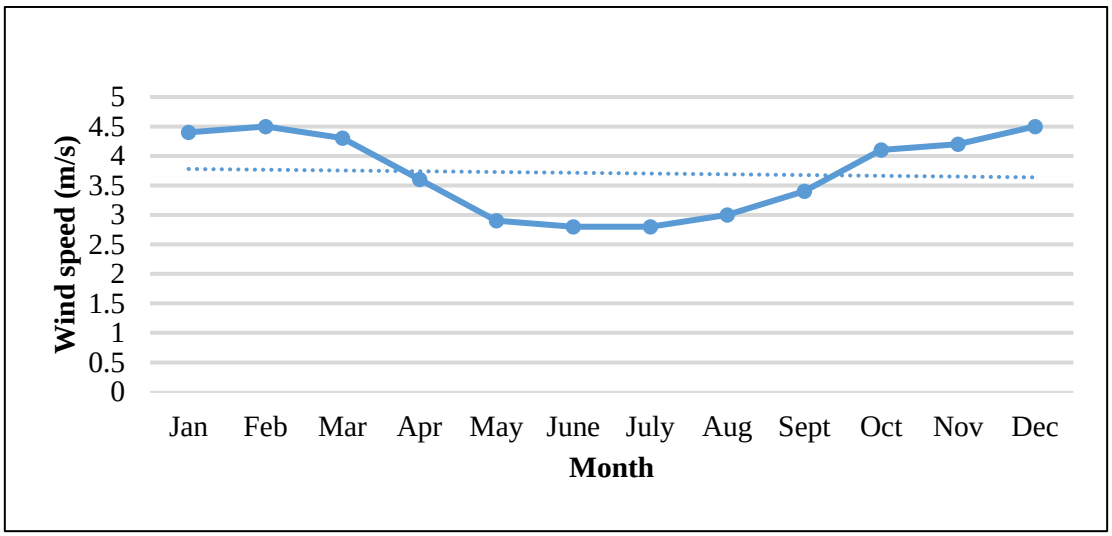

Figure 4. 12: Trend of monthly wind speed in Stony Athi sub-catchment

4.2.2 Sub-catchment Physical Characteristics

Topography and Slope

Digital Elevation Model (DEM) shown in Figure 4.13 indicates that the maximum altitude is 2,082 m situated in the western part while the minimum altitude of 1,493 m occurs in the central areas with a mean of 1,787 m. Large portions of the central areas are moderately flat plains, popularly referred to as the Kapiti Plains, while isolated high areas occur in the eastern margins. The slope map in Figure 4.14 was generated from the DEM and indicates that the surface of the sub-catchment generally slopes from west to east and can be divided into three classes, namely; class 1 (0 – 4%), class 2 (4 – 10%) and class 3 (10 – 30%).

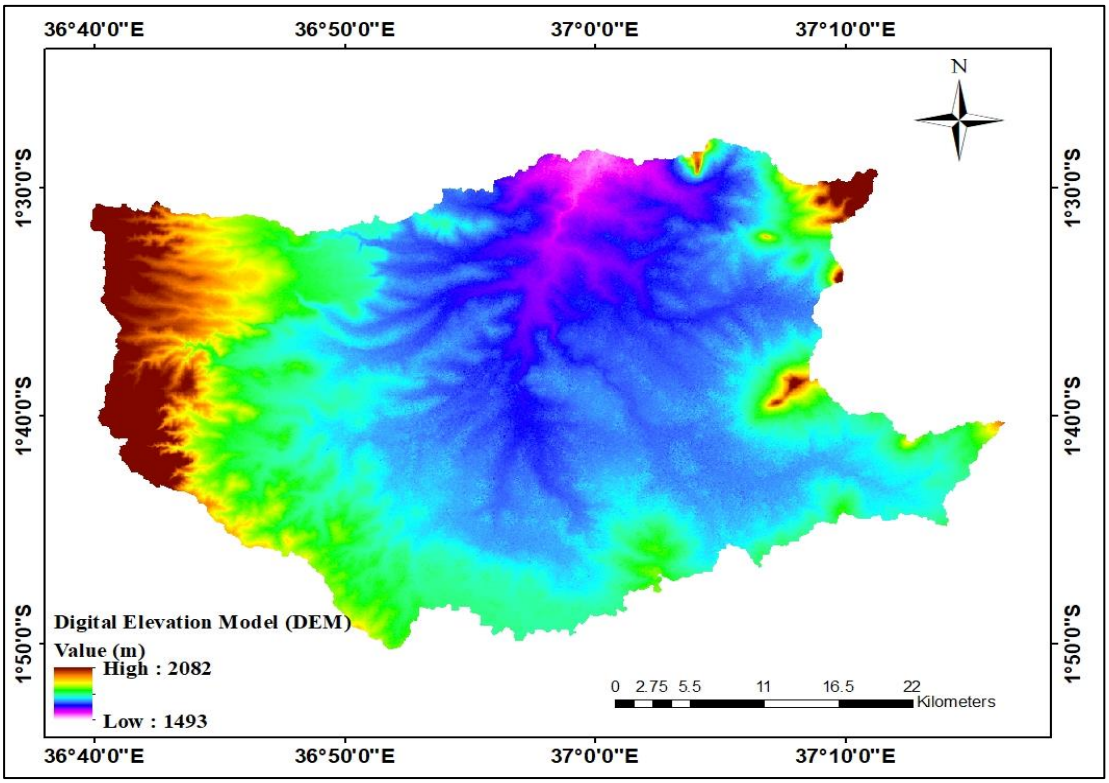

Figure 4. 13: Digital Elevation Model (DEM) of the study area

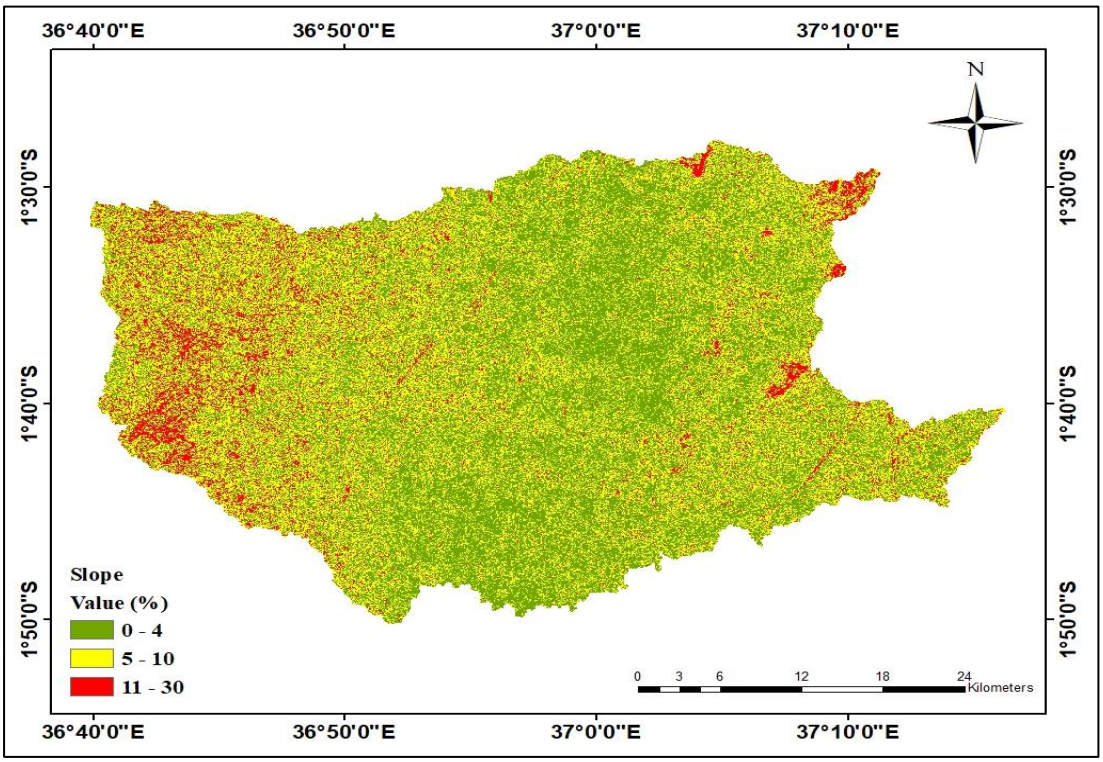

Figure 4. 14: Slope map of the study area

Soil Texture

Soil types were categorized based on USDA soil textural classes as presented in Table 4.12 while the spatial distribution of soil texture is shown in Figure 4.15. Five soil textures were identified namely sandy loam covering 2.2% of the total area, sandy clay loam (20.5%), sandy clay (4.4%), clay loam (10.7%) and clay (62.1%). The study area is therefore dominated by clay covering an area of 1,027.4 km^2 followed by sandy clay loam (338.8 km^2) and sandy clay (1,77.3 km^2). Clay loam (73.1 km^2) and sandy loam (36.9 km^2) cover relatively small portions of the area. Sandy loam has the hydraulic conductivity of 1.4 x 10^{-5} m/s while clay has the lowest of 3.0 x 10^{-7} m/s **(**Saxton & Rawls, 2006). Soil texture is dependent on the parent material. Soils on volcanic rocks have low sand percentages and are mainly clays and clay loams. Soils developed on basement rocks are generally sandy clay loams and sandy clays. Red sandy clays dominate the basement rocks rich in ferro-magnesian minerals while brown sandy clay loams prevail on the undifferentiated basement rocks.

Table 4. 12: Soil texture area coverage in the Stony Athi sub-catchment

Soil texture	Area covered (km^2)	Percentage covered (%)	Hydraulic conductivity (m/s)
Sandy loam	36.9	2.2	1.4 x 10^{-5}
Sandy clay loam	338.8	20.5	3.1 x 10^{-6}
Sandy clay	177.3	10.7	1.2 x 10^{-6}
Clay loam	73.1	4.4	3.9 x 10^{-7}
Clay	1,027.4	62.1	3.0 x 10^{-7}

Groundwater Depth

Groundwater depth was found to be in the range of between 2 and 130m below the surface (Figure 4.16). It was observed that the depth in the central parts, which are also low in elevation have shallower groundwater levels relative to the higher elevations in the western and eastern regions. Gebreyohannes *et al*. (2013) observed that groundwater depths of than 20 m have an insignificant effect on the WetSpass-M model simulations.

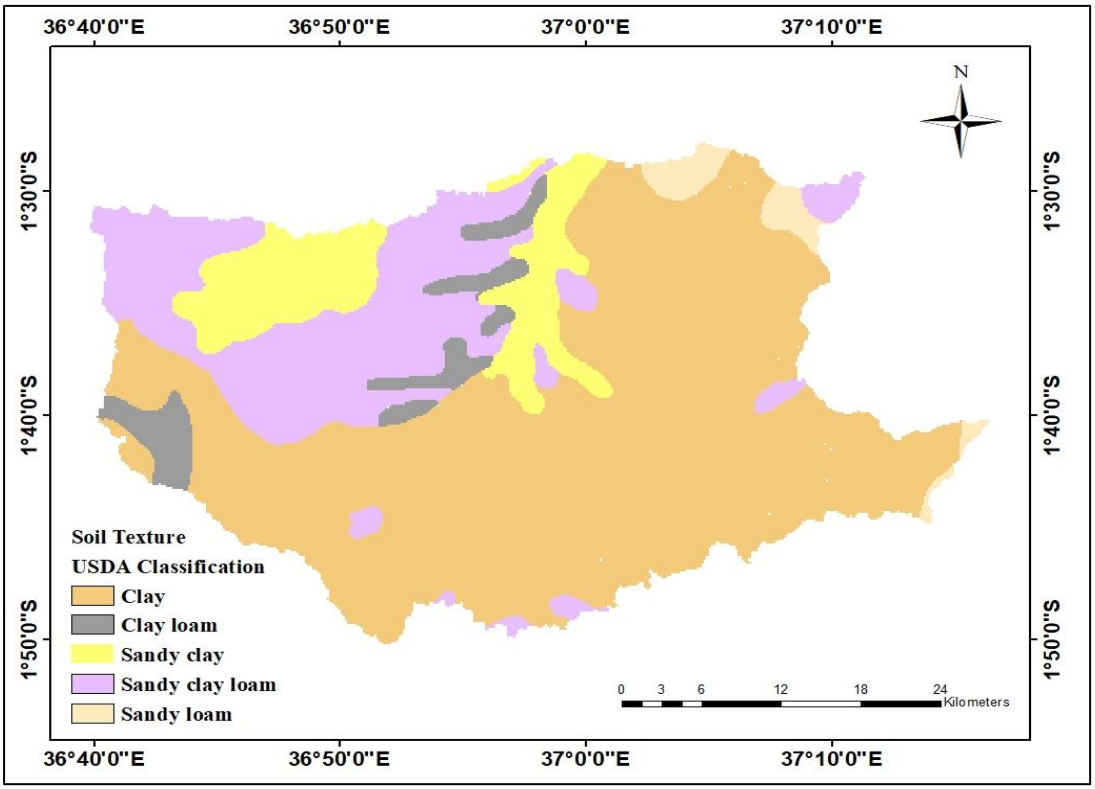

Figure 4. 15: Spatial distribution of soil texture

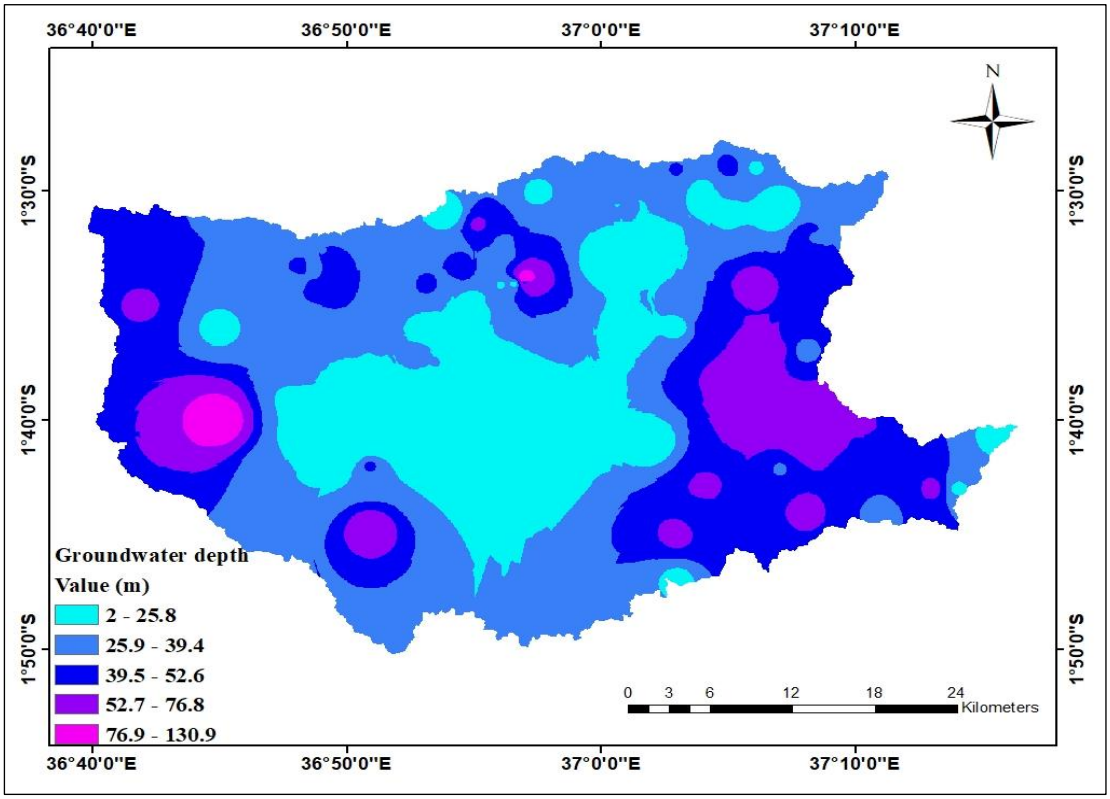

Figure 4. 16: Spatial groundwater depth map

4.2.3 Temporal Variations of Groundwater Recharge

WetSpass-M model outputs for the average monthly water balance components between 1984 and 2017 are presented in Table 4.13. The monthly groundwater recharge varied from 1.83 mm in July to 11.2 mm in March. Actual evapotranspiration ranged between 2.8 mm to 109.3 mm in the months of July and April, respectively, Surface runoff was found to be lowest in July and August with a value of 0.03, which are the months with the lowest rainfall while the highest was recorded in April with an average of 24.9 mm. July and August are the months with the lowest rainfall while the highest was recorded in March and April. The results indicated that of the annual rainfall of 633.5 mm, 63% of the groundwater recharge occurs during the two rainy seasons of March to April and October to December while the rest 36% occur in the dry season between June and September and January and February.

Elsewhere. Kahsay *et al*. (2018b) demonstrated that out of the average annual rainfall of 710 mm in Raya valley, northern Ethiopia, 84% of the recharge occurs in summer (wet season), while 16% ocurs during winter (dry season). Rwanga (2018) reported that about 88.04% of the annual groundwater recharge occurs during the wet season (summer) and the remaining 11.96% during dry season (winter) in Central Limpopo province of South Africa.

Al-Kuisi and El-Naqa (2013) showed that 95% of the recharge in the Jafr basin, Jordan occurs during winter and the remaining 5% in summer. Gebremeskel and Kebede (2017) reported that of the 77% annual rainfall received during the rainy season in the Werii watershed of the Tekeze River Basin, Ethiopia, 65% is recharged while 35% is recharged in the dry season. The differences in the recharge values in different seasons were attributed to other factors that contribute to recharge such as soil type, topography, type of land use and land cover among others.

Table 4. 13: Monthly and annual hydrologic components between 1984 and 2017

	Jan	Feb	March	April	May	June	July	Aug	Sept	Oct	Nov	Dec	Total
Average Rainfall	41.6	39.8	77.6	137.9	77.3	15.1	4.7	6.7	8.7	38.7	113.1	72.3	633.5
1984													
Actual ET.	31.15	28.26	53.76	109.27	60.84	10.70	2.89	4.24	4.68	28.51	89.91	53.62	**477.8**
Surface Runoff	1.23	1.42	12.81	24.45	9.00	0.13	0.03	0.03	0.14	0.93	14.18	9.29	**73.63**
GW Recharge	9.30	10.16	11.31	7.81	7.90	4.34	1.79	2.39	3.88	9.27	10.43	9.69	**88.28**
1995													
Actual ET.	30.96	28.06	53.36	109.44	60.64	10.64	2.87	4.21	4.62	28.31	89.83	53.27	**476.2**
Surface Runoff	1.14	1.35	12.58	23.38	8.68	0.12	0.03	0.03	0.14	0.85	13.29	8.99	**70.58**
GW Recharge	9.53	10.38	11.69	8.13	8.19	4.39	1.81	2.42	3.93	9.49	10.85	10.08	**90.89**
2005													
Actual ET.	30.71	27.81	53.31	109.73	60.46	10.45	2.79	4.12	4.52	28.04	90.23	53.25	**475.4**
Surface Runoff	1.52	1.71	13.37	24.84	9.45	0.22	0.06	0.07	0.20	1.20	14.53	9.76	**76.94**
GW Recharge	9.43	10.29	11.15	7.29	7.76	4.48	1.85	2.47	3.97	9.44	9.97	9.53	**87.62**
2017													
Actual ET.	30.46	27.59	53.06	108.86	59.99	10.34	2.76	4.08	4.49	27.81	89.58	53.01	**472.0**
Surface Runoff	1.93	2.12	14.30	27.06	10.51	0.36	0.10	0.13	0.27	1.57	16.22	10.63	**85.18**
GW Recharge	9.30	10.14	10.68	6.88	7.43	4.47	1.85	2.45	3.93	9.33	9.39	9.08	**84.95**
TOTALs	**41.7**	**39.8**	**77.6**	**137.9**	**77.3**	**15.1**	**4.7**	**6.7**	**8.7**	**38.7**	**113.1**	**72.3**	**633.6**

Figure 4.17 shows the monthly values represented on a bar chart. From the table, there was an indication that the actual evapotranspiration and runoff increased with rainfall increase, while groundwater recharge reduced with increased rainfall. This was expected because the infiltration capacity of clay soils, which cover the greatest percentage does not necessarily match with an increase in rainfall.

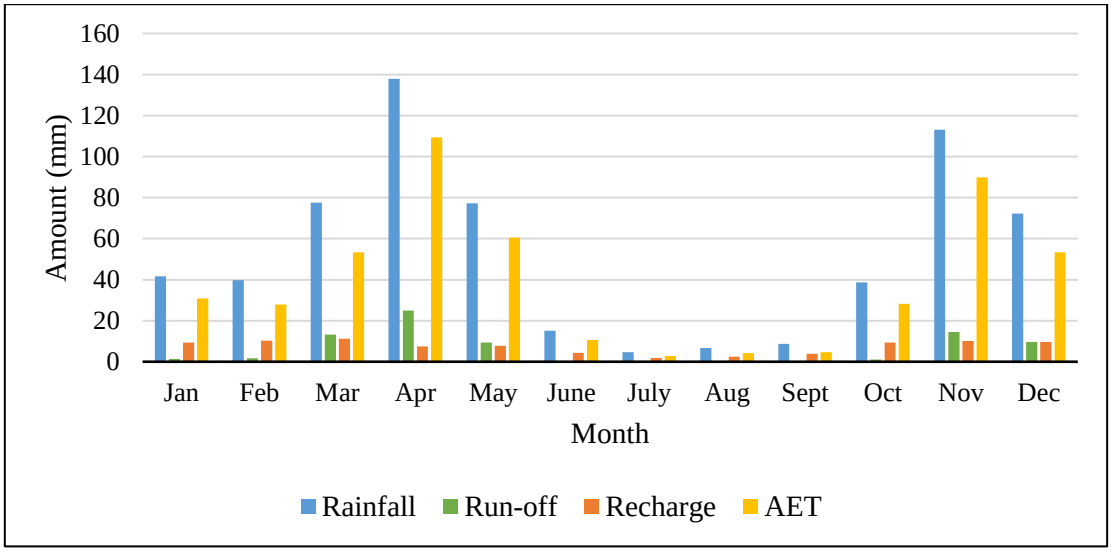

Figure 4. 17: Average monthly hydrological components

Table 4.14 presents the lumped up annual water balance for the four different temporal periods. Actual evapotranspiration varied from 478 mm in 1984 to 472 mm in 2017 while runoff showed an increase from 74 mm in 1984 to 85 mm in 2017. Annual recharge varied from 88 mm to 84 mm for the years 1984 and 2017, respectively. Results indicated that the annual rainfall of 633.5 mm is divided as 14% recharge, 12% runoff and 75% is lost through evapotranspiration. Both recharge and evapotranspiration indicated decreasing trends while surface runoff showed an increase over the study period.

The calculated hydrological components compared well with values reported by studies done elsewhere using WetSpass. Saghravani *et al*. (2013) showed that 12, 32 and 56% of rainfall received in Selangor, Malaysia was converted to recharge, surface runoff and evapotranspiration, respectively. Rwanga (2018) reported that the average annual groundwater recharge was 22.1% of the average annual precipitation of 475.8 mm in

Central Limpopo province of South Africa. Gebremeskel and Kebede (2017) reported that the long-term average annual precipitation (717 mm) is distributed as 90.7% evapotranspiration, 6% runoff, and 4.2% recharge. The annual rainfall of 53.5 mm received in Jafr basin, Jordan, is distributed as 4.9% surface runoff, 94.6%) evapotranspiration, and 0.5% recharge (Al-Kuisi and El-Naqa, 2013). According to Aish (2014), 77% of the precipitation received in the Gaza Strip is evapotranspiration, 11% is runoff and 12% becomes recharge.

Table 4. 14: Water balance components for the four temporal periods

	1984		1995		2005		2017	
Component	**Amount (mm)**	**%**	**Amount (mm)**	**%**	**Amount (mm)**	**%**	**Amount (mm)**	**%**
Actual Evapotranspiration								
Range	190-608		142-567		148-608		143-571	
Mean	478	75.3	476	75.1	475	74.9	472	74.4
Std, Dev.	39		42		44		54	
Surface runoff								
Range	25-420		24-488		25-512		24-512	
Mean	74	11.7	71	11.2	77	12.1	85	13.4
Std, Dev.	40		25		55		72	
Recharge								
Range	0-325		0-325		0-325		0-325	
Mean	88	13.8	91	14.3	87	13.7	84	13.2
Std, Dev.	38		37		35		34	

Figure 4.18 presents the percentage of each water balance component for the four temporal periods under different LULC. Actual evapotranspiration constituted 75.3% in 1984, 75.1% in 1995, 74.9 in 2005 and 74.4% in 2017 with an overall average of 75% while surface runoff was 11.7%, 11.2%, 12.1% and 13.4% for the same years. Groundwater recharge constituted 13.8%, 14.3%, 13.7% and 13.2% over the same period. The overall average of surface runoff and recharge was calculated as 12% and 14% of the annual rainfall. These values indicated a decrease in actual evapotranspiration and recharge and an increase in surface runoff.

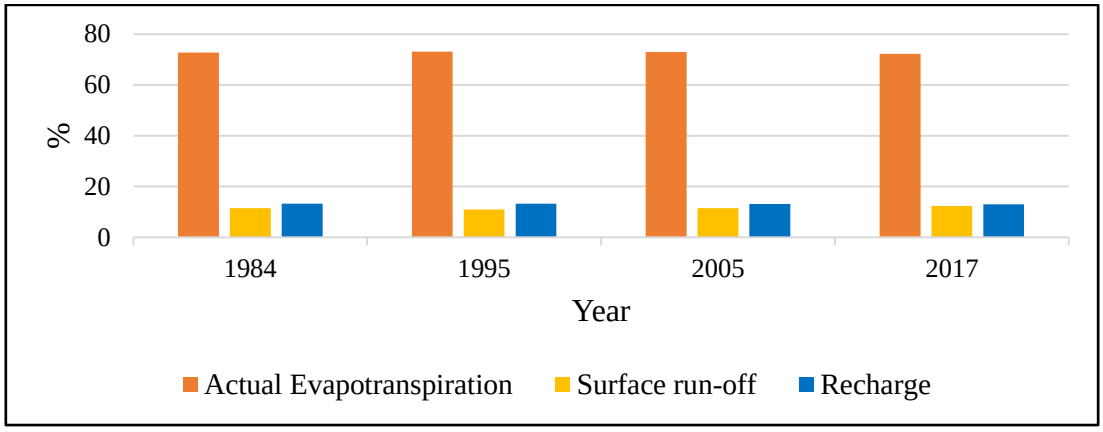

Figure 4. 18: Annual water balance components for the four temporal periods

Figure 4.19 presents the temporal trend of recharge and runoff in the sub-catchment from 1984 to 2017, which clearly indicated a decreased recharge but an increased runoff over the study period. Annual recharge varied from 88 mm to 84 mm for the years 1984 and 2017, respectively. The temporal variations were attributed to the fact that forested area, shrub and grass land in the sub-catchment were lost over time and converted to agricultural and built-up areas. Rangeland coverage as of 1984 was 98% while this has progressively reduced to 94% by the year 2017. On the other hand, agricultural and built-up areas increased from 0.1% to 4%. These LULC changes also contributed to a decrease in actual evapotranspiration and an increase in surface runoff.

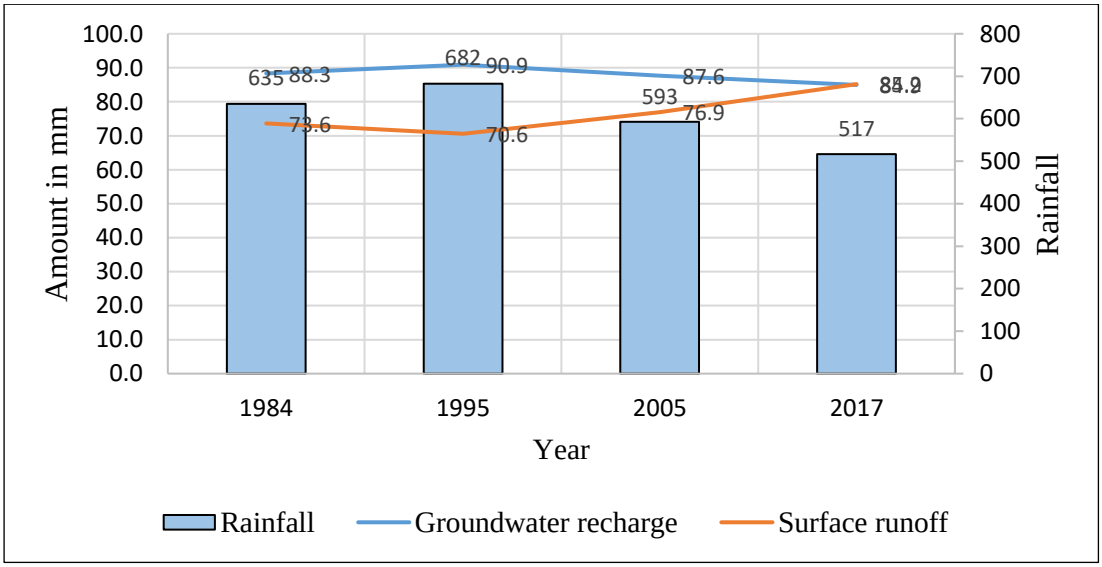

Figure 4. 19: Trend of annual recharge and surface runoff

Annual recharge in terms of volume was calculated as 153 million m^3 while the mean annual surface runoff was about 134 million m^3, which is about 11 million m^3 per month. Estimated annual recharge values in the neighbouring Nairobi County range between 109 to 320 million m^3 (Oiro *et al*., 2020). Kitheka, 2019 reported that the discharge of Stony Athi is 14 million m^3 per month. The figures of the present study compare favourably well with those of Oiro *et al*. (2020) and Kitheka (2019).

4.2.4 Spatial Variations of Groundwater Recharge

Spatial variability maps for groundwater recharge for the years 1984 and 2017 are presented in Figures 4.20 and 4.21. The maps show the different areas of low and high recharge potentials. The study showed that spatial recharge variation is strongly controlled by LULC and soil texture. The highest recharge was observed on sandy loam soils and forest cover, which was attributed to the fact that vegetation intercepts and slows down surface runoff in forested areas and hence allows more infiltration by the relatively high permeable sandy loam soils.

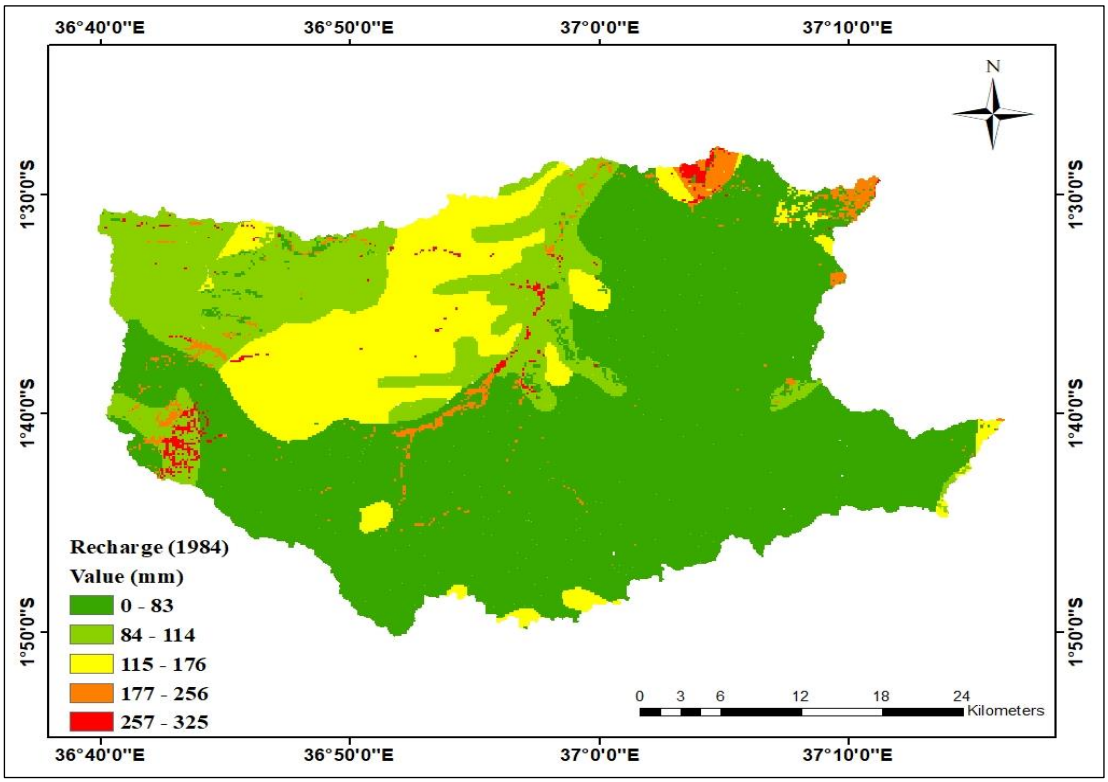

Figure 4. 20: Map of spatial distribution of annual recharge for 1984

The lowest recharge was observed on clay soil and built up areas due to the higher percentage of impervious surfaces in built up areas while clay soils have low permeability, which inhibits infiltration, but increase surface runoff. Agricultural and grassland show relatively similar recharge values for the same soil textures. Generally, areas located in the central and south-eastern parts have lower annual recharge because of heavy presence of clay soils while areas in the north-western parts show relatively high recharge due to more loamy and sandy soils. The high-altitude areas also show a relatively high annual recharge due to higher precipitation and high vegetation cover. However, much of the central parts of the sub-catchment have less amount of recharge due to lower precipitation. Higher values of recharge were observed in areas with permeable, sandy loam soils while low values are associated with clay soils. Areas with the highest recharge rates had the lowest runoff rates.

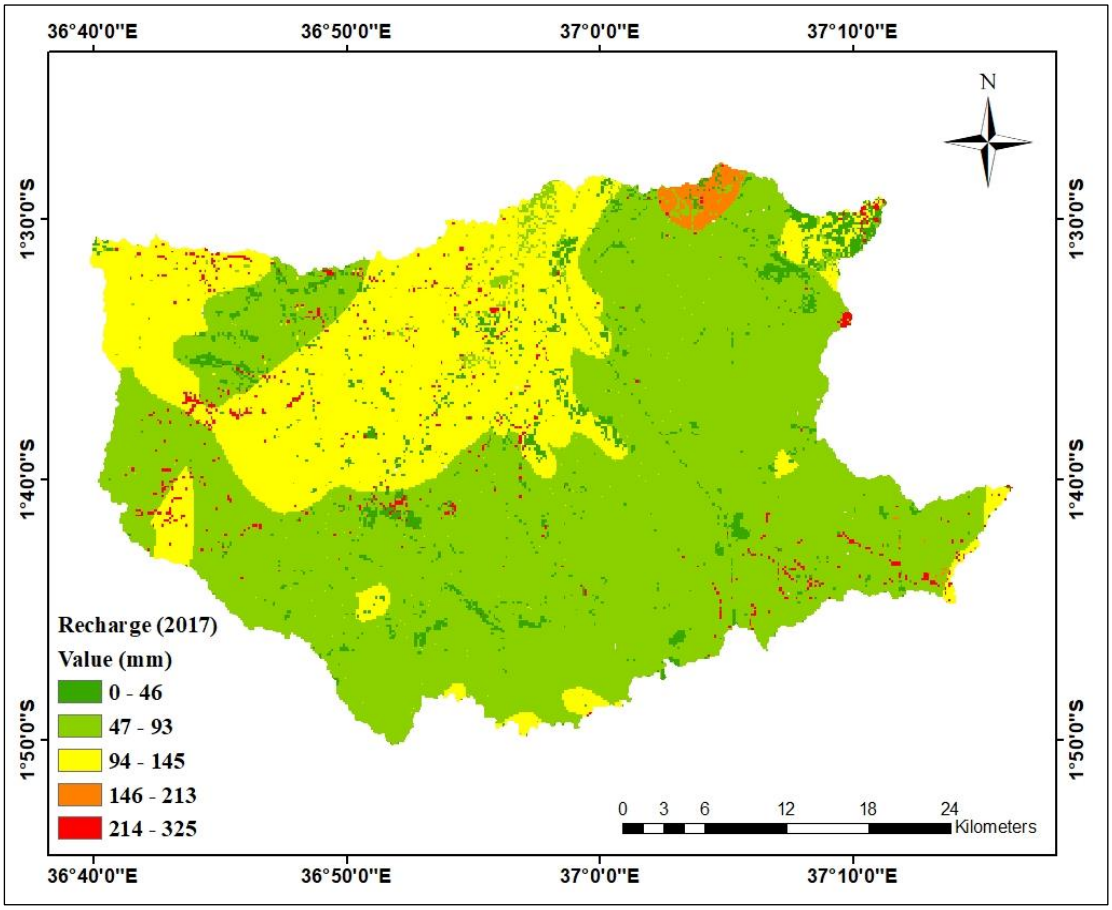

Figure 4. 21: Map of spatial distribution of annual recharge for 2017

4.2.5 LULC and Groundwater Recharge

Relationship between LULC and annual recharge is presented in Table 4.15 and Figure 4.22. In the forested area category, recharge rates are highest at 42.4% of the total recharge, followed by grassland, shrub land and agricultural land with 17.9%, 17.4%, and 15.6%, respectively. In the built-up areas, the annual recharge was found to be 6.6% while it is almost insignificant in bare land at 0.1%. Bare land and built up areas have low recharge rates due to increased soil compaction and impervious surfaces as well as presence of rock, which reduce water infiltration and increase runoff. In the case of forested areas, grassland and shrub land, there is higher water infiltration than surface runoff. The same case applies to agricultural land mainly because tilling favours infiltration capacity.

Table 4. 15: Relationship between LULC and groundwater recharge

LULC category	Recharge (mm)	%
Bare land	0.4	0.1
Built up area	38.9	6.6
Agricultural land	92.3	15.6
Shrub land	102.8	17.4
Grass land	106.1	17.9
Forested area	251.1	42.4

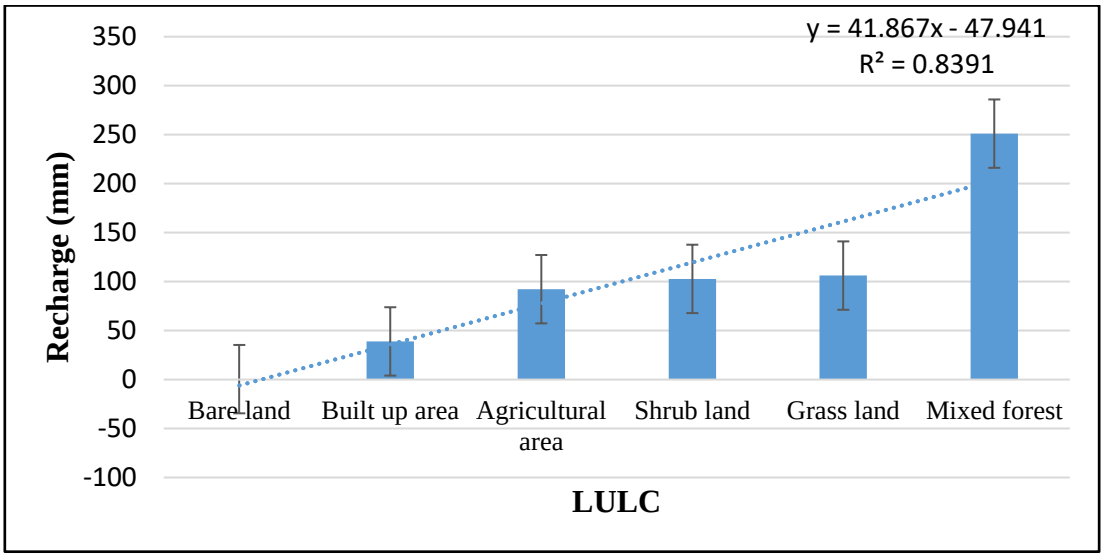

Figure 4. 22: Average annual recharge for different LULC categories

Presently, Kajiado County has a forest cover of 3.6%, which is 7.4% short of the constitutionally accepted 10% forest cover. According to the findings of this study, forest cover in the sub-catchment was 2.5% in 1984, which reduced to 1.4% in 2017. Therefore, the County Government should continuously promote tree planting campaigns in an effort to achieve the desired 10% forest cover.

4.2.6 Soil Texture and Groundwater Recharge

Soil texture plays a major role in recharge because it influences the rate of water infiltration. Coarse textured soils such as sandy loam have a higher capacity of infiltration than fine textured soils such as clay soils, which limits infiltration, leading to increased runoff. Table 4.16 and Figure 4.23 gives the mean recharge as a function of soil texture in the Stony Athi sub-catchment. The highest recharge occurs on sandy loam (30.6%) and sandy clay loam (21.8%) followed by sandy clay (17.9%), clay loam (17.6%) while clay has the least values of 12.0% of the total annual recharge.

Table 4. 16: Groundwater recharge for different soil textures

Soil texture	Hydraulic conductivity (m/s)	Average recharge (mm)	Percentage (%)
Sandy loam	3.45×10^{-5}	168.9	30.6
Sandy clay loam	6.31×10^{-6}	120.5	21.8
Sandy clay	2.45×10^{-6}	98.8	17.9
Clay loam	2.17×10^{-6}	97.1	17.6
Clay	1.28×10^{-6}	66.2	12.0

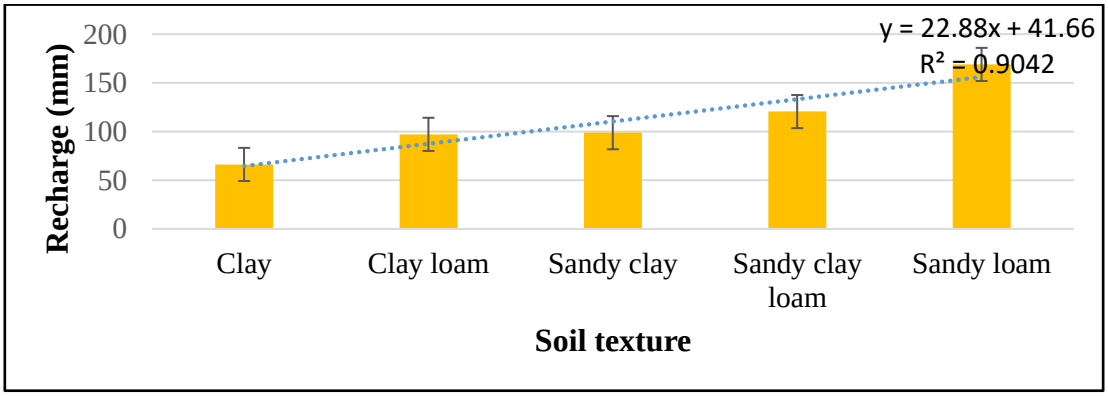

Figure 4. 23: Groundwater recharge for different soil textures

Table 4.17 and Figure 4.24 shows the annual groundwater recharge for various LULC and soil texture combinations. The highest recharge was observed on sandy loam soils and forested area at 197 mm/year while the lowest recharge is on clay soils and built up areas at 35 mm/year. Agricultural and grassland show relatively similar recharge values for the same soil textures. Shrub land show relatively higher values than grassland, but less than forested area while bare land exhibit relatively higher values compared to the built-up areas.

Table 4. 17: Average recharge for different combinations of LULC and soil texture

Soil texture / LULC	Sandy loam	Sandy clay loam	Clay loam	Sandy clay	Clay
Built-up area	49	46	44	45	35
Bare land	84	73	59	52	36
Agricultural land	136	130	107	102	67
Grassland	146	125	114	101	69
Shrub land	172	127	105	100	73
Forested area	197	181	171	170	138

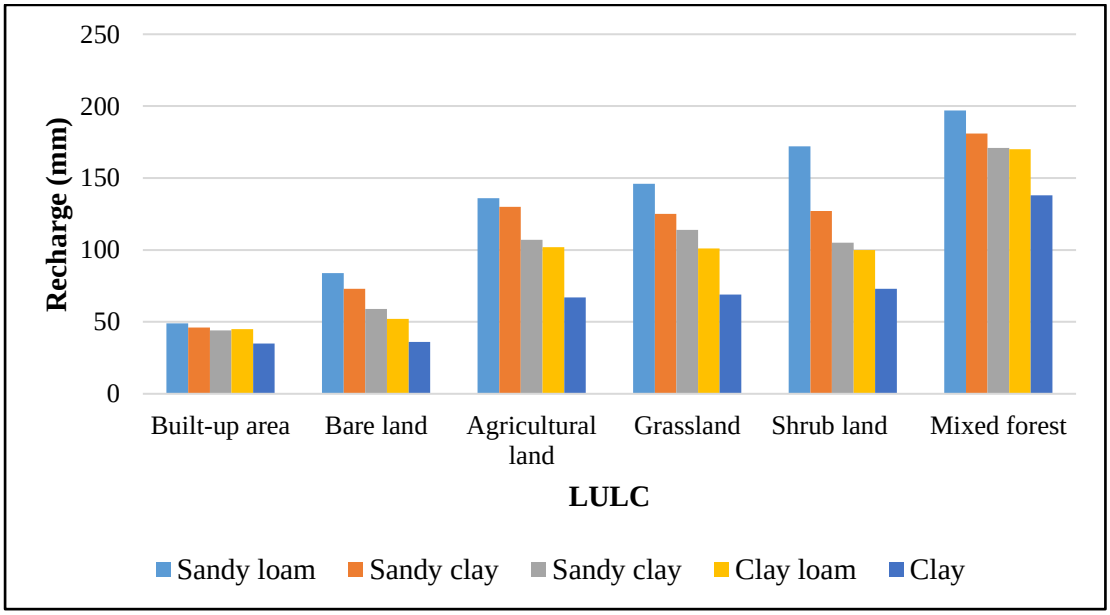

Figure 4. 24: Groundwater recharge for different combinations of LULC and soil texture

4.2.7 WetSpass-M model Validation

Comparison of the WetSpass-M generated groundwater recharge and the global modelled data of river discharge downloaded from the Global Flood Awareness System (GloFAS) is presented in Table 4.18 and Figure 4.25. Surface runoff is at its peak in April during the long March – May rainy season and lowest in August and September. High runoff is again observed during the short October – December rainy season. Moderate runoff is observed in January and February.

Table 4. 18: Comparison of GloFAS runoff and WetSpass simulated runoff

Month	GloFAS runoff data (mm)	Wetspass runoff data (mm)
January	7.68	1.45
February	9.43	1.65
March	10.12	13.27
April	23	24.93
May	11.64	9.40
June	4.51	0.21
July	0	0.05
August	0	0.06
September	0	0.19
October	0.92	1.14
November	7.21	14.56
December	4.44	9.67

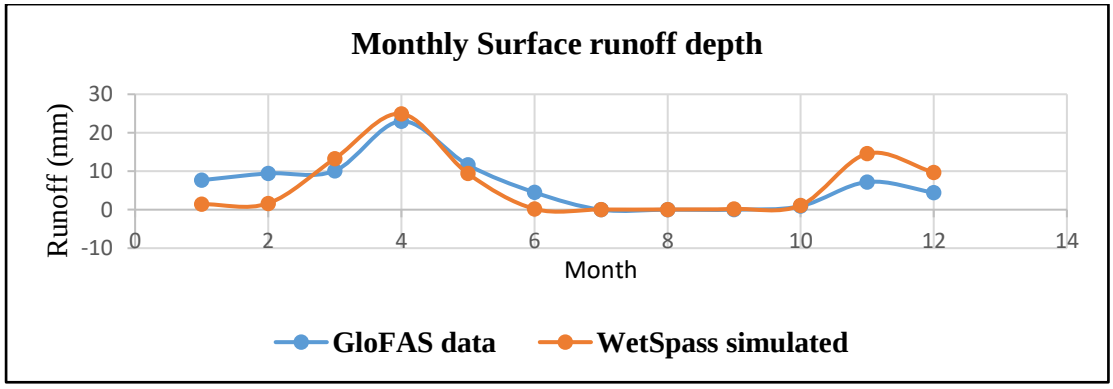

Figure 4. 25: GloFAS surface runoff versus WetSpass simulated surface runoff for the year 2017

4.2.8 Significance of Temporal Groundwater Recharge Variations

The second hypothesis stated that the land use and land cover changes that have occurred between 1984 and 2017 have a significant influence on groundwater recharge. The WetSpass-M simulated results indicated that although variations were observed, the changes were not statistically significant at $p < .05$ as shown in Table 4.19.

Table 4. 19: Chi-Square goodness of fit for water balance - 1984 - 2017

	1984	1995	2005	2017		
Component	**Amount (mm)**	**Amount (mm)**	**Amount (mm)**	**Amount (mm))**	**df**	**p-value**
Actual Evapotranspiration	478	476	475	472	3	0.998
Surface runoff	74	71	77	85	3	0.701
Recharge	88	91	87	84	3	0.962

4.3 Groundwater Vulnerability to Pollution

The third specific objective was to evaluate the influence of LULC changes on groundwater vulnerability to pollution in Stony Athi sub-catchment. This was achieved by using the Modified DRASTIC model; a modification of the conventional DRASTIC vulnerability model to include the LULC factor.

4.3.1 Depth to Water Level (D)

Depth to the water level in the study area was grouped into five classes with a range of between 4.6 m to more than 30 m below the surface. The ratings ranged between 1 and 7 (Table 4.20). The depth to water rating map is shown in Figure 4.26.

Table 4. 20: Depth to water level (Weight (Dw) = 5)

Range (m)	**Rating (Dr)**	**Total Weight (Dw x Dr)**
4.6 – 9.1	7	35
9.1 – 15.2	5	25
15.2 – 22.8	3	15
22.8 – 30.4	2	10
>30.4	1	5

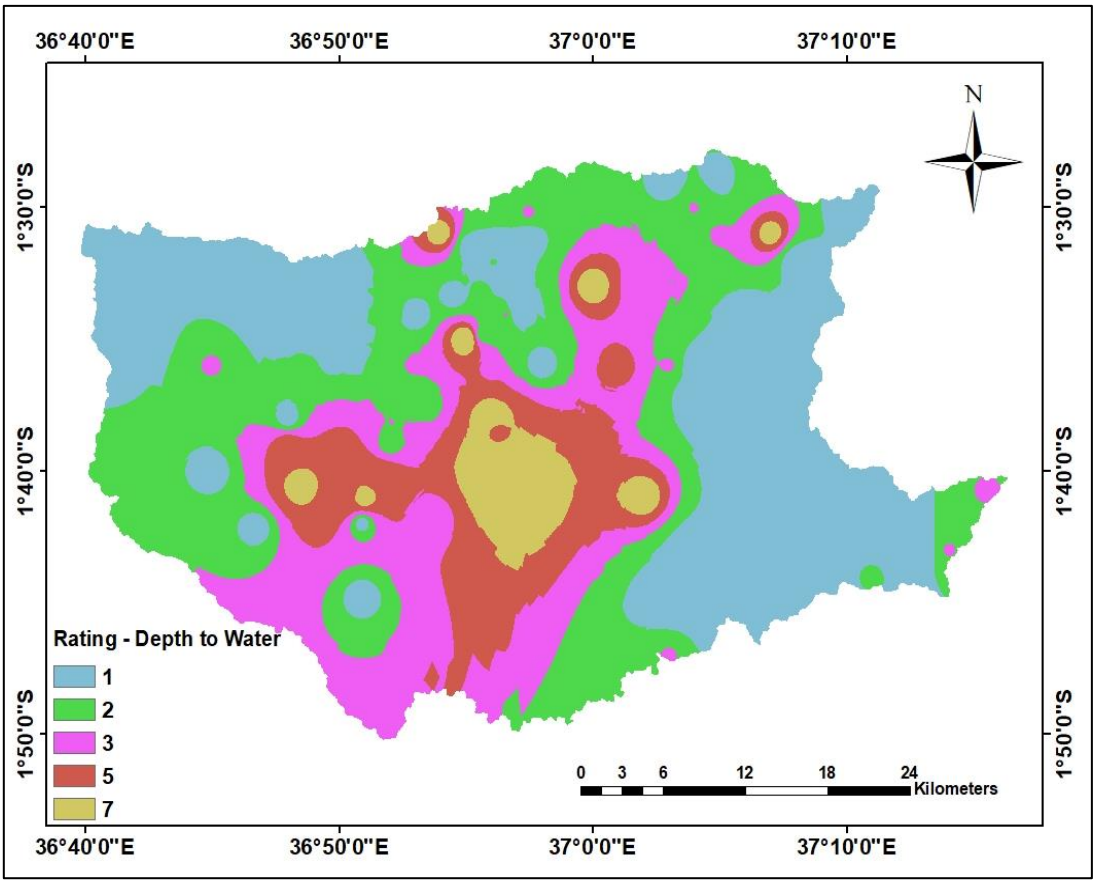

Figure 4. 26: Depth to groundwater rating map

4.3.2 Net Recharge (R)

Net recharge was generated from the WetSpass-M Model, which gave values in the range of 0 – 357 mm/year. The ranges were grouped into four classes while rating values were between 1 and 8 (Table 4.21). The rating map is presented in Figure 4.27.

Table 4. 21: Net Recharge (Weight (Rw) = 4)

Range (mm)	Rating (Rr)	Total Weight (Rw x Rr)
0 – 50.8	1	4
50.8 – 101.6	3	12
101.6 – 177.8	6	24
177.8 – 254.0	8	32

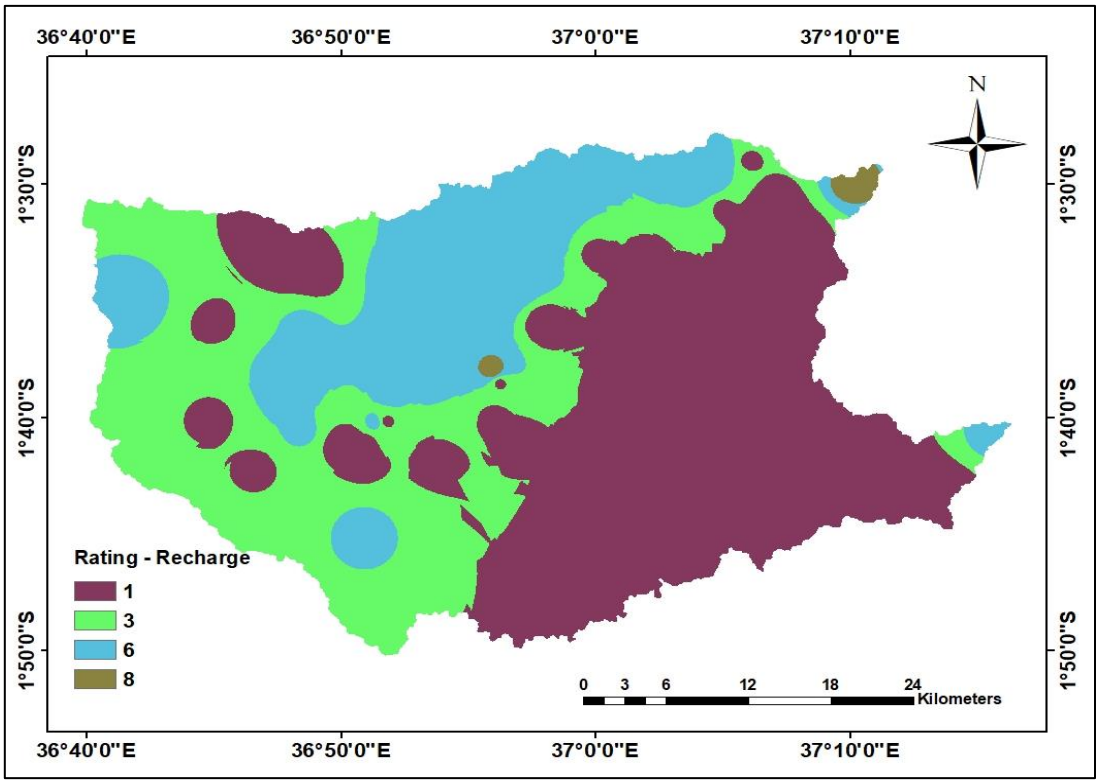

Figure 4. 27: Net recharge rating map

4.3.3 Aquifer Media (A)

The aquifers were classified into the different rock systems with differing hydraulic characteristics. Basement metamorphic rock aquifers, comprised of quartzo-feldspathic and granitoid gneisses, have the least permeability. The volcanic aquifers, comprised of phonolites and tuffs show moderate permeability. Areas where the volcanic rocks are highly fractured have high values of transmissivity. The contact zones between the two rock formations, comprised of sediments have a relatively higher permeability. The rates and weights of the aquifer media were classified into the three groups (Table 4.22). The interpolated raster map of the aquifer media is shown in Figure 4.28.

Table 4. 22: Aquifer Media (Weight (Aw) = 3)

Range	Rating (Ar)	Total Weight (Aw x Ar)
Sediments	8	24
Volcanics	4	12
Basement	3	9

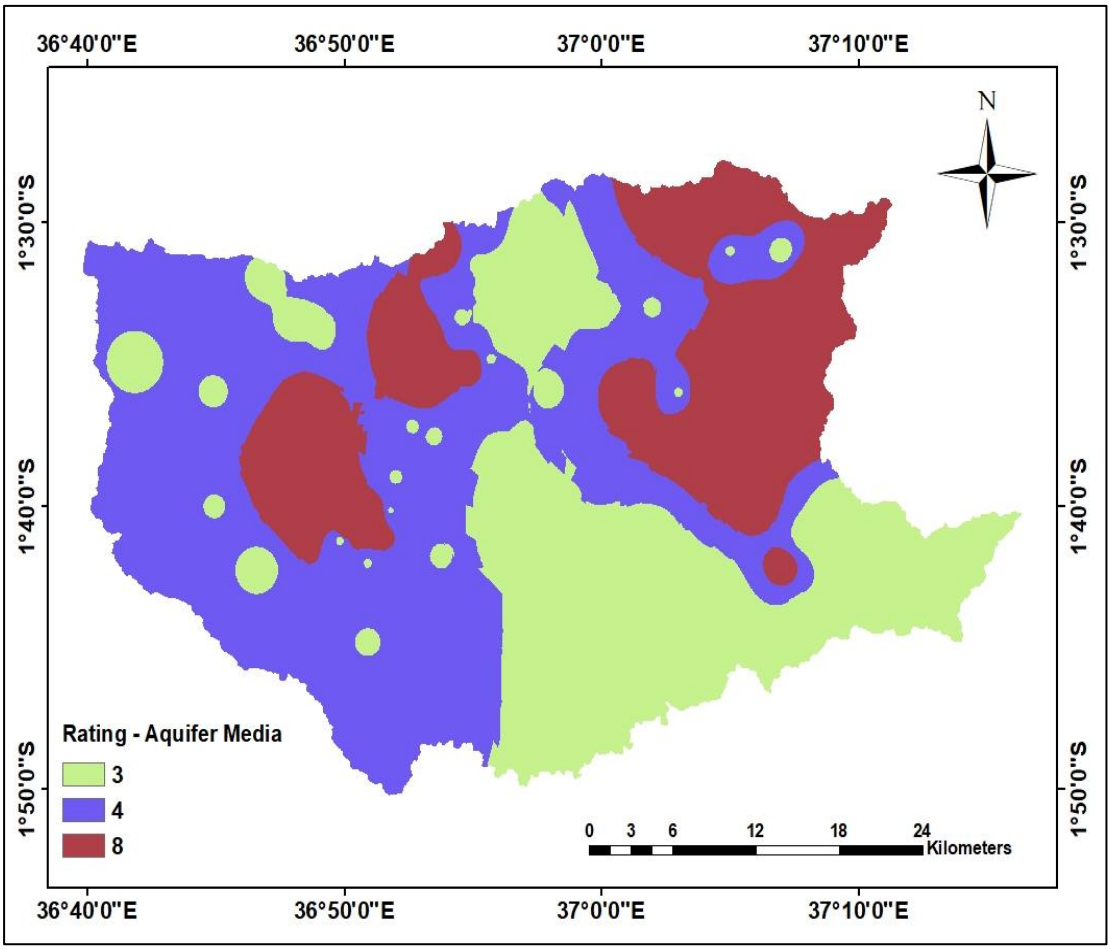

Figure 4. 28: Aquifer media rating map

4.3.4 Soil Media (S)

Soils in the study area comprises of sandy loam, sandy clay loam, clay loam, sandy clay and clay (Table 4.23). The rates were assigned as per the original DRASTIC values ranging between 1 and 6 for the different soil types. The soils were classified into four groups as shown in the rating map (Figure 4.29).

Table 4. 23: Soil Media (Weight (Sw) = 2)

Range	Rating (Sr)	Total Weight (Sw x Sr)
Clay	1	2
Clay loam	3	6
Loam	5	10
Sandy loam	6	12

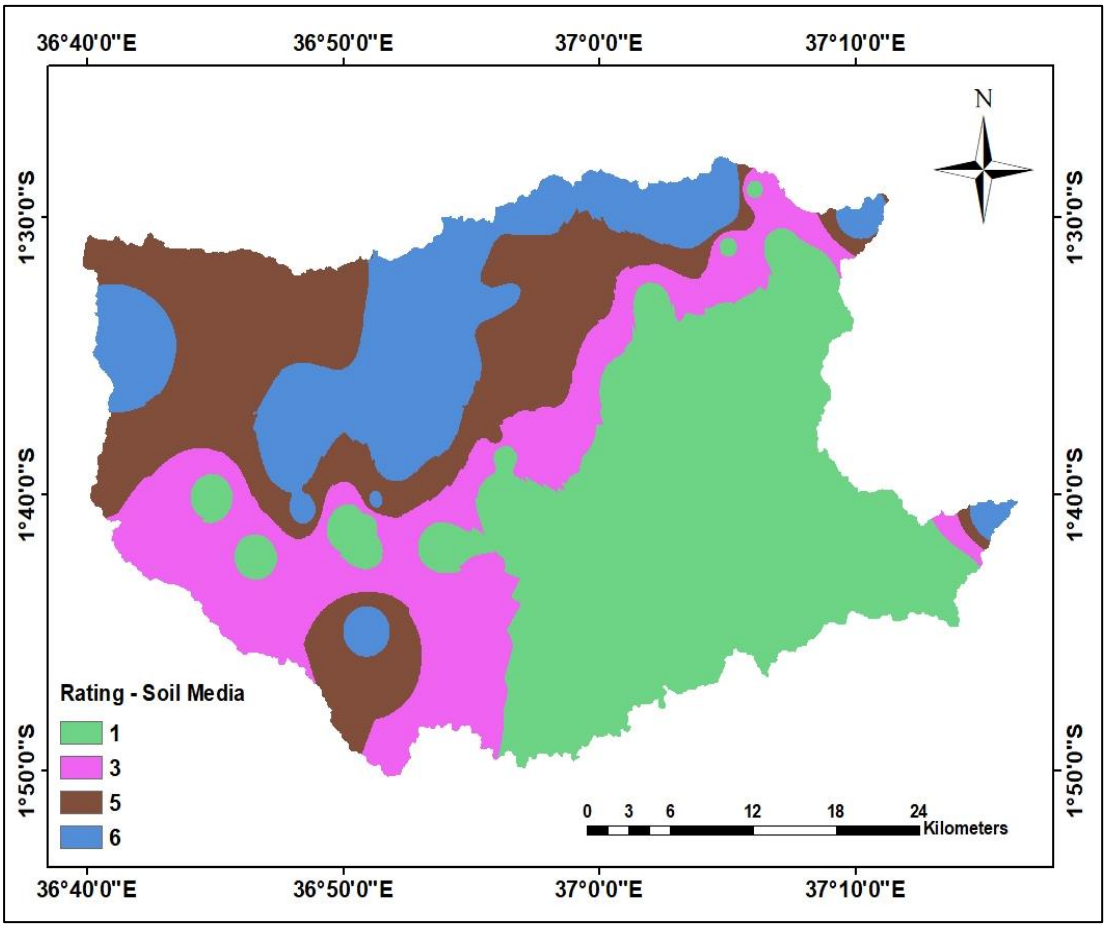

Figure 4. 29: Soil media rating map

4.3.5 Topography (T)

Topography was split into four classes in the range of 0 – 2%, 2 – 6% and 6 – 12% and 12 – 18% and assigned rates as per the original DRASTIC model ranging between 3 and 10 (Table 4.24). The rating map is presented in Figure 4.30.

Table 4. 24: Topography (Weight (Tw) = 1)

Range (%)	Rating (Tr)	Total Weight (Tw x Tr)
0-2	10	10
2-6	9	9
6-12	5	5
12-18	3	3

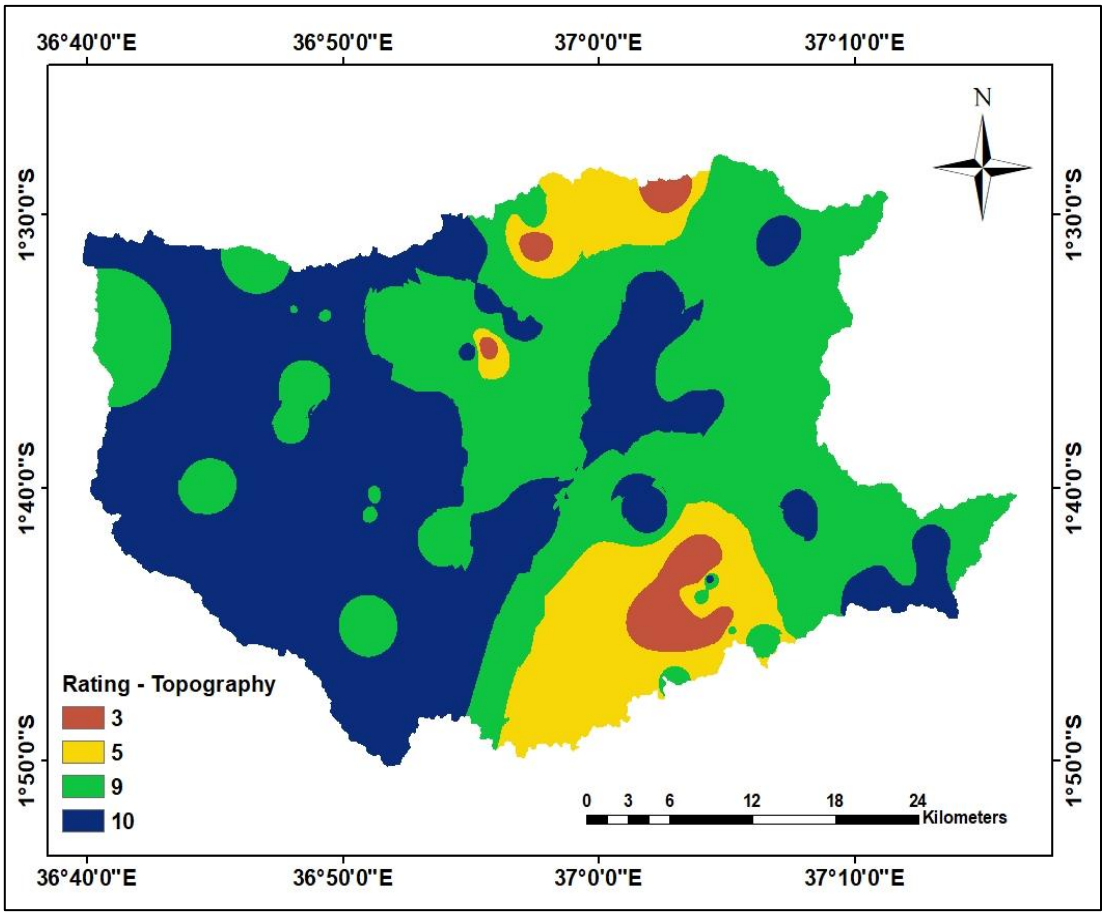

Figure 4. 30: Topography (slope) rating map

4.3.6 Impact of the Vadose Zone (I)

Vadose zone was designated with clay in areas covered with volcanic tuff. Clay is the main product of weathering of tuff. Areas covered by phonolite were designated as a confining layer, since the phonolites are not intensely weathered. Areas covered by the basement rocks were designated as sand and gravel with silt. The parameters were converted into a grid map and values assigned as presented in Table 4.25 and Figure 4.31, with ratings ranging between 1 and 6.

Table 4. 25: Impact of vadose zone (Weight (Iw) = 5)

Range	Rating (Ir)	Total Weight (Iw x Ir)
Confining layer	1	5
Clay	3	15
Sand and gravels with silt	6	30

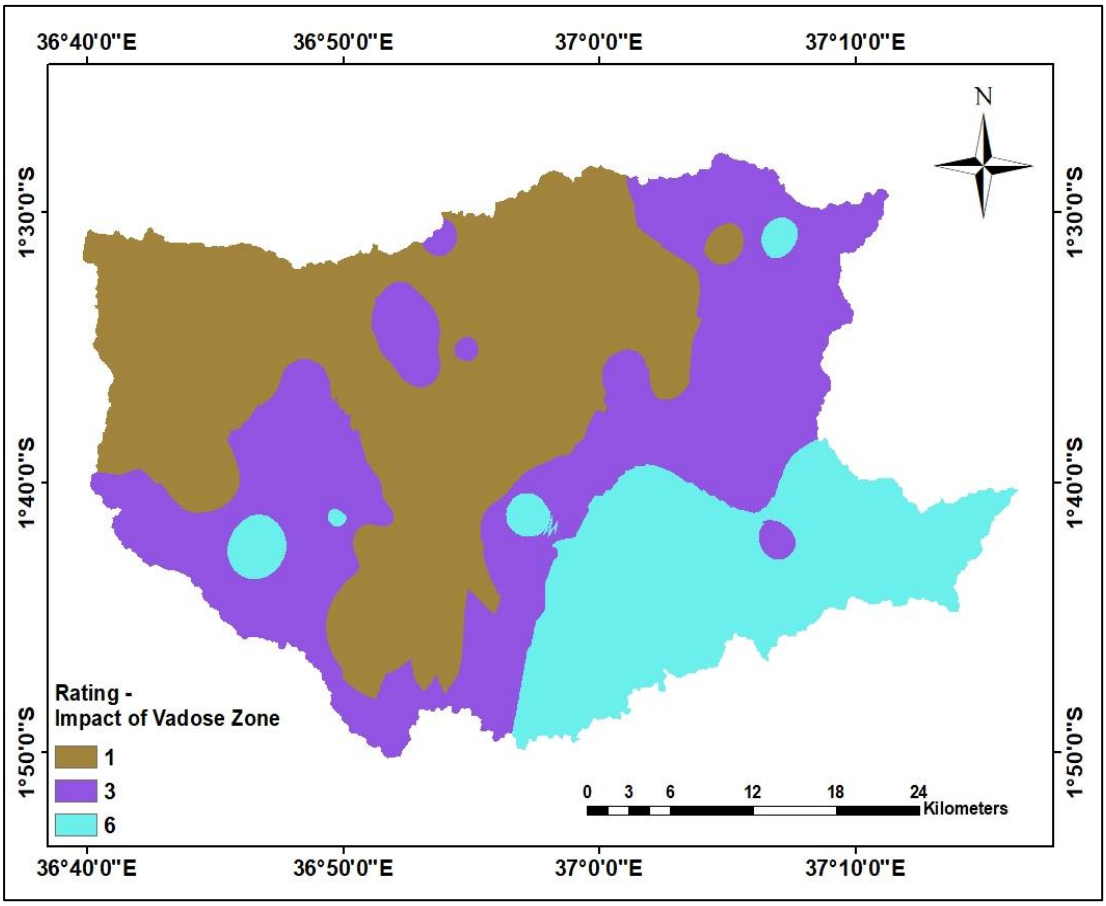

Figure 4. 31: Impact of vadose zone rating map

4.3.7 Hydraulic Conductivity (C)

Aquifer types were grouped into 3 classes, namely fractured basement, fractured volcanic rocks and sediments with values of hydraulic conductivity ranging between 0.04 and 28.7 m/day (Table 4.26). The spatial distribution of the hydraulic conductivity ratings is presented in Figure 4.32.

Table 4. 26: Hydraulic conductivity (Weight (Cw) = 3)

Aquifer type	Range (m/day)	Rating (Cr)	Total Weight (Cw x Cr)
Fractured basement	0.04 – 4.1	1	3
Fractured volcanic rocks	4.1 – 12.3	2	6
Sediments	12.3 – 28.7	4	12

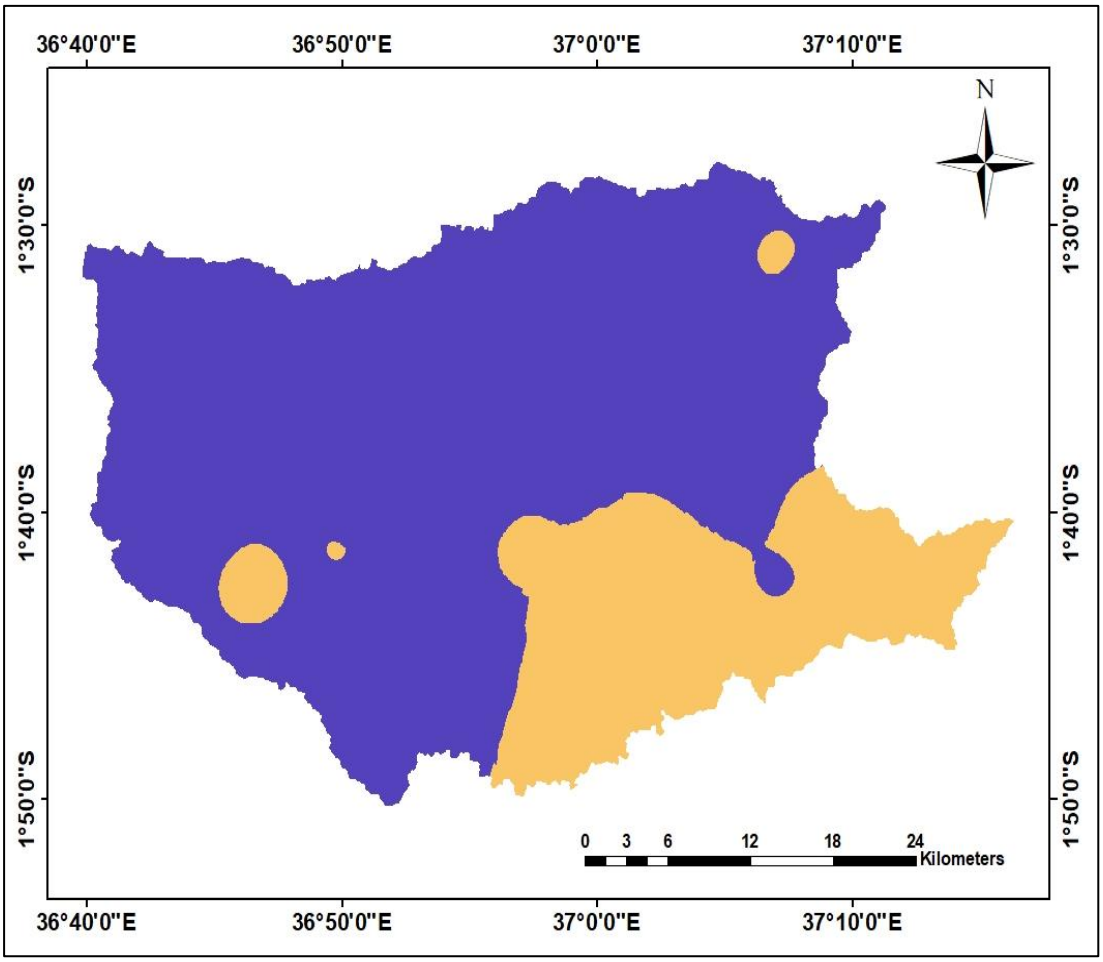

Figure 4. 32: Hydraulic conductivity rating map

4.3.8 DRASTIC Vulnerability Index (DVI)

DRASTIC vulnerability index values ranged between a minimum of 40 and 130. Based on the USEPA DRASTIC Index, the study area falls under low to moderate vulnerability category when LULC has not been factored. The vulnerability map shown in Figure 4.33 shows that the central regions are more vulnerable to groundwater pollution. This observation was attributed to the lower slope terrains that is mostly covered with loam and sandy loam soils which allow enhanced infiltration. Furthermore, the centrally located areas have the most human activities, including real estate developments and horticultural farms.

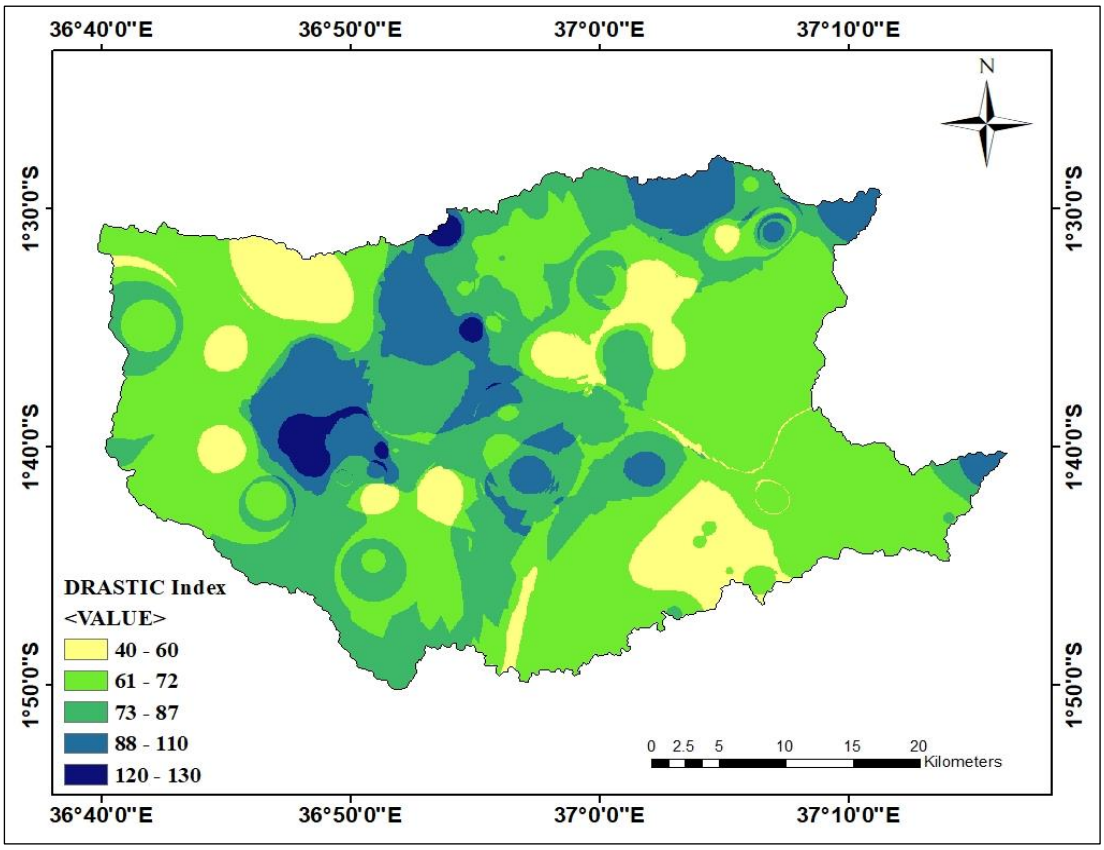

Figure 4. 33: DRASTIC vulnerability Index map

4.3.9 Modified DRASTIC Vulnerability Index (MDVI)

The Modified DRASTIC model is a modification of the conventional DRASTIC model to include the LULC parameter. The five categories of LULC were assigned ratings ranging between 2 and 7 (Table 4.27), with built up areas having the highest vulnerability and forested area with the least vulnerability rating.

Table 4. 27: Land use and land cover (Weight (Lw) = 5)

Range	Rating (Sr)	Total Weight (Sw x Sr)
Built up area	7	35
Agricultural land	5	25
Bare land	3	15
Grass land	2	10
Shrub land	2	10
Forested area	2	10

The LULC rating maps were overlaid on the DVI map to generate modified DRASTIC vulnerability index (MDVI) maps for the four temporal periods. MDVI maps for 1984 and 2017 are presented in Figures 4.34 and 4.35. Basing on US EPA classification, the MDVI results were classified into low, moderate and high vulnerability. The areal coverage and percentage of vulnerability categories is presented in Table 4.28.

Table 4. 28: Modified DRASTIC indexes between 1984 and 2017

		1984		1995		2005		2017	
Vulnerability class	**Range**	**Area (km^2)**	**%**	**Area (km^2)**	**%**	**Area (km^2)**	**%**	**Area (km^2)**	**%**
Low	<100	1,431	87	1,437	87	1,436	87	1,433	87
Moderate	101-140	198	12	188	11	188	11	148	9
High	140-150	24	1	28	2	29	2	72	4

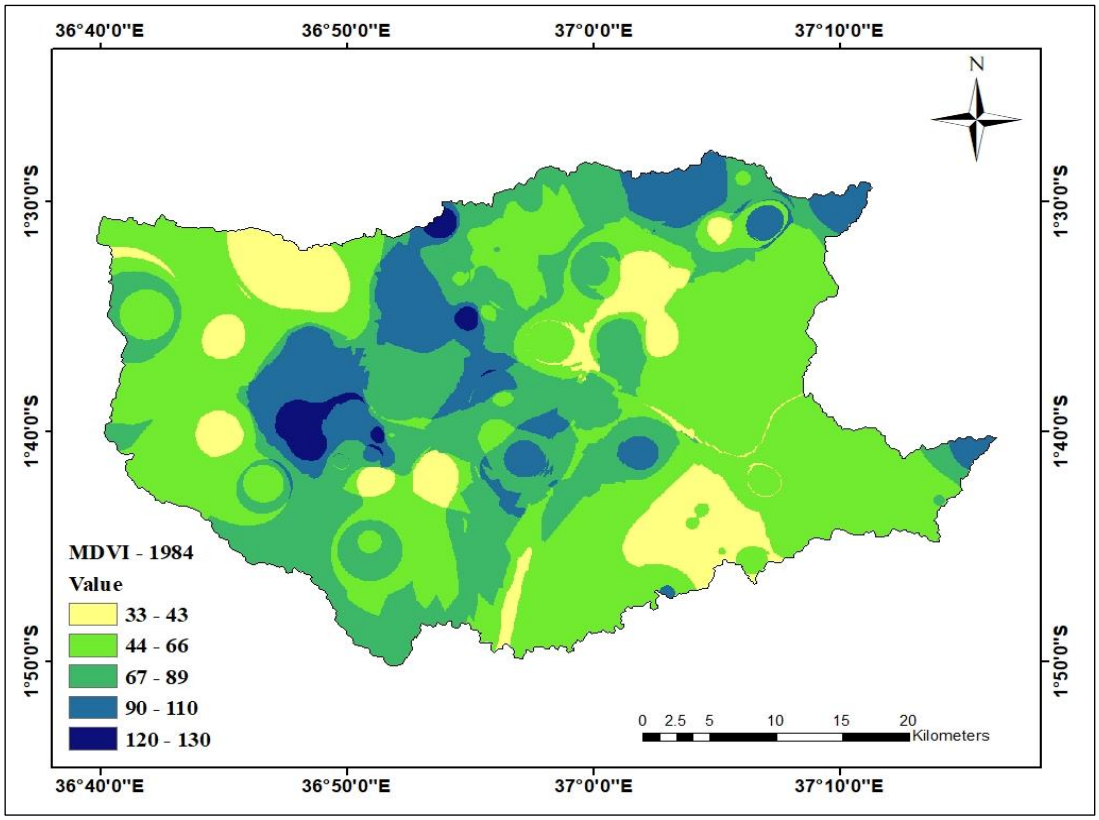

Figure 4. 34: Modified DRASTIC vulnerability Index map for 1984

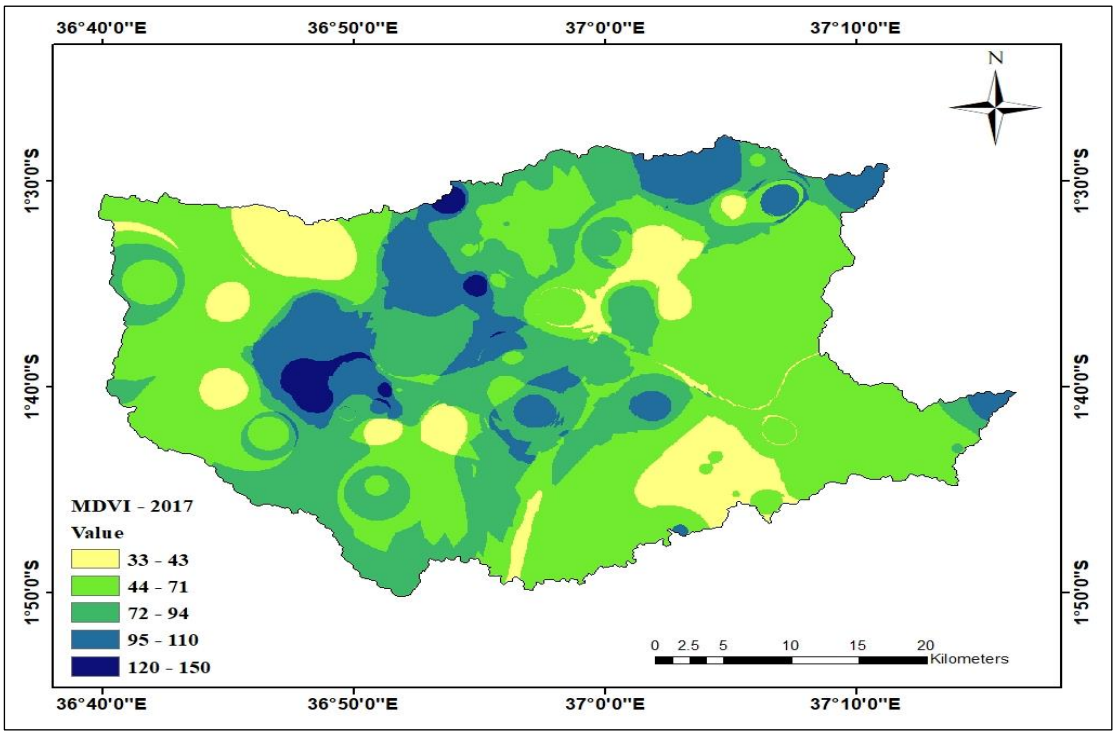

Figure 4. 35: Modified DRASTIC vulnerability Index map for 2017

Area coverage with low vulnerability varied from 1,431 km^2 in 1984, 1,437 km^2 in 1995, 1,436 km^2 in 2005 and 1,433 km^2 in 2017, indicating very minor changes. Moderate vulnerability category ranged from 198 km^2 in 1984 to 148 km^2 while the area with high vulnerability was 24 km^2 and 72 km^2 in 1984 and 2017, respectively. Results indicated that although 87% area coverage remained under low vulnerability category between 1984 and 2017, areas with high vulnerability increased from 1% in 1984 to 4% in 2017 while the area with moderate vulnerability decreased from 12 to 9% over the same period.

The spatial MDVI vulnerability maps show that moderate to high vulnerability areas occur along a stretch extending from the north east to south west and tend to be aligned to the major roads and towns. These are the areas that witnessed accelerated land development and agricultural activities. The vulnerability classes in this stretch had MDVI that ranged from 101 to 150. Low vulnerability areas occur in the north-western and much of the south-eastern flanks, which are largely rangelands that have not been altered and have MDVI of less than 100.

Since all the parameters, apart from LULC, were kept constant, then this indicated that changes in LULC transformed 3% of the area from moderate to high vulnerability category over the period under study. Moreover, groundwater vulnerability index ranged from 40 – 130 for the DRASTIC model while the range was 33 – 150 for the Modified DRASTIC model. This difference was attributed to the increase in agricultural and built up areas and the decrease in forested areas.

4.3.10 Modified DRASTIC Model Validation

The derived results of MDVI were correlated with nitrate concentration data measured in selected boreholes that were spatially distributed within the study area to validate the modified vulnerability index map as presented in Table 4.29. The trend line of the scatter plot of nitrate concentration against the MDVI index in Figure 4.36 indicates a positive correlation between the two parameters at $R^2 = 0.4489$.

Table 4. 29: Nitrate concentration and vulnerability index for 2017

Longitude	Latitude	Nitrate concentration (mg/l)	MDVI
36.8402	-1.6797	5.99	61
36.7792	-1.7025	6.8	89
36.8641	-1.6784	1.4	38
36.8952	-1.6958	13.7	102
36.774	-1.629	6	89
36.839	-1.689	6.1	84
36.838	-1.685	6.8	84
36.905	-1.678	15.38	84

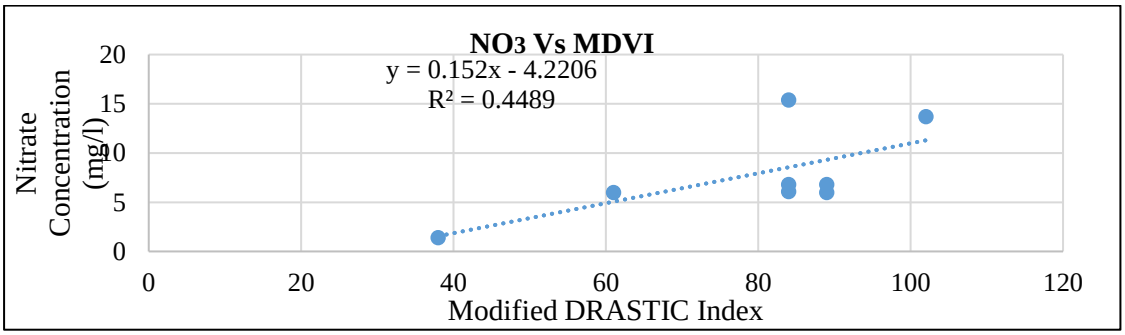

Figure 4. 36: Correlation between nitrate concentration and MDVI

4.3.11 Significance of Temporal Groundwater Pollution Vulnerability

The third hypothesis stated that LULC changes have a significant influence on the vulnerability to pollution in Stony Athi sub-catchment. Results indicated that 87% of the study area has a very low vulnerability (Table 4.30), while areas with moderate vulnerability decreased from 12% to 9% between 1984 and 2017. Areas with high vulnerability increased from 1% to 4% in 2017. Chi-test goodness of fit test showed that changes in areas with moderate and high vulnerability were significant while changes in areas with low vulnerability were insignificant at $p< 0.05$ (Table 4.30),

Table 4. 30: Chi-Square goodness of fit for pollution vulnerability

		1984	**1995**	**2005**	**2017**		
Vulnerability class	**Range**	**Area (km^2)**	**Area (km^2)**	**Area (km^2)**	**Area (km^2)**	**df**	***P value***
Low	<100	1,431	1,437	1,436	1,433	3	0.9994
Moderate	101-140	198	188	188	148	3	0.0426
High	140-150	24	28	29	72	3	<0.00001

CHAPTER FIVE: SUMMARY, CONCLUSSION AND RECOMMENDATIONS

5.1 Summary

This study's main objective was to establish the influence of LULC changes on groundwater recharge and its vulnerability to pollution in the Stony Athi sub-catchment between 1984 and 2017. The objective was accomplished through three specific objectives that sought to quantify the extent and magnitude of LULC changes that have occurred in the sub-catchment between 1984 and 2017; to estimate the spatial-temporal variations of recharge due to land use and land cover changes; and to evaluate the influence of land use and land cover changes on groundwater vulnerability to pollution. The specific objectives assisted in answering the research questions outlined in section 1.3 herein.

Significant ($p<0.05$) land use and land cover changes were observed in the study area between 1984 and 2017. The observed LULC changes means an increased demand for water leading to more abstraction as was evidenced by increased sinking of boreholes. The observed LULC changes were also associated with the observed decreased groundwater recharge and increased surface runoff, which cause high flooding during the rainy season. The LULC changes also contributed to more vulnerability of groundwater pollution. However, the LULC impacts on groundwater recharge and pollution vulnerability were found to be statistically insignificant.

Overall, changes in land use/land cover accounted for only 0.6% reduction in mean annual groundwater recharge between 1984 and 2017. Although, the 0.6% reduction recharge appears minute, this might become pronounced if the current rate of population growth, urbanization and agricultural growth continues. Therefore, proper and regulated land development should be policy priorities to reduce loss of rangelands and promote groundwater recharge for sustainability. On a spatial scale, variation of groundwater recharge was found to be highly controlled by LULC and soil texture.

This study also demonstrated the importance of WetSpass, a GIS-based physically-based spatially-distributed model in assessing the influence of LULC to groundwater recharge. The WetSpass-M model gives results in both numerical values and maps of the spatial distribution of three hydrological components, namely recharge, surface runoff and actual evapotranspiration. On the other hand. the GIS-based DRASTIC application used in this study produced groundwater vulnerability maps that can be used as a predictor of relative groundwater vulnerability.

5.2 Conclusions

Based on the results of this study, the following conclusions were made:

1. The study provided valuable insights on the extent, nature and magnitude of LULC changes that has occurred in Stony Athi sub-catchment between 1984 and 2017. Built-up area coverage increased from 0.04% in 1984 to 3.4% in 2017 while agricultural land increased from 0.06% in 1984 to 0.7% in 2017. On the other hand, rangelands decreased from 95.3% in 1984 to 92.7% in 2017 while forested area decreased from 2.5% in 1984 to 1.4% in 2017. Gains in built-up areas and agricultural land were associated with loss of rangelands and forested area. The study results indicated significant changes ($p<0.05$) for all LULC classes. Thus, the alternative hypothesis for the first objective was accepted.

2. Groundwater recharge in Stony Athi sub-catchment decreased from 88 mm in 1984 to 84 mm in 2017. Comparison between the groundwater recharge and LULC over the investigated period indicated that areas with reduced recharge rates correspond to increased built-up and agricultural areas. Increased urban developments were associated with the creation of more impervious surfaces, which impede infiltration. Similarly, cultivated areas promote surface runoff while vegetated areas promote recharge and impede runoff. Results from the study indicated that the LULC changes that have occurred between 1984 and 2017 do not have a significant ($p<0.05$) influence on groundwater recharge. Therefore, the alternative hypothesis for the second objective was rejected.

3. Groundwater vulnerability to pollution indicated that area coverage with low vulnerability was 198 km^2 (12%) in 1984 and 148 km^2 (9%) in 2017 while areas with moderate vulnerability was 24 km^2 (1%) and 72 km^2 (4%) in 1984 and 2017, respectively. 87% of the sub-catchment area was categorized as having low pollution vulnerability. Statistics indicated that changes in LULC transformed 3% of the area from low to moderate vulnerability category over the period under study. However, the LULC impact on groundwater vulnerability to pollution was not statistically significant. Thus, the alternative hypothesis was rejected.

5.3 Recommendations

The following recommendations were made:

i) The National and the Kajiado County Government should continuously update and enforce land use and zoning policies and frameworks. Such frameworks should be anchored by appropriate laws to mitigate against uncontrolled land use practices and to manage urban and industrial expansion. The study is a foundation for further research with the aim of modeling and predicting future LULC scenarios.

ii) The study further recommends more studies on spatially distributed long-term groundwater recharge across the country with the ultimate objective of producing a spatial groundwater recharge map of Kenya. The WetSpass-M model has been found to be a useful tool for evaluating the long term spatially distributed recharge. The model is also useful for assessing effects of LULC changes as well as climate change on the water regime in a catchment, especially in areas undergoing rapid LULC changes. Moreover, the WetSpass-M model can also be used for evaluation of surface runoff and actual evapotranspiration.

iii) Continuous quantitative monitoring of groundwater pollution risk should be conducted and other areas undergoing rapid LULC changes to prevent detrimental effects of groundwater pollution due to anthropogenic activities.

iv) Future research in the study area could focus on other possible factors, which might affect groundwater flow dynamics in the study area. Moreover, further studies could be carried out to take into account the impact of climate change in conjunction with land use and land cover changes to both surface and groundwater resources.

REFERENCES

Abdollahi, K., Bashir, I., Verbeiren, B., Harouna, M. R., Griensven, A. V., Huysmans, M., & Batelaan, O. (2017). A distributed monthly water balance model: formulation and application on Black Volta Basin. *Environmental Earth Science*, *76*(5)

Abdollahi, K., Bazargan, A., & McKay, G. (2018). Water balance models in environmental modelling. *Handbook of Environmental Materials Management*, 1-16. https://doi.org/10.1007/978-3-319-58538-3_119-1

Abdulrafiu, O. M., Adebola, A., & Oladele, O. (2016). Vulnerability assessment of groundwater pollution in the vicinity of an active dumpsite (Olusosun), Lagos, Nigeria. *Chemistry International*, *2*(4), 232-241

Adenuga, K.I., Mahmoud, A.S., Dodo, Y.A., Albert, M., Kori, S.A., Danlami, N.J. (2021). Climate change adaptation and mitigation in sub-Saharan African countries. In: Asif M (ed) Energy and environmental security in developing countries. Advanced sciences and technologies for security applications. Springer, Cham. https://doi.org/10.1007/978-3-030-63654-816

African Development Bank (2019). East Africa Economic Outlook 2019. Macroeconomic Developments and Prospects. Political Economy of Regional Integration**.** https://www.afdb.org/en/documents/document/regional- economic-outlook-2019-east-africa-108658

Aish, A.M. (2014). Estimation of water balance components in the Gaza Strip with GIS based WetSpass model.2014. *Civil and Environmental Research*, *6*(11). https://www.iiste.org

Al-Abadi, A.M., Al-Shamma'a, A.M., & Aljabbar, M.H. (2017). A GIS-based DRASTIC model for assessing intrinsic groundwater vulnerability in north-eastern Missan governorate, Southern Iraq. *Applied Water Science, 7*(1), 89-101

Albhaisi, M., Brendonck, L., & Batelaan, O. (2013). Predicted impacts of land use change on groundwater recharge of the upper Berg catchment, South Africa. *Water SA, 39*(2). https://doi: 10.4314/wsav39i2.4

Ali, M., & Mubarak, S. (2017). Approaches and methods of quantifying natural groundwater recharge – A Review. *Asian Journal of Environment and Ecology, 5*(1), 1-27. https://doi.org/10.9734/ajee/2017/36987

Al-Kuisi, M., & El-Naqa, A. (2013). GIS based spatial groundwater recharge estimation in the Jafr basin, Jordan - Application of WetSpass models for arid regions: *Revista Mexican de Ciencias Geologicas, 30*(1), 96-109

Aller, L., Bennet, T., Lehr, J. H., Petty, R. J., & Hachet, G. (1987). DRASTIC: A standardized system for evaluating groundwater pollution potential using hydro-geological settings. EPA/600/2-87/035. U.S. Environmental Protection Agency, Ada, OK, USA

Amwata, D. A., Nyariki, D. R., & Musimba, N. R. (2015). Factors influencing pastoral and agropastoral household vulnerability to food insecurity in the Dry lands of Kenya: A case study of Kajiado and Makueni Counties. *Journal of International Development, 28*(5), 771-787. https://doi.org/10.1002/jid.3123

Anderson, W., Taylor, C., McDermid, S., Ilboudo-Nébié, E., Seager, R., Schlenker, W., Cottier, F., de Sherbinin, A., Mendeloff, D., & Markey, K. (2021). Violent conflict exacerbated drought-related food insecurity between 2009 and 2019 in sub-Saharan Africa. *Nature Food, 2*(8), 603–615. https://doi.org/10.1038/s43016-021-00327-4

Armanuos, A. M., Negm, A., Yoshimura, C., & Valeriano, O. C. (2016). Application of WetSpass model to estimate groundwater recharge variability in the Nile Delta aquifer. *Arabian Journal of Geosciences*, *9*. https://DOI 10.1007/s12517-016-2580-x

Arneth, A., F. Denton, F. Agus, A. Elbehri, K. Erb, B. Osman Elasha, M. Rahimi, M. Rounsevell, A. Spence, R. & Valentini, (**2019)**. Framing and Context. In: *Climate Change and Land: an IPCC special report on climate change, desertification, land degradation, sustainable land management, food security, and greenhouse gas fluxes in terrestrial ecosystems* (eds. Shukla, P. R. *et al*.) Ch. 1 (IPCC, 2019)

Asada, K., Eguchi, S., Ikeba, M., Kato, T., Yada, S., Nakajima, Y., & Itahashi, S. (2017). Modelling nitrogen leaching from Andosols amended with different composted manures using LEACHM. *Nutrient Cycling in Agro-ecosystems*, *110*(2), 307-326. https://doi.org/10.1007/s10705-017-9899-x

Barbash, J. E., & Voss, F. D. (2016). Design and testing of a process-based groundwater vulnerability assessment (P-GWAVA) system for predicting concentrations of agrichemicals in groundwater across the United States. *Scientific Investigations Report*. https://doi.org/10.3133/sir20145189

Batelaan, O., & De Smedt, F. (2001). WetSpass: A flexible, GIS based distributed recharge methodology for regional groundwater modelling. In: Gehrels, H., Peters, J., Hoehn, E., Jensen, K., Leibundgut, C., Griffioen, J., Webb, B., & Zaadnoordijk, W-J (eds). Impact of human activity on groundwater dynamics, Publ. no. 269. IAHS, Wallingford, 11–17

Batelaan, O., & Woldeamlak, S.T. (2007). User guide of WetSpass-M. http://www.vub.ac.be/WetSpa/introduction_WetSpass-M. htm

Bobadoye, A. O., Ogara, W. O., Ouma, G. O., & Onono, J. O. (2014). Comparative analysis of rainfall trends in different sub-counties in Kajiado County, Kenya. *International Journal of Innovative Research & Studies (IJRS)*, *3*(12), 179-195

Boretti, A., & Rosa, L. (2019). Re-assessing the projections of the world water development report. *Npj Clean Water*, *2*(1). doi: 10.1038/s41545-019-0039-9

Bullock, E. L., Healey, S. P., Yang, Z., Oduor, P., Gorelick, N., Omondi, S., Ouko, E., & Cohen, W. B. (2021). Three Decades of Land Cover Change in East Africa. *Land*, *10*(2), 150. https://doi.org/10.3390/land10020150

Butt, A., Shabbir, R., Ahmad, S. S., & Aziz, N. (2015). Land use change mapping and analysis using Remote Sensing and GIS: A case study of Simly watershed, Islamabad, Pakistan. *The Egyptian Journal of Remote Sensing and Space Science*, *18*(2), 251-259. https://doi.org/10.1016/j.ejrs.2015.07.003

Cassardo, C. (2014). Global warming and water sustainability. *E3S Web of Conferences*, *2*, 02006. https://doi.org/10.1051/e3sconf/20140202006

Chen, Q., Chen, H., Wang, J., Zhao, Y., Chen, J., & Xu, C. (2019). Impacts of climate change and land-use change on hydrological extremes in the Jinsha River Basin. *Water*, *11*(7), 1398. https://doi.org/10.3390/w11071398

Chiaka, J. C., & Zhen, L. (2021). Land Use, Environmental, and Food Consumption Patterns in Sub-Saharan Africa, 2000–2015: A Review. *Sustainability*, *13*(15), 8200. https://doi.org/10.3390/su13158200

CIDP, (2018). *Kajiado County Integrated Development Plan*, 2018-2022. https://www.kajiado.go.ke

Congalton, R. G., & Green, K. (2019). Assessing the Accuracy of Remotely Sensed Data, Principles and Practices, Third Edition, CRC Press. 328p

Dassargues A. (2018). *Hydrogeology: Groundwater Science and Engineering*. Taylor & Francis CRC press, 472p

Dimitriadou, S., & Nikolakopoulos, K.G. (2021). Evapotranspiration Trends and Interactions in Light of the Anthropogenic Footprint and the Climate Crisis: A Review. Hydrology 2021, 8, 163. https://doi.org/10.3390/ hydrology8040163

Duarte, L., Espinha M., J., & Teodoro, A. (2019). An open source GIS-based application for the assessment of groundwater vulnerability to pollution. *Environments, 6*(7), 86. doi.org/10.3390/environments 6070086

Durães, M. F., & De Mello, C. R. (2013). Groundwater recharge behavior based on surface runoff hydrographs in two basins of the Minas Gerais State. *Ambiente E Agua - an Interdisciplinary Journal of Applied Science*, *8*(2). https://doi.org/10.4136/ambi-agua.1127

El Mansouri, B., Kili, M., Chao, J., Fekri, A., & Mridekh, A. (2013). Mathematical Models as Tools for Prevention and Risk Estimates of Groundwater Pollution: Contributions and Challenges. *The Handbook of Environmental Chemistry*, 175-191. doi: 10.1007/698_2013_240

Earle, S. (2019). *Physical Geology – 2nd Edition*. Victoria, B.C.: BC campus. https://opentextbc.ca/physicalgeology2ed/

Edwards, P. J., Williard, K. W., & Schoonover, J. E. (2015). Fundamentals of watershed hydrology. *Journal of Contemporary Water Research & Education, 154*(1), 3-20. https://doi.org/10.1111/j.1936-704x.2015.03185.x

Ewusi, A., Asante-Annor, A., Seidu, J., & Fosu-Gyeabour, L. O. (2016). Groundwater vulnerability assessment using Drastic Index and GIS in Kumasi Metropolitan Assembly, Ghana. *Ghana Mining Journal*, *16*(1), 21 – 30

FAO, 2016. State of the World's Forests 2016. Forests and agriculture: land-use challenges and opportunities. Rome

Framing and Context, (2022). *Global Warming of 1.5°C*, 49–92. https://doi.org/10.1017/9781009157940.003

Ghazavi, R., & Ebrahimi, Z. (2015). Assessing groundwater vulnerability to contamination in an arid environment using DRASTIC and GOD models. *International Journal of Environmental Science Technology*, *12*, 2909–2918

Gebremeskel, G., & Kebede, A. (2017). Spatial estimation of long-term seasonal and annual groundwater resources: application of WetSpass model in the Werii watershed of the Tekeze River Basin, Ethiopia. *Physical Geography*, *38*(4), 338-359. http://doi.org/10.1080/02723646.2017.1302791

Gebreyohannes, T., De Smedt, F., Walraevens, K., Gebresilassie, S., Hussien, A., & Hagos, M., & Gebrehiwot, K. (2013). Application of a spatially distributed water balance model for assessing surface water and groundwater resources in the Geba basin, Tigray, Ethiopia. *Journal of Hydrology*, *499*, 110-123. https://doi: 10.1016/j.jhydrol.2013.06.026

Gleeson, T., Befus, K. M., Jasechko, S., Luijendijk, E., & Cardenas, M. B. (2015). The global volume and distribution of modern groundwater. *Nature Geoscience*, *9*(2), 161-167. https://doi.org/10.1038/ngeo2590

Government of the Republic of Kenya, (2014). State of the ASALs; Report for the Medium Term ASAL Program, Kajiado County; Ministry of Devolution and Planning, Directorate of Arid and Semi-arid Lands, Nairobi-Kenya

Government of the Republic of Kenya, (2018). National Climate Change Action Plan, 2018-2022. Ministry of Environment and Forestry, Nairobi

Gong, J., Hu, Z., Chen, W., Liu, Y., & Wang, J. (2018). Urban expansion dynamics and models in metropolitan Guangzou, China. *Land use policy, 72*, 100-109

Goswami, K. B., & Bisht, P. S. (2017). The Role of Water Resources in Socio-Economic Development. *International Journal for Research in Applied Science and Engineering Technology (IJRASET), 5*(XII), 1669-1674

Graf, R., & Przybyłek, J. (2018). Application of the WetSpass simulation model for determining conditions governing the recharge of shallow groundwater in the Poznań Upland, Poland. *Geologos, 24*(3), 189–205. https://doi: 10.2478/logos-2018-0020

Guth, A., & Wood, J (2013). Geology of the Kajiado Region, Kenya. *Maps of the Southern Kenya Rift*. https://doi:10.1130/2014.dmch016.s4

Guigui, X., Xiaosi, S., Yiwu, Z., & Bing, Y. (2021). Identifying potential sites for artificial recharge in the plain area of the Daqing river catchment using GIS-based multi-criteria analysis. *Sustainability 13*:3978. https://doiorg/103390/su13073978

Gupta, N. (2014). Groundwater vulnerability assessment using DRASTIC method in Jabalpur District of Madhya Pradesh. *International Journal of Recent Technology and Engineering*, *3*(3). ISSN: 2277-3878

Hall, J.W. Grey D., Garrick, D., Fung, F., Brown, C., Dadson, S.J., Sadof C.W. (2014). "Coping with the curse of freshwater variability," *Science*, *346*(6208), pp. 429–430. https://doi.org/10.1126/science.1257890

Harrigan, S., Zsoter, E., Alfieri, L., Prudhomme, C., Salamon, P., Wetterhall, F., Barnard, C., Cloke, H., and Pappenberger, F., (2020). GloFAS-ERA5 operational global river discharge reanalysis 1979–present, Earth Syst. Sci. Data, 12, 2043–2060. https://doi.org/10.5194/essd-12-2043-2020

Hughes, A., Mansour, M., Ward, R., Kieboom, N., Allen, S., Seccombe, D., Charlton, M., & Prudhomme, C. (2021). The impact of climate change on groundwater recharge: National-scale assessment for the British mainland. *Journal of Hydrology*, *598*, 126336. https://doi.org/10.1016/j.jhydrol.2021.126336

Islam, S., Singh, R. K., & Khan, R. A. (2016). Methods of estimating ground water recharge. *International Journal of Engineering Associates*, *5*(2). ISSN: 2320-0804) # 6

Jaseela, C., Prabhakar, K., & Harikumar, P. S. P. (2016). Application of GIS and DRASTIC Modeling for Evaluation of Groundwater Vulnerability near a Solid Waste Disposal Site. *International Journal of Geosciences*, *07*(04), 558–571. https://doi.org/10.4236/ijg.2016.74043

Jiménez, A. A., Vilchez, F.F., González, O.N., & Susana M. L. (2018). Analysis of the land use and cover changes in the Metropolitan Area of Tepic-Xalisco (1973–2015) through Landsat Images; *Sustainability*, *10*, 1860

Kahsay, G. H., Gebreyohannes, T., Gebremedhin, M. A., Gebrekirstos, A., Birhane, E., Gebrewahid, H., & Welegebriel, L. (2018b). Spatial groundwater recharge estimation in Raya basin, Northern Ethiopia: an approach using GIS based water balance model. *Sustainable Water Resources Management*, *5*(2), 961–975. https://doi.org/10.1007/s40899-018-0272-2

Karim, A., & Saeid, A. V. (2019). Harmonized world soil database in SWAT https://doi.org/10.1594/PANGAEA.901309

Kenya National Bureau of Statistics, & Statistics, (2019). *Kenya Population and Housing Census Results*. Kenya National Bureau of Statistics. https://docs.edtechhub.org/lib/5MHY2Y9G

Khosravi, K., Sartaj, M., Tsai, F. T.-C., Singh, V. P., Kazakis, N., Melesse, A. M., Prakash, I., Tien Bui, D., & Pham, B. T. (2018). A comparison study of DRASTIC methods with various objective methods for groundwater vulnerability assessment. *Science of the Total Environment*, *642*, 1032–1049. https://doi.org/10.1016/j.scitotenv.2018.06.130

Khouni, I., Louhichi, G., & Ghrabi, A. (2021). Use of GIS based Inverse Distance Weighted interpolation to assess surface water quality: Case of Wadi El Bey, Tunisia. *Environmental Technology and Innovation*, *24*, 101892. https://doi.org/10.1016/j.eti.2021.101892

Kitheka, J. (2019). Salinity and salt fluxes in a polluted tropical river: The case study of the Athi River in Kenya. *Journal of Hydrology: Regional Studies*, *24*, 100614. doi: 10.1016/j.ejrh.2019.100614

Klemas, V., & Pieterse, A. (2015). Using remote sensing to map and monitor water resources in arid and semi-arid regions. *The Handbook of Environmental Chemistry*, 33-60. https://doi.org/10.1007/978-3-319-14212-8_2

Kohfahl, C., Molano-Leno, L., Martínez, G., Vanderlinden, K., Guardiola-Albert, C., & Moreno, L. (2019). Determining groundwater recharge and vapor flow in dune sediments using a weighable precision meteo lysimeter. *Science of the Total Environment*, *656*, 550–557. https://doi.org/10.1016/j.scitotenv.2018.11.415

Kumar, C. P. (2016). Assessing the Impact of Climate Change on Groundwater Resources. National Institute of Hydrology, India

Kumar, G., Sena, D.R., Kurothe, R.S., Pande, V.C., Rao, B.K., Vishwakama, A.K., Bagdi, G.L., & Mishra, P.K. (2014). Watershed impact evaluation using remote sensing. *Journal of Current Science 106(10):*1369-1378

Kuria, Z. (2013). Groundwater Distribution and Aquifer Characteristics in Kenya. *Developments in Earth Surface Processes*, 83–107. https://doi.org/10.1016/b978-0-444-59559-1.00008-6

Lang, D., Zheng, J., Shi, J., Liao, F., Ma, X., Wang, W., Chen, X., & Zhang, M. (2017). A Comparative Study of Potential Evapotranspiration Estimation by Eight Methods with FAO Penman–Monteith Method in Southwestern China. *Water*, *9*(10), 734. https://doi.org/10.3390/w9100734

MacDonald, A. M., Lark, R. M., Taylor, R. G., Abiye, T., Fallas, H. C., Favreau, G., Goni, I. B., Kebede, S., Scanlon, B., Sorensen, J. P. R., Tijani, M., Upton, K. A., & West, C. (2021). Mapping groundwater recharge in Africa from ground observations and implications for water security. *Environmental Research Letters*, *16*(3), 034012. https://doi.org/10.1088/1748-9326/abd661

Machiwal, D., Jha, M. K., Singh, V. P., & Mohan, C. (2018). Assessment and mapping of groundwater vulnerability to pollution: Current status and challenges. *Earth-Science Reviews*, *185*, 901–927. https://doi.org/10.1016/j.earscirev.2018.08.009

Malaki, P. A., Kironchi, G., Mureithi, S., & Kathumo, V. (2017). Assessing land use and land cover change using participatory geographical information system (PGIS) approach in Nguruman Sub-catchment, Kajiado North Sub County, Kenya. *Journal of Geography and Regional Planning*, *10*(8), 219-228. https://doi.org/10.5897/jgrp2016.0606

Maqsoom, A., Aslam, B., Khalil, U., Ghorbanzadeh, O., Ashraf, H., Faisal Tufail, R., Farooq, D., & Blaschke, T. (2020). A GIS-based DRASTIC Model and an Adjusted DRASTIC Model (DRASTICA) for Groundwater Susceptibility Assessment along the China–Pakistan Economic Corridor (CPEC) Route. *ISPRS International Journal of Geo-Information*, *9*(5), 332. https://doi.org/10.3390/ijgi9050332

Maria, R. (2018). Comparative studies of groundwater vulnerability assessment. *IOP Conference Series: Earth and Environmental Science*, *118*, 012018. https://doi.org/10.1088/1755-1315/118/1/012018

Matheson, F.J. (1966). *Geology of the Kajiado Area; Report No. 70*. Ministry of Natural Resources and Wildlife; Geological Survey of Kenya. https://library.wur.nl/isric/fulltext/isricu_i2753_001.pdf

Mehran, A., AghaKouchak, A., Nakhjiri, N., Stewardson, M. J., Peel, M. C., Phillips, T. J., Wada, Y., & Ravalico, J. K. (2017). Compounding impacts of human-induced water stress and climate change on water availability, *Scientific Reports*, *7*(1). https://doi.org/10.1038/s41598-017-06765-0

Meresa, E., Girmay, A., & Gebremedhin, A. (2019). Water Balance Estimation Using Integrated GIS-Based WetSpass Model in the Birki Watershed, Eastern Tigray, Northern Ethiopia. *Physical Science International Journal*, *22*(3), 1-17. https://doi: 10.9734/psij/2019/v22i330133

Moges, S.S., & Dinka M.O. (2021). Assessment of groundwater vulnerability using the DRASTIC model: A case study of Quaternary catchment A21C, Limpopo River Basin, South Africa. *Journal of Water and Land Development*, *49*(IV– VI) 35–46. doi 10.24425/jwld.2021.137094

Mohan, C., Western, A. W., Wei, Y., & Saft, M. (2018). Predicting groundwater recharge for varying land cover and climate conditions – a global meta-study. *Hydrology and Earth System Sciences*, *22*(5), 2689–2703. https://doi.org/10.5194/hess-22-2689-2018

Morara, M. K., MacOpiyo, L., & Kogi-Makau, W. (2014). Land-use, land cover change in urban pastoral interface: A case study of Kajiado County, Kenya;

Journal of Geography and Regional Planning, *7*(9), 192-202. https://doi.org/10.5897/jgrp2014.0448

Mulyadi, A., Dede, M., & Widiawaty, M. A. (2020). Spatial interaction of groundwater and surface topographic using geographically weighted regression in built-up area. *IOP Conference Series: Earth and Environmental Science*, *477*, 012023. https://doi.org/10.1088/1755-1315/477/1/012023

Mundia, C.N., & Njagi N. W. (2018). Modelling of Potential Sites for Underground Water in Semi-arid Areas. (2018a). *Journal of Applied Science, Engineering and Technology for Development*. https://doi.org/10.33803/jasetd.2017.3-1.5

Nyamasyo, S. K., & Kihima, B. O. (2014). Changing land use patterns and their mpacts on wild ungulates in Kimana Wetland Ecosystem, Kenya. *International Journal of Biodiversity;* Volume 2014, Article ID 486727, 10 pages

Ogutu, J.O., Piepho, H.P., Said, M.Y., & Shem C. Kifugo, S.C. (2014). Herbivore dynamics and range contraction in Kajiado County Kenya: Climate and land use changes, population pressures, governance, policy and human-wildlife conflicts. *The Open Ecology Journal, 7*, 9-31

Oiro, S., Comte, J., Soulsby, C., MacDonald, A., & Mwakamba, C. (2020). Depletion of groundwater resources under rapid urbanisation in Africa: recent and future trends in the Nairobi Aquifer System, Kenya. *Hydrogeology Journal*, *28*(8), 2635-2656. doi: 10.1007/s10040-020-02236-5

Olumuyiwa, O. F., Yemisi, A., & Olajumoke, O. (2017). Groundwater assessment and its intrinsic vulnerability studies using aquifer vulnerability index and GOD Methods. *International Journal of Energy and Environmental Science*, *2*(5), 103-116. https://doi: 10.11648/j.ijees.20170205.13

Onyancha, C. Sagi Dalyot, S. David Siriba, D. & Monika Sester, M. (2012). Modelling of spatial and temporal variations in groundwater rest levels in Nairobi City using Geographic Information System, *Nile Basin Water Science and Engineering Journal, 5*(1)

Oroji, B. (2019). Assessing groundwater vulnerability by pollution mapping in Iran: Case study Hamadan – Bahar Plain. *Geofísica Internacional, 57*(3), 161-174

Owuor, S. O., Butterbach-Bahl, K., Guzha A. C., Rufino M. C., Pelster, D. E., Díaz-Pinés, E., & Breuer, L. (2016a). Groundwater recharge rates and surface runoff response to LULC changes in semi-arid environments. *Ecological Processes, 5(*1) https://doi: 10.1186/s13717-016-0060-6

Owuor, S.O., Schüth, C., Lehné, R., Hoppe, A., Obiri, J., Nyaberi, D.M. & Kibet, M.C. (2016b). Estimation of hydraulic properties from pumping tests data of Nairobi area, Kenya. *Int. J. Res. Engineer. Technol. 5*(2), 331-3398. doi: 10.15623/ijret.2016.0502060

Ozerskiy, A. (2017). Hydrogeology of the Archean Crystalline Rock Massif in the Southern Part of the Yenisseyskiy Ridge (Siberian Craton). *Universal Journal of Geoscience, 5*(5), 151-155. https://doi.org/10.13189/ujg.2017.050505

Padilla, L., Winchell, M., Peranginangin, N., & Grant, S. (2017). Development of groundwater pesticide exposure modeling scenarios for vulnerable spring and winter wheat-growing areas. *Integrated Environmental Assessment and Management, 13*(6), 992–1006. https://doi.org/10.1002/ieam.1925

Papa, F., Crétaux, J.-F., Grippa, M., Robert, E., Trigg, M., Tshimanga, R. M., Kitambo, B., Paris, A., Carr, A., Fleischmann, A. S., de Fleury, M., Gbetkom, P. G., Calmettes, B., & Calmant, S. (2022). Correction to: Water Resources in Africa under Global Change: Monitoring Surface Waters from space, *Surveys in Geophysics.* https://doi.org/10.1007/s10712-022-09729-w

Parece, T., & Campbell, J. (2015). Land Use/Land Cover Monitoring and Geospatial Technologies: An Overview. *The Handbook of Environmental Chemistry*, 1-32. https://doi.org/10.1007/978-3-319-14212-8_1

Potapov, P., Hansen, M. C., Pickens, A., Hernandez-Serna, A., Tyukavina, A., Turubanova, S., Zalles, V., Li, X., Khan, A., Stolle, F., Harris, N., Song, X.-P., Baggett, A., Kommareddy, I., & Kommareddy, A. (2022). The Global 2000-2020 Land Cover and Land Use Change Dataset Derived from the Landsat Archive: First Results. *Frontiers in Remote Sensing*, *3*. https://doi.org/10.3389/frsen.2022.856903

Pulido-Velazquez, M., Peña-Haro, S., García-Prats, A., Mocholi-Almudever, A., Henriquez-Dole, L., Macian-Sorribes, H., & Lopez-Nicolas, A. (2015). Integrated assessment of the impact of climate and land use changes on groundwater quantity and quality in the Mancha Oriental system (Spain). *Hydrology and Earth System Sciences*, *19*(4), 1677-1693. https://doi: 10.5194/hess-19-1677-2015

Rendilicha, H. G., Home, P.G., & Raude, J.M. (2018). A review of groundwater vulnerability assessment in Kenya. *Acque Sotterranee - Italian Journal of Groundwater*, *7*(2). https://doi.org/10.7343/as-2018-328

Rukundo, E., & Doğan, A. (2019). Dominant Influencing Factors of Groundwater Recharge Spatial Patterns in Ergene River Catchment, Turkey. *Water*, *11*(4), 653. https://doi.org/10.3390/w11040653

Rwanga, S. S. (2013). A review on groundwater recharge estimation using WetSpass model. *International Conference on Civil and Environmental Engineering* (CEE'2013) Nov. 27-28

Rwanga, S. S. (2018). *Modelling groundwater flow under recharge uncertainty: an application to central Limpopo, South Africa*. PhD thesis, Tshwane University of Technology, 160p

Rwanga, S. S., & Ndambuki, J. M. (2017). Approach to quantify groundwater recharge using GIS based water balance model: *A Review International Journal of Research in Chemical, Metallurgical and Civil Engineering*, *4*(1) (2017) ISSN 2349-1442 EISSN 2349-1450

Said, M. Y., Ogutu, J. O., Kifugo, S. C., Makui, O., Robin S., Reid, R. S., & de Leeuw, J. (2016). Effects of extreme land fragmentation on wildlife and livestock population abundance and distribution. *Journal for Nature Conservation*, *34*, 151–164

Saghravani, S. R., Yusoff, I., Mustapha, S., & Saghravani, S. F. (2013). Estimating groundwater recharge using empirical method: A case study in the Tropical Zone. *Sains Malaysiana*, *42*(5), 553–560

Saghravani, S., Yusoff, I., Wan Md Tahir, W. Z., & Othman, Z. (2014). Comparison of water table fluctuation and chloride mass balance methods for recharge estimation in a tropical rainforest climate: a case study from Kelantan River catchment, Malaysia. *Environmental Earth Sciences*, *73*(8), 4419-4428. https://doi.org/10.1007/s12665-014-3727-2

Salahat, M., Al-Qinna, M., Mashal, K., & Hammouri, N. (2014). Identifying major factors controlling groundwater quality in semi-arid area using advanced statistical techniques. *Water Resources Management*, *28*(11), 3829-3841. https://doi.org/10.1007/s11269-014-0712-1

Salem, A., Dezs˝o, J., & El-Rawy, M. (2019). Assessment of groundwater recharge, evaporation, and runoff in the Drava Basin in Hungary with the WetSpass model. *Hydrology 2019*, *6*(23). https://doi: 10.3390/hydrology6010023

Saxton, K., & Rawls, W. (2006). Soil water characteristic estimates by texture and organic matter for hydrologic solutions. *Soil Science Society of America Journal*, *70*(5), 1569-1578. https://doi: 10.2136/sssaj2005.0117

Scanlon, B. R., Healy, R. W., Cook, P. G. (2002). Choosing appropriate techniques for quantifying groundwater recharge. *Hydrogeology Journal*, *10*, 18–39. http://dx.doi.org/10.1007/s10040-001-0176-2

Sombroek, W. G., Braun, H. M. H., & Van der Pouw, B. J. A. (1982). *Exploratory soil map and agro-climatic zone map of Kenya*, 1980. Kenya Soil Survey

Syombua, J. (2013). Land use and land cover changes and their implications for human-wildlife conflicts in the semi-arid rangelands of southern Kenya. *Journal of Geography and Regional Planning*, *6*(5), 193-199. https://doi.org/10.5897/jgrp2013.0365

Talabi, A. O., & Kayode, T. J. (2019). Groundwater Pollution and Remediation. *Journal of Water Resource and Protection*, *11*(01), 1. https://doi.org/10.4236/jwarp.2019.111001

Thielen, J., Alfieri, L., Burek, P., Kalas, M., Salamon, P., Thiemig, V., de Roo, A., Muraro, D., Pappenberger, F., & Dutra, E. (2012). The Global Flood Awareness System (GloFAS). *Comprehensive Flood Risk Management*. https://doi.org/10.1201/b13715-225

Thomas, B., Behrangi, A., & Famiglietti, J. (2016). Precipitation Intensity Effects on Groundwater Recharge in the Southwestern United States. *Water*, *8*(3), 90. https://doi.org/10.3390/w8030090

Tramberend, S., Burtscher, R., Burek, P., Kahil, T., Fischer, G., Mochizuki, J., Greve, P., Kimwaga, R., Nyenje, P., Ondiek, R., Nakawuka, P., Hyandye, C., Sibomana, C., Luoga, H. P., Matano, A. S., Langan, S., & Wada, Y. (2021).

Co-development of East African regional water scenarios for 2050. *One Earth, 4*(3), 434–447. https://doi.org/10.1016/j.oneear. 2021.02.012

Tuinhof A., Foster S., Frank S., Amal, T., & Wishart, M. (2011). Appropriate Groundwater Management Policy for Sub-Saharan Africa in face of demographic pressure and climatic variability GW•MATE Strategic Overview Series 4 World Bank (Washington DC–USA)

World Bank, (2016). "High and Dry: Climate Change, Water, and the Economy." World Bank, Washington, DC. License: Creative Commons Attribution CC BY 3.0 IGO

United Nations, (2018). Sustainable Development Goal 6: Synthesis Report 2018 on Water and Sanitation. New York

United Nations (2019). Department of Economic and Social Affairs, Population Division. World Population Prospects 2019: Volume I: Comprehensive Tables.https://population.un.org/wpp/Publications/Files/WPP2019Volume-I

U.S. EPA, (1993). A review of methods for assessing aquifer sensitivity and ground water vulnerability to pesticide contamination. US.EPA. EPA/813/R-93/002

Varamesh, S., Hosseini, S. M., & Rahimzadegan, M. (2017). Detection of land use changes in Northeastern Iran by Landsat Satellite Data. *Applied Ecology and Environmental Research, 15*(3), 1443-1454

Wang, L., Dochartaigh, B. O., & Macdonald, D. (2010). A literature review of recharge estimation and groundwater resource assessment in Africa. *British Geological Survey Internal Report*, IR/10/051, 31pp

Winkler, K., Fuchs, R., Rounsevell, M., & Herold, M. (2021). Global land use changes are four times greater than previously estimated. *Nature Communications, 12*(1), 2501. https://doi.org/ 10.1038/ s41467-021-22702-2

World Bank, (2016). "*High and Dry: Climate Change, Water, and the Economy*." World Bank, Washington, DC. License: Creative Commons Attribution CCBY 3.0 IGO

Xu, Y., Seward, P., Gaye, C., Lin, L., & Olago, D. O. (2019). Preface: Groundwater in Sub-Saharan Africa. *Hydrogeology Journal, 27*(3), 815–822. https://doi.org/10.1007/s10040-019-01977-2

Yıldız, D. (2017). "The Importance of Water in Development ", World Water Diplomacy & Science News. Hydro-politics Academy, Ankara, Turkey

Young, N.E., Anderson, R.S., Chignell, S.M., Vorster, A.G., Lawrence, R., & Evangelista, P.H. (2017). A survival guide to Landsat pre-processing. *Ecology, 98*(4), 920–932

Zarei, M., Ghazavi, R., Vli, A., & Abdollahi, K. (2016). Estimating groundwater recharge, evapotranspiration and surface runoff using land-use data: A Case Study in Northeast Iran. *Biological Forum – An International Journal 8*(2), 196-202. https://www.researchtrend.net

Zeng, X., Wang, D., & Wu, J. (2015). Evaluating the three methods of goodness of fit test for frequency analysis. *Journal of Risk Analysis and Crisis Response, 5*(3), 178-187. https://doi.org/10.2991/jrarc.2015.5.3.5

Zhang, Q., Wang, L., Wang, H., Zhu, X., & Wang, L. (2020). Spatio-Temporal Variation of Groundwater Quality and Source Apportionment Using Multivariate Statistical Techniques for the Hutuo River Alluvial-Pluvial Fan, China.

International Journal of Environmental Research and Public Health, *17*(3), 1055. https://doi.org/10.3390/ijerph17031055

Zomlot, Z., Verbeiren, B., Huysmans, M., & Batelaan, O. (2015). Spatial distribution of groundwater recharge and base flow: Assessment of controlling factors. *Journal of Hydrology: Regional Studies*, *4*, 349–368. http://dx.doi.org/10.1016/j.ejrh. 2015.07.005

APPENDICES

Appendix I: Confusion (error) matrices for 1984 to 2017 LULC maps

1984	Reference data						
Classified data	Class 1	Class 2	Class 3	Class 4	Class 5	Class 6	Total
Class 1	**33**	0	0	0	1	0	34
Class 2	0	**38**	0	0	0	0	38
Class 3	5	0	**40**	0	0	0	45
Class 4	0	4	0	**39**	2	0	45
Class 5	1	0	0	0	**37**	0	38
Class 6	0	0	0	0	0	**42**	42
Total	39	42	40	39	40	42	242

User's Accuracy, %	**Producer's Accuracy, %**	
97.05	84.61	Class 1 - Built - up
100	90.47	Class 2 - Agricultural area
88.89	100	Class 3 - Grasslands
		Class 4 - Shrub land
86.67	100	Class 5 - Forested area
97.34	92.5	Class 6 - Bare ground
100	100	

Overall Accuracy = 94.6% **Kappa Coefficient = 0.93**

1995	Reference data						
Classified data	Class 1	Class 2	Class 3	Class 4	Class 5	Class 6	Total
Class 1	**53**	0	1	0	0	0	54
Class 2	0	**27**	0	0	0	3	30
Class 3	3	1	**40**	0	0	3	47
Class 4	0	2	0	**41**	0	0	43
Class 5	0	0	0	0	**37**	0	37
Class 6	0	1	0	0	0	**43**	44
Total	56	31	41	41	37	49	255

User's Accuracy, %	**Producer's Accuracy, %**	
98.14	94.64	Class 1 - Built - up
90	87.09	Class 2 - Agricultural area
85.1	97.56	Class 3 - Grasslands
95.34	100	Class 4 - Shrub land
100	100	Class 5 - Forested area
97.72	87.75	Class 6 - Bare ground

Overall Accuracy = 94.5% **Kappa Coefficient = 0.93**

Appendix I: Confusion (error) matrices (Cont'd)

2005	Reference data						
Classified data	Class 1	Class 2	Class 3	Class 4	Class 5	Class 6	Total
Class 1	**40**	0	0	0	1	0	41
Class 2	0	**35**	0	0	0	0	35
Class 3	0	0	**40**	0	2	0	42
Class 4	0	7	0	**41**	0	0	48
Class 5	0	0	0	0	**37**	0	37
Class 6	0	0	0	0	0	**39**	39
Total	40	42	40	41	40	39	242

User's Accuracy, %	**Producer's Accuracy, %**	
97.56	100	Class 1 - Built - up
100	83.33	Class 2 - Agricultural area
95.23	100	Class 3 - Grasslands
85.41	100	Class 4 - Shrub land
100	92.5	Class 5 - Forested area
100	100	Class 6 - Bare ground
Overall Accuracy = 95.8%	**Kappa Coefficient = 0.95**	

2017	Reference data						
Classified data	Class 1	Class 2	Class 3	Class 4	Class 5	Class 6	Total
Class 1	**55**	0	0	0	0	0	55
Class 2	3	**60**	0	0	0	3	66
Class 3	0	0	**60**	7	0	0	67
Class 4	0	0	0	**60**	0	0	60
Class 5	2	0	0	0	**60**	0	62
Class 6	0	0	0	0	0	**57**	57
Total	60	60	60	67	60	60	367

User's Accuracy, %	**Producer's Accuracy, %**	
97.56	100	Class 1 - Built - up
100	83.33	Class 2 - Agricultural area
95.23	100	Class 3 - Grasslands
85.41	100	Class 4 - Shrub land
100	92.5	Class 5 - Forested area
100	100	Class 6 - Bare ground
Overall Accuracy = 95.9%	**Kappa Coefficient = 0.95**	

Appendix II: Climatic data used in this study (source: KMD and en.climate-data.org**)**

Station	**Rainfall (mm)**												
	Jan	**Feb**	**Mar**	**Apr**	**May**	**June**	**July**	**Aug**	**Sept**	**Oct**	**Nov**	**Dec**	**Annual**
JKIA	51	37	72	128	115	25	10	14	14	52	140	78	737
Isinya	49	42	83	130	70	16	3	8	8	41	106	80	637
Katumani	52	36	85	133	59	8	3	5	4	39	151	101	676
Machakos	47	49	107	179	69	9	5	4	8	53	191	109	830
Kajiado	43	39	60	107	55	11	5	3	8	24	62	48	466
Konza	30	34	67	132	62	9	2	2	6	30	100	57	531
Kitengela	35	39	69	138	80	16	7	6	10	35	100	57	592
Athi River	34	39	73	137	77	17	6	6	10	37	107	56	599
Kiserian	56	46	82	180	160	31	11	16	17	45	111	78	833

Station	**Temperature (degree C)**												
	Jan	**Feb**	**Mar**	**Apr**	**May**	**June**	**July**	**Aug**	**Sept**	**Oct**	**Nov**	**Dec**	**Mean**
JKIA	19.7	20.3	20.7	20.0	19.2	17.7	16.5	16.9	18.1	19.2	19.0	18.4	18.8
Isinya	19.6	20.4	20.6	20.0	19	17.5	16.7	17.0	18.5	19.8	19.4	19.3	19.0
Katumani	19.2	19.6	20.6	19.9	18.9	17.4	16.6	16.7	18.6	19.4	19.5	18.2	18.7
Machakos	19.5	20.3	20.7	20.0	19.0	17.4	16.5	17.0	18.5	20.1	19.4	19.2	19.0
Kajiado	19.5	20.3	20.5	19.8	18.8	17.5	16.5	17.1	18.3	19.7	19.2	19.1	18.9
Konza	19.4	20.3	20.6	20.0	18.9	17.3	16.5	16.9	18.4	19.8	19.3	19.0	18.9
Kitengela	19.8	20.5	20.9	20.4	19.4	17.7	16.9	17.2	18.7	20.0	19.5	19.5	19.2
Athi River	20.0	20.8	21.0	20.7	19.6	18.0	17.0	17.5	18.9	20.2	19.8	19.6	19.4
Kiserian	18.3	19.0	19.3	19.0	18.0	16.5	15.5	15.8	17.3	18.6	18.2	18.0	17.8

Appendix II: Climatic data (Cont'd)

Station	Potential Evapotranspiration (PET) (mm)												
	Jan	**Feb**	**Mar**	**Apr**	**May**	**June**	**July**	**Aug**	**Sept**	**Oct**	**Nov**	**Dec**	**Annual**
JKIA	179	179	197	140	108	93	98	101	147	169	138	167	1716
Isinya	133	146	149	139	124	101	88	93	116	136	130	129	1485
Katumani	129	142	153	121	102	81	86	100	136	158	116	115	1436
Machakos	132	144	150	139	124	99	85	93	116	141	130	127	1482
Kajiado	132	144	147	136	121	101	85	95	113	135	127	126	1462
Konza	130	144	149	139	122	98	85	92	115	136	129	124	1463
Kitengela	136	147	153	146	130	104	92	96	119	139	132	132	1527
Athi River	139	152	155	150	133	109	93	101	122	143	136	133	1567
Kiserian	113	124	129	124	109	85	70	75	98	118	112	109	1264

	Wind Speed (m/s)												
	Jan	**Feb**	**Mar**	**Apr**	**May**	**June**	**July**	**Aug**	**Sept**	**Oct**	**Nov**	**Dec**	
JKIA	4.4	4.4	4.2	3.3	2.8	2.6	2.6	4.4	3.2	4.0	3.9	4.4	3.68
Isinya	4.4	4.4	4.2	3.3	2.8	2.6	2.6	4.4	3.2	4.0	3.9	4.4	3.68
Katumani	4.4	4.4	4.2	3.3	2.8	2.6	2.6	4.4	3.2	4.0	3.9	4.4	3.68
Machakos	4.4	4.4	4.2	3.3	2.8	2.6	2.6	4.4	3.2	4.0	3.9	4.4	3.68
Kajiado	4.4	4.4	4.2	3.3	2.8	2.6	2.6	4.4	3.2	4.0	3.9	4.4	3.68
Konza	4.4	4.4	4.2	3.3	2.8	2.6	2.6	4.4	3.2	4.0	3.9	4.4	3.68
Kitengela	4.4	4.4	4.2	3.3	2.8	2.6	2.6	4.4	3.2	4.0	3.9	4.4	3.68
Athi River	4.4	4.4	4.2	3.3	2.8	2.6	2.6	4.4	3.2	4.0	3.9	4.4	3.68
Kiserian	4.4	4.4	4.2	3.3	2.8	2.6	2.6	4.4	3.2	4.0	3.9	4.4	3.68

Appendix III: WetSpass-M land use parameters used in this study (source: WetSpass-M user guide)

CODE	LAND USE TYPE	RUN-OFF VEG	VEG_ CLASS (No.)	IMP_RO CLASS (No.)	VEG AREA (FRAC)	BARE AREA (FRAC)	IMPER. AREA (FRAC)	OPEN WATER AREA (FRAC)	ROOT_ DEPTH	LAI	MIN. STOMATA OPENING	INTER. %	VEG. HEIGHT
2	Built-up areas	Grass	2.0	2.0	0.2	0.0	0.8	0.0	0.3	2.0	100.0	10.0	0.12
7	Bare land	bare soil	4.0	0.0	0	1.0	0.0	0.0	0.05	0.0	110.0	0.0	0.001
21	Agriculture	Crop	1.0	0.0	0.8	0.2	0.0	0.0	0.4	4.0	180.0	35.0	0.6
23	Savannah Grassland	Grass	2.0	0.0	1.0	0.0	0.0	0.0	0.3	2.0	100.0	10.0	0.2
31	Trees and riverine vegetation	Forest	3.0	0.0	1.0	0.0	0.0	0.0	2.0	5.0	375.0	25.0	16.0
36	Shrub savannah	Grass	2.0	0.0	1.0	0.0	0.0	0.0	0.6	6.0	110.0	40.0	2.0

Land use attribute table descriptions: *CODE* - land use number; *LAND USE TYPE* – land use type*; RUN_OFF VEG* - runoff vegetation; *VEG_CLASS* - runoff class for vegetation type; *IMP_RO class* - runoff class for impervious area; *VEG AREA (FRAC)* - fraction of vegetated area; BARE AREA (FRAC) - fraction of bare area; *IMPER. AREA (FRAC)* **–** fraction of impervious area; *OPEN WATER AREA (FRAC)* – fraction of open water area; *ROOT_DEPTH* – root depth; *LAI* – leaf area index; *MIN. STOMATA OPENING* – minimum stomatal opening; *INTER. %* - interception percentage; *VEG. HEIGHT* – vegetation height

Appendix IV: WetSpass-M soil parameters used in this study (source: WetSpass-M user guide)

CODE	SOIL	FIELD CAPACITY	WILTING POINT	PLANT AVAILABLE WATER	RESIDUAL WATER CONTENT	A1	EVAPO-DEPTH	TENSION SATURATED HEIGHT	P_FRACTION SUMMER	P_FRACTION WINTER
3	Sandy loam	0.21	0.01	0.20	0.04	0.35	0.05	0.61	0.09	0.01
7	Sandy clay loam	0.5	0.33	0.13	0.09	0.21	0.05	0.37	0.95	0.85
9	Clay loam	0.33	0.19	0.14	0.075	0.27	0.05	0.26	0.62	0.41
10	Sandy clay	0.32	0.23	0.09	0.109	0.25	0.05	0.29	0.8	0.68
12	Clay	0.46	0.33	0.13	0.09	0.21	0.05	0.37	0.95	0.85

Soil texture attribute table descriptions: *CODE* - soil type number; *SOIL* - soil type; *FIELD CAPACITY* – field capacity*; WILTING POINT* - wilting point*; PLANT AVAILABLE WATER* - plant available water *; RESIDUAL WATER CONTENT* - residual water content*; A1* (calibration parameter dependent on the sand content); *EVAPO-DEPTH* (bare soil evaporation depth); *TENSION SATURATED HEIGHT* – tension saturated height*; P_FRACTION SUMMER* (fraction of summer precipitation contributing to runoff); *P_FRACTION WINTER* (fraction of summer precipitation contributing to runoff).

Appendix V: Soil analyses data (source: this study)

No.	1st Hydrometer Reading	2nd Hydrometer Reading	Sand %	Silt %	Clay %	Texture	WetSpass -M Code
1	20	7	40	14	46	clay	12
2	30	11	60	22	18	sandy loam	3
3	30	7	60	14	26	sandy clay loam	7
4	25	6	50	12	38	sandy clay	10
5	30	8	60	16	24	sandy clay loam	7
6	21	5	42	10	48	clay	12
7	28	9	56	18	26	sandy clay loam	7
8	30	10	60	20	20	sandy clay loam	7
9	22	10	44	20	36	clay loam	9
10	16	6	32	12	56	clay	12
11	30	12	60	24	16	sandy loam	3
12	23	5	46	10	44	sandy clay	10
13	26	7	52	14	34	sandy clay loam	7
14	30	12	60	24	16	sandy loam	3
15	27	10	54	20	26	sandy clay loam	7
16	27	8	54	16	30	sandy clay loam	7
17	20	10	40	20	40	clay	12
18	26	14	52	28	20	loam	5
19	24	5	48	10	42	sandy clay	10
20	27	6	54	12	34	sandy clay loam	7
21	29	11	58	22	20	sandy clay loam	7
22	28	4	56	8	36	sandy clay	10
23	25	6	50	12	38	sandy clay	10
24	30	9	60	18	22	sandy clay loam	7
25	28	20	56	40	4	sandy loam	3
26	25	13	50	26	24	sandy clay loam	7
27	26	1	52	2	46	sandy clay	10
28	10	3	20	6	74	clay	12
29	24	11	48	22	30	sandy clay loam	7
30	22	11	44	22	34	clay loam	9
31	18	6	36	12	52	clay	12
32	13	1	26	2	72	clay	12
33	30	15	60	30	10	sandy loam	3
34	14	3	28	6	66	clay	12

Appendix V: Soil analyses data (Cont'd)

No.	1st Hydrometer Reading	2nd Hydrometer Reading	Sand %	Silt %	Clay %	Texture	WetSpass -M Code
35	23	10	26	20	54	clay	12
36	19	5	38	10	52	clay	12
37	17	10	34	20	46	clay	12
38	21	8	42	16	42	clay	12
39	12	1	24	2	74	clay	12
40	12	7	24	14	62	clay	12
41	24	19	48	38	14	loam	5
42	12	6	24	12	64	clay	12
43	26	20	52	8	40	sandy clay	10
44	13	7	26	14	60	clay	12
45	24	11	48	22	30	sandy clay loam	7
46	26	21	52	6	42	sandy clay	10
47	18	9	36	18	46	clay	12
48	15	10	30	20	50	clay	12
49	22	15	44	30	26	loam	5
50	16	9	32	18	50	clay	12
51	19	14	38	28	34	clay loam	9
52	17	9	34	18	48	clay	12
53	29	13	58	26	16	sandy loam	3
54	26	16	52	32	16	loam	5
55	18	8	36	38	16	loam	5
56	23	12	46	24	30	sandy clay loam	7
57	13	10	26	20	54	clay	12
58	14	5	28	10	62	clay	12
59	22	10	44	20	36	clay loam	9
60	28	15	56	30	14	sandy loam	3
61	24	8	48	16	36	sandy clay	10
62	25	12	50	24	26	sandy clay loam	7
63	24	13	48	26	26	sandy clay loam	7
64	22	12	44	24	32	clay loam	9
65	25	15	50	30	20	loam	5
66	25	21	50	8	42	sandy clay	10
67	15	8	30	16	54	clay	12

Appendix VI: Groundwater depth data (source: present study and WRA)

No.	**Location**	**Longitude**	**Latitude**	**Depth (m)**
1.	Isinya	36.8402	-1.6797	14
2.	Steel factory	36.8552	-1.6705	15
3.	Latia resource centre	36.8313	-1.6866	13
4.	Inkiito Manoh	36.7792	-1.7025	31
5.	Sathya Sai school	36.8088	-1.6005	27
6.	Inkukuon	36.8008	-1.5616	33
7.	Tumate borehole	37.0719	-1.7219	53
8.	Ilpolosat	37.0861	-1.7533	45
9.	Konza	37.1033	-1.7591	49
10.	Konza	37.0811	-1.75	45
11.	Ereteti	36.7833	-1.5333	36
12.	Olturoto	36.9375	-1.6419	11
13.	P J Dave	36.8952	-1.6958	20

Serial no.	**Location**	**Longitude**	**Latitude**	**Depth (m)**
5785	Iloitayiok	36.75000	-1.60000	80.0
7454	Kisaju	36.80000	-1.63330	70.0
8103	Isenya	36.80000	-1.65000	80.0
9298	Kitengela	36.95000	-1.48330	152.0
9520	Isinya	36.80890	-1.67670	38.0
10026	Olooloit koshi	36.82780	-1.52080	102.0
10081	Kitengela	36.95000	-1.56390	165.0
10252	Isinya	36.86330	-1.66940	82.0
10317	Langau	36.78330	-1.44440	100.0
10331	Kitengela	36.90920	-1.55610	89.0
10508	Kitengela	36.88470	-1.56830	122.0
10513	Kitengela	36.96670	-1.59860	90.0
10556	Kipeto	36.82640	-1.71390	123.0
10700	Kaputei	36.93890	-1.54720	92.0
10747	Kipeto	36.69860	-1.60000	130.0
10754	Kitengela	36.95780	-1.50360	120.0
10758	Kisaju	36.92780	-1.58060	100.0
10880	Masai farm	36.93470	-1.53390	101.0
10924	Kitengela	36.93330	-1.53060	174.0
10966	Isinya	36.89170	-1.62500	148.0
11173	Kisaju	36.87780	-1.61940	107.0
11264	Isinya	36.84860	-1.70000	100.0
11266	Kaputei	36.80610	-1.81030	105.0

Appendix VII: Approval of Research Proposal

KENYATTA UNIVERSITY
GRADUATE SCHOOL

E-mail: kubps@yahoo.com
dean-graduate@ku.ac.ke
Website: www.ku.ac.ke

P.O. Box 43844, 00100
NAIROBI, KENYA
Tel. 810901 Ext. 57530

Internal Memo

FROM: Dean, Graduate School

DATE: 9th November, 2016

TO: Mr. Morris W. Mathenge
C/o Department of Environmental Science
KENYATTA UNIVERSITY

REF: N85/31028/15

SUBJECT: APPROVAL OF RESEARCH PROPOSAL

This is to inform you that the Graduate School Board at its meeting 19th October, 2016 approved your Ph.D. Research Proposal entitled "Influence of Land Use and Land Cover Changes on Groundwater Resources in the Stony Athi Sub-Catchment, Kajiado County, Kenya".

You may now proceed with your Data collection, subject to clearance with the Director General, National Commission for Science, Technology & Innovation.

As you embark on your data collection, please note that you will be required to submit to Graduate School completed supervision Tracking Forms per semester. The form has been developed to replace the progress Report Forms. The Supervision Tracking Forms are available at the University's Website under Graduate School webpage downloads.

By copy of this letter, the Registrar (Academic) is hereby requested to grant you substantive registration for your Ph.D. studies.

Thank you.

JOHN M. ODONGI
FOR: DEAN, GRADUATE SCHOOL

c.c. Chairman, Department of Environmental Sciences
Registrar (Academic) Att; Mr. Likam
Supervisors:

1. Dr. Gladys Gathuru
   C/o Department of Environmental Sciences
   KENYATTA UNIVERSITY
2. Dr. Esther Kitur
   C/o Department of Environmental Sciences
   KENYATTA UNIVERSITY

JMO/cao

Appendix VIII: Research Authorization

KENYATTA UNIVERSITY
GRADUATE SCHOOL

E-mail: kubps@yahoo.com
dean-graduate@ku.ac.ke
Website: www.ku.ac.ke

P.O. Box 43844, 00100
NAIROBI, KENYA
Tel. 8710901 Ext. 57530

Our Ref: N85/31028/15 **Date:** 9th November, 2016

The Director General,
National Commission for Science, Technology & Innovation,
P.O. Box 30623-00100,
NAIROBI

Dear Sir/Madam,

RE: RESEARCH AUTHORIZATION FOR MR.MORRIS W. MATHENGE REG. NO. N85/31028/15

I write to introduce Mr. Mathenge who is a Postgraduate Student of this University. He is registered for a Ph.D. degree programme in the **Department of Environmental Sciences in the School of Environmental Studies.**

Mr. Mathenge intends to conduct research for Ph.D. thesis entitled, **"Influence of Land Use and Land Cover Changes on Groundwater Resources in the Stony Athi Sub-Catchment, Kajiado County, Kenya".**

Any assistance given will be highly appreciated.

Yours faithfully,

MRS. LUCY N. MBAABU
FOR: DEAN, GRADUATE SCHOOL

JMO/cao

Appendix IX: NACOSTI Research Authorization

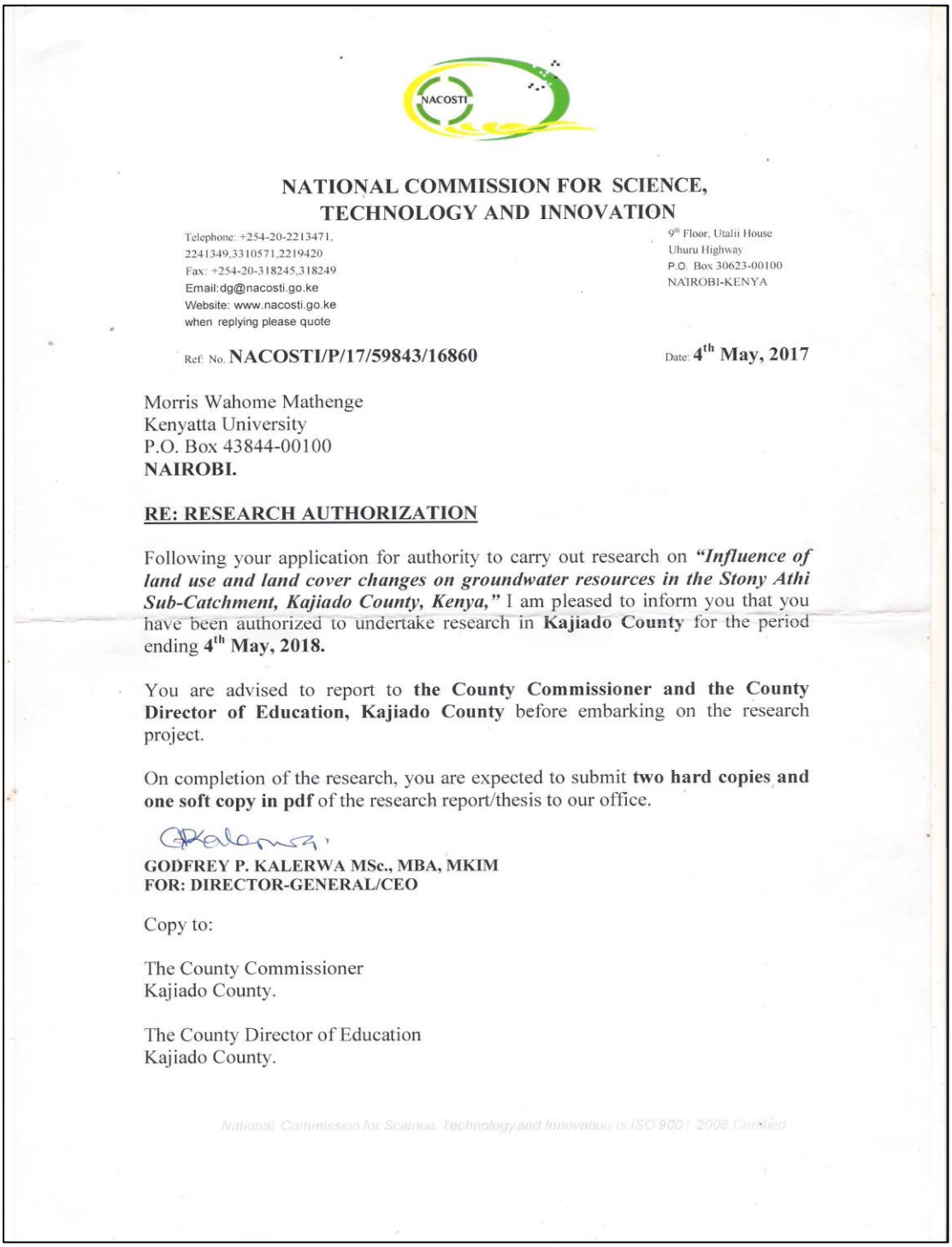

NATIONAL COMMISSION FOR SCIENCE,
TECHNOLOGY AND INNOVATION

Telephone: +254-20-2213471,
2241349,3310571,2219420
Fax: +254-20-318245,318249
Email:dg@nacosti.go.ke
Website: www.nacosti.go.ke
when replying please quote

9th Floor, Utalii House
Uhuru Highway
P.O. Box 30623-00100
NAIROBI-KENYA

Ref: No. **NACOSTI/P/17/59843/16860**

Date: **4th May, 2017**

Morris Wahome Mathenge
Kenyatta University
P.O. Box 43844-00100
NAIROBI.

RE: RESEARCH AUTHORIZATION

Following your application for authority to carry out research on ***"Influence of land use and land cover changes on groundwater resources in the Stony Athi Sub-Catchment, Kajiado County, Kenya,"*** I am pleased to inform you that you have been authorized to undertake research in **Kajiado County** for the period ending **4th May, 2018.**

You are advised to report to **the County Commissioner and the County Director of Education, Kajiado County** before embarking on the research project.

On completion of the research, you are expected to submit **two hard copies and one soft copy in pdf** of the research report/thesis to our office.

GODFREY P. KALERWA MSc., MBA, MKIM
FOR: DIRECTOR-GENERAL/CEO

Copy to:

The County Commissioner
Kajiado County.

The County Director of Education
Kajiado County.

Appendix X: Research Clearance Permit

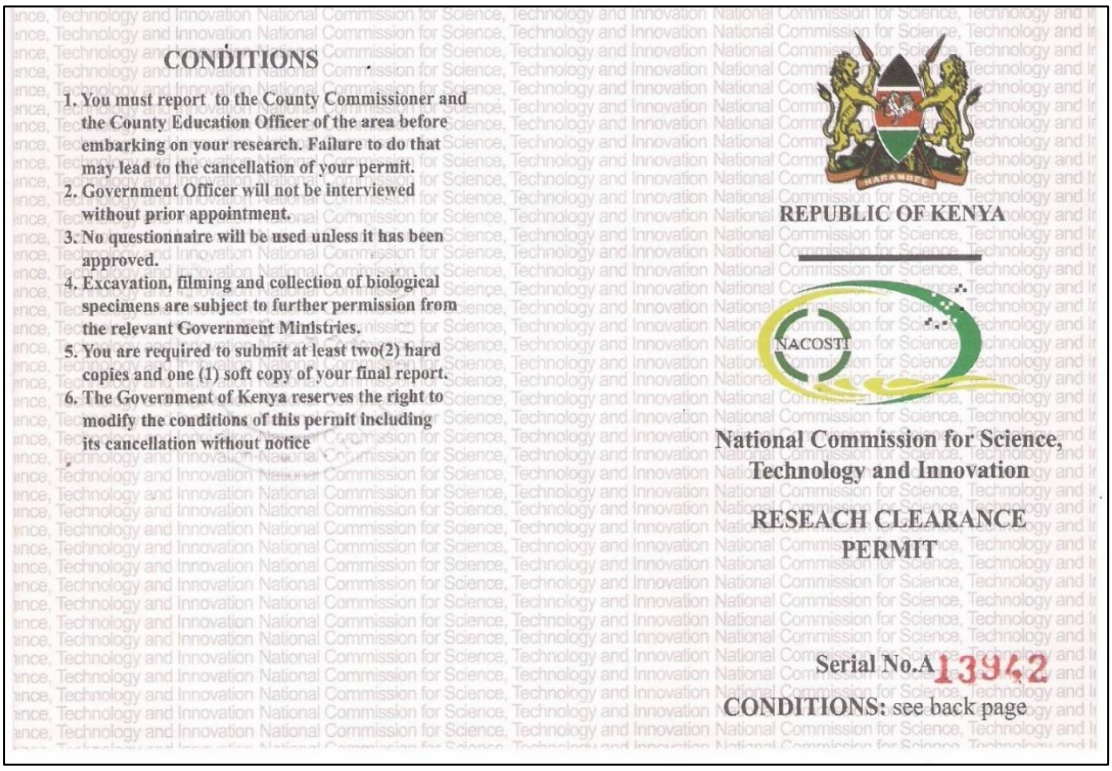

CONDITIONS

1. You must report to the County Commissioner and the County Education Officer of the area before embarking on your research. Failure to do that may lead to the cancellation of your permit.
2. Government Officer will not be interviewed without prior appointment.
3. No questionnaire will be used unless it has been approved.
4. Excavation, filming and collection of biological specimens are subject to further permission from the relevant Government Ministries.
5. You are required to submit at least two(2) hard copies and one (1) soft copy of your final report.
6. The Government of Kenya reserves the right to modify the conditions of this permit including its cancellation without notice

REPUBLIC OF KENYA

NACOSTI

National Commission for Science, Technology and Innovation

RESEACH CLEARANCE PERMIT

Serial No.A 13942

CONDITIONS: see back page

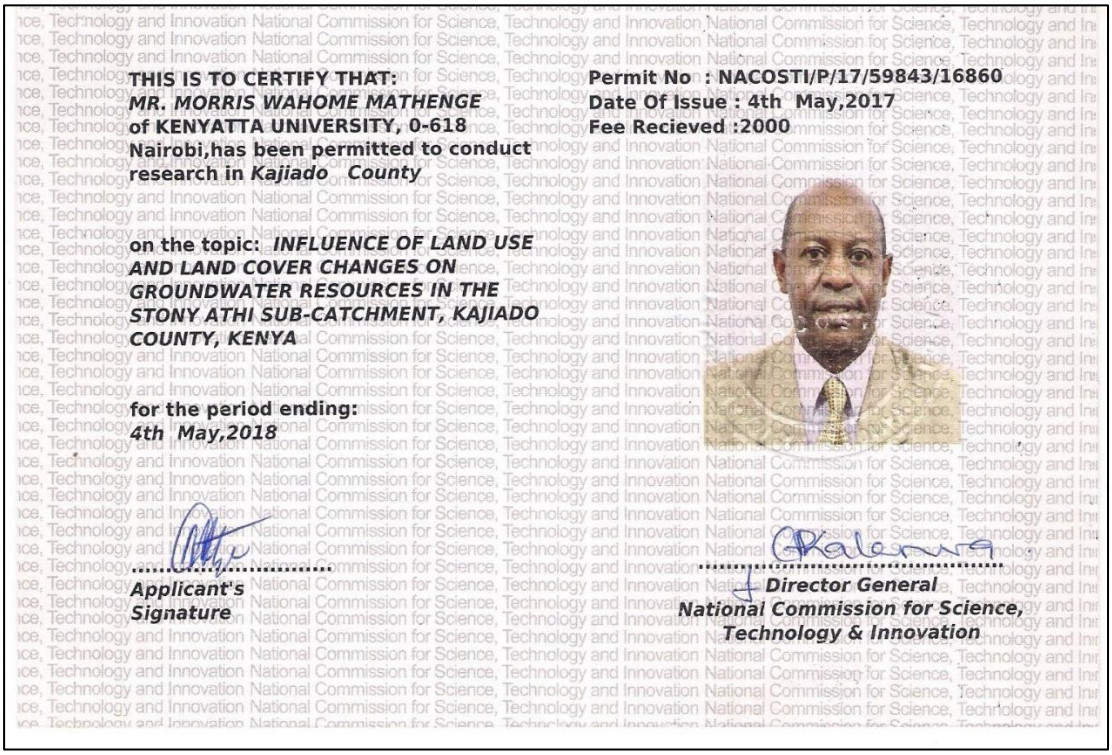

THIS IS TO CERTIFY THAT:
MR. MORRIS WAHOME MATHENGE
of KENYATTA UNIVERSITY, 0-618
Nairobi,has been permitted to conduct research in *Kajiado County*

on the topic: *INFLUENCE OF LAND USE AND LAND COVER CHANGES ON GROUNDWATER RESOURCES IN THE STONY ATHI SUB-CATCHMENT, KAJIADO COUNTY, KENYA*

for the period ending:
4th May,2018

Permit No : NACOSTI/P/17/59843/16860
Date Of Issue : 4th May,2017
Fee Recieved :2000

.....
Applicant's Signature

.....
Director General
National Commission for Science, Technology & Innovation